UNIVERSIDADE DA BEIRA INTERIOR
Ciências

Biophysical study of therapeutic antibody adsorption in affinity chromatography

Gonçalo Fradique Lopes da Silva

Tese para obtenção do Grau de Doutor em
Bioquímica
(3º ciclo de estudos)

Orientador: Prof. Doutor Ana Cristina Mendes Dias Cabral
Co-orientador: Prof. Doutor Alois Jungbauer

Covilhã, julho de 2019

Um brinde aos avós.

Acknowledgements

To Prof. Cristina Cabral, Prof. Alois Jungbauer, and Astrid Dürauer, for their prompt availability whenever I needed and scientific input. Also, for their kind and useful advice during the course of these four years. But mostly, for their patience.

To Sir Rupert Tschelieβnig, for aiming for eternal fame. Thank you for all the help and the shiny models, because “seeing is believing”.

To Jacek Plewka, for sharing the burden with me.

To all my friends and colleagues involved in the 25.011 project, Alois’ lab in Vienna, and Cristina’s lab in Portugal, for the good work environment, coffee breaks, beer breaks, and all the fun and interesting discussions we had.

À minha família, um muito obrigado por todo o suporte, carinho, e motivação durante estes anos.

I also want to acknowledge Fundação para a Ciência e Tecnologia for the grant and the Austrian Centre of Industrial Biotechnology, Novartis/Sandoz, and Boehringer Ingelheim for the cooperation.

Resumo alargado

O mercado de anticorpos monoclonais (mAbs – do inglês *monoclonal antibodies*) tem vindo a crescer exponencialmente ao longo das últimas décadas devido à elevada capacidade de resposta, selectividade, e robustez destas biomoléculas. O número de áreas de aplicação terapêutica dos mAbs tem também vindo a aumentar, sendo o cancro e as doenças autoimunes as mais representadas. Existem actualmente mais de 50 produtos aprovados e comercializados, representando uma receita de cerca de 100 mil milhões de dólares em vendas. Deste modo, devido à elevada procura e concomitante necessidade de aumento da produção destas biomoléculas, a indústria farmacêutica tem estado em constante evolução e optimização dos processos de produção e purificação de mAbs. Existem ainda critérios cada vez mais apertados para o controlo de qualidade destas biomoléculas por parte das principais agências reguladoras mundiais, nomeadamente a *U.S. Food and Drug Administration* (FDA) e a Agência Europeia do Medicamento (EMA – do inglês *European Medicines Agency*), de modo a assegurar a formulação de um produto seguro e de elevada pureza. É, por isso, necessário haver uma compreensão completa de todos os passos envolvidos em toda a cadeia de produção de anticorpos monoclonais.

Um dos passos mais críticos, dispendiosos, e limitante é o passo de captura dos anticorpos durante a fase de purificação, nomeadamente o uso de cromatografia de afinidade com resinas de proteína A. A cromatografia de proteína A é o método mais aplicado para a purificação de anticorpos devido à sua elevada selectividade e também devido à sua robustez. As resinas de cromatografia utilizadas têm elevadas capacidades de ligação dinâmica, muito devido ao facto de os seus ligandos serem cadeias com múltiplos locais de ligação. Apesar da ligação dos anticorpos à proteína A ser amplamente conhecida, ainda não existe muita informação acerca do mecanismo através do qual a interação ocorre. Há certos aspectos como a estequiometria, a ligação preferencial, e a orientação tanto da cadeia de proteína A como do anticorpo que ainda não estão muito claros. Este conhecimento pode ser utilizado para optimizar a performance da captura de mAbs, quer seja através do melhoramento das resinas, quer seja através da minimização de custos devido a melhores previsões através do estabelecimento de modelos que incorporem estes parâmetros.

Na cromatografia de proteínas são utilizados alguns sensores que têm por base fornecer informação acerca da concentração (UV), pureza (cromatografia de exclusão molecular em HPLC – SEC-HPLC do inglês), potência (ressonância de plasma de superfície – SPR do inglês), e estrutura (dicroísmo circular – CD do inglês e dispersão de luz por ângulo múltiplo – MALS do inglês). No entanto, todos estes sensores recolhem informação após as moléculas terem passado pela coluna de cromatografia operando *online* no sistema, ou então são usadas *offline*. Nenhum dos detectores fornece informação sobre a ligação anticorpo-proteína A realmente *in situ*.

Este trabalho de doutoramento teve como objectivo a compreensão da interacção entre anticorpos e resinas de proteína A com recurso a técnicas de operação *in situ*, de modo a poder

estabelecer um modelo que consiga prever a adsorção de anticorpo, a sua organização estrutural aquando da ligação, a sua migração ao longo da coluna, a sua eluição e consequente pureza e potência. Para tal, foram usadas duas resinas de proteína A comerciais (MabSelect SuRe e TOYOPEARL AF-rProtein A HC) conhecidas pelas suas cadeiras com múltiplos domínios de ligação (4 e 6, respectivamente) e foi utilizado um mAb comercial (trastuzumab).

A microcalorimetria de fluxo (FMC – do inglês) foi usada extensivamente para obter os parâmetros termodinâmicos associados à adsorção de anticorpos às resinas de proteína A. O microcalorímetro consiste numa coluna cilíndrica de 6 mm de diâmetro interno e 6 mm de altura com dois sensores térmicos acoplados às paredes da coluna capazes de detectar pequenas variações de potencial durante o processo cromatográfico. O perfil de adsorção mostrou ser de natureza exotérmica com dois passos subjacentes. Um primeiro momento é relativo à ligação em si, que resulta em grandes libertações de calor. Posteriormente, há uma reorganização dos anticorpos nos ligandos de modo a arranjarem a posição energeticamente mais favorável.

De modo a caracterizar as alterações estruturais do complexo anticorpo-proteína A e avaliar a sua influência na topologia da superfície na adsorção, foi utilizada a técnica difracção de raios-X de pequeno ângulo (SAXS – do inglês *small angle X-ray scattering*). Foi usado um pequeno capilar de quartzo transparente aos raios-X em que foram empacotadas as resinas de proteína A. Foi possível acompanhar a formação da camada de anticorpo à superfície das resinas à medida que o anticorpo era introduzido. Foi demonstrada a possibilidade de ligação heterogénea dependendo da saturação da resina. Um modelo aplicado para interpretar os resultados foi o "*broken rod model*", que sugere que as moléculas de anticorpo se ligam aos ligandos de proteína A no domínio mais exterior. Uma investigação posterior envolvendo diferentes concentrações de anticorpo foi realizada para avaliar a estequiometria de ligação em diferentes zonas da isotérmica. Os dados experimentais foram comparados com modelos cristalográficos reproduzindo o anticorpo e uma cadeia com quatro domínios de ligação semelhante à usada na resina MabSelect SuRe. Foi verificado que a baixas concentrações a estequiometria mais favorável é de 1:1 e que a concentrações intermédias 2:1 torna-se mais favorável, sendo sempre uma mistura de ambas. A estequimetria 3:1 foi igualmente testada e tida como possível, mas posteriormente desconsiderada como provável devido aos elevados efeitos estéricos presentes, pelo que esta condição carece de uma modelação mais avançada para poder ter em conta a flexibilidade das moléculas. Todos estes resultados confirmam a natureza heterogénea das resinas de proteína A.

A abordagem oferecida por esta tese permitiu avaliar in situ a adsorção de anticorpos a proteína A durante o passo cromatográfico de afinidade, no entanto pode ser aplicada a qualquer tipo de cromatografia e para qualquer tipo de biomolécula, permitindo assim, abrir portas a uma investigação mais aprofundada para todos os tipos de cromatografia de alta relevância industrial, onde compreender o mecanismo de ligação biomolécula-ligando é de extrema importância.

Palavras-chave

Anticorpos monoclonais; proteína A; cromatografia de afinidade; isotérmica de adsorção; *shrinking core model*; microcalorimetria de fluxo; entalpia de adsorção; raios-X de pequeno ângulo; *broken rod model*; *pearl necklace model*.

Abstract

The monoclonal antibody market has been growing rapidly in the past decades, and the number of therapeutic areas where monoclonal antibodies (mAbs) are employed has been increasing, with cancer and autoimmune diseases being the most represented. There are already more than 50 approved products, representing a staggering $100 billion in global sales. Because of this high demand, antibody manufacturing has been in constant evolution and asking for new, more efficient, and more optimized methods to be applied both in the upstream and downstream processing.

Protein A chromatography is step of choice of most of the pharmaceutical companies for the antibody capture in the downstream processing. It is a core unit operation that has been in constant evolution, with the new resins coming to the market having higher binding capacities than their predecessors and improved alkaline stability. Despite of this extensive improvement in Protein A resins, there are still some aspects that lack understanding and deep investigation, specifically the mechanism of interaction between the antibodies and the Protein A ligands, both under linear and overloaded conditions. This knowledge can be used for further enhancement of performance in the mAbs capture step.

The knowledge accumulated during the last decades by studying chromatography for proteins bioprocess development has shed some light to the mechanistic understanding of protein–ligand interactions, though based on indirect measurements. Chromatography processes in general are characterized with online and offline sensors that probe the concentration (UV detector), purity (SEC-HPLC), potency (SPR), and structure (MALS, CD) of the product, as well as conductivity and pH that can be measured directly in the chromatography stations (ÄKTA). However, none of these probes operate *in situ*, *i.e.* in the chromatographic column where the interaction occurs. The online sensors tackle the elution peak, and the offline sensors analyse the sample afterwards. Therefore, this research consists in a biophysical study on the antibody adsorption to commercial Protein A resins with *in-situ* sensors, which resulted in an improved understanding of antibody–Protein A interactions, both under linear and overloaded conditions.

Flow microcalorimetry was extensively used to retrieve the thermodynamic parameters during antibody adsorption. The microcalorimeter consists on a ID 6 mm × 6 mm column with two thermistors coupled on the column walls that are able to detect small changes in potential during a chromatographic process. The application of the technique to two commercial Protein A resins (MabSelect SuRe with a tetrameric Protein A ligand and TOYOPEARL AF-rProtein A HC with a hexameric Protein A ligand) showed an adsorption profile of exothermic nature with two sub-processes involved. The first and stronger moment was associated to the adsorption process itself. The second moment, less energetic, was associated either to reorganization of the antibody layer and the Protein A chain upon binding, or to antibody binding to a ligand where

an antibody molecule would already be bound. These interpretations were reinforced by the small angle X-ray scattering (SAXS) studies.

To characterize the changes in the antibody-Protein-A ligand complex and evaluate the influence of the surface topology on adsorption, SAXS was employed using a miniaturized, X-ray-transparent chromatography column packed with the resin. In this way, the protein absorption process could be followed and the formation of a protein layer on the chromatography resin fibres can be observed at the nanoscale and in a time-resolved manner. For the first time it was possible to directly correlate the nanostructure changes inside the column, upon adsorption and during elution. It was demonstrated the possibility of heterogeneous binding throughout the bead network depending on the resin saturation. By application of the broken rod model and under resin saturation it was proposed that an average of 1.2 antibodies adsorb per Protein A ligand in MabSelect SuRe at the outermost domains. Further investigation was performed at different surface concentrations in order to evaluate differences in the organization and stoichiometry in the different zones of the isotherm. The experimental data, analysed by the pearl necklace model, was compared with crystallographic structures of an IgG1 and a tetrameric chain of the B domain of Staphylococcal Protein A (the native form of the Protein A ligand present in MabSelect SuRe). It was found that at low isotherm concentrations the antibody to Protein A ratio was 1:1 and that at intermediate and high concentrations the 2:1 stoichiometry became favoured. The stoichiometry of 3:1 was also tested but was disregarded because of the strong steric effects.

The offered approach in this thesis follows the adsorption process *in situ*, in the column and opens up new prospects to deeper investigation of all modes of chromatography of high industrial relevance, where the understanding of biomolecule–resin mechanism of interaction is of utmost importance.

Keywords

Monoclonal antibodies; Protein A; affinity chromatography; adsorption isotherm; shrinking core model; flow microcalorimetry; adsorption enthalpy; small angle X-ray scattering; broken rod model; pearl necklace model.

List of publications

I. Antibody adsorption in Protein A affinity chromatography – In situ measurement of nanoscale structure by small angle X-ray scattering

Jacek Plewka, Gonçalo L. Silva, Rupert Tscheließnig, Harald Rennhofer, Cristina Dias-Cabral, Alois Jungbauer, Helga Lichtenegger
Published in Journal of Separation Science 2019; 41:4122-4132 (DOI: 10.1002/jssc.201800776)

II. Antibody binding heterogeneity of Protein A resins

Gonçalo F. L. Silva, Jacek Plewka, Rupert Tscheließnig, Helga Lichtenegger, Alois Jungbauer, Ana C. M. Dias-Cabral
Published in Journal of Biotechnology 2019; 1800632:1-8 (DOI: 10.1002/biot.201800632)

III. The pearl necklace model in Protein A chromatography – molecular mechanisms at the resin interface

Gonçalo L. Silva, Jacek Plewka, Helga Lichtenegger, Cristina Dias-Cabral, Alois Jungbauer, Rupert Tscheließnig
Published by Biotechnology and Bioengineering 2019; 116:76-86 (DOI: 10.1002/bit.26843)

List of communications

Oral communications

I. 3D model of antibody-protein A complex rearrangement on the surface of commercial affinity resins

Goncalo Silva, Alois Jungbauer, Rupert Tscheließnig
Affinity (2019) Stockholm, Sweden

II. 3D model of antibody adsorption on TOYOPEARL AF-rProtein A HC and Mabselect SuRe

Goncalo Silva, Jacek Plewka, Helga Lichtenegger, Ana C. Dias-Cabral, Alois Jungbauer, Rupert Tscheließnig
HIC/DSP Bioseparation Conference (2019) Interlaken, Switzerland

III. Structural and thermodynamic characterization of antibody-staphylococcal Protein A complex on chromatography surface

G. L. Silva, A. C. Dias-Cabral, A. Jungbauer, R. Tscheließnig
European Symposium on Biochemical Engineering Sciences (ESBES) (2018) Lisbon, Portugal

IV. 3D structure of the antibody-staphylococcal Protein A complex on chromatography surface by small angle X-ray scattering and molecular simulation

G. L. Silva, A. C. Dias-Cabral, A. Jungbauer, R. Tscheließnig
International Symposium on Preparative and Process Chromatography (PREP) (2018) Baltimore, USA

V. Thermal and structural analysis of mAb binding to Protein A in affinity chromatography

G. L. Silva, J. Plewka, R. Tscheließnig, A. Jungbauer, A. C. Dias-Cabral
Biopartitioning and Purification Conference (BPP) (2017) Copenhagen, Denmark

VI. Online and in situ monitoring of mAb adsorption on Protein A chromatography resins

G. L. Silva, J. Plewka, R. Tscheließnig, H. Lichtenegger, A. C. Dias-Cabral, A. Jungbauer
International Congress in Health Sciences Research: Trends in Biotechnology for Biomedical Applications (2017) Covilhã, Portugal

VII. Thermodynamic overview of mAb adsorption on Protein A

G. L. Silva, A. Rodler, R. Tscheließnig, A. Jungbauer, A. C. Dias-Cabral
International Symposium on the Separation of Proteins, Peptides & Polynucleotides (ISPPP) (2016) Salzburg, Austria

Poster communications

I. Thermal and structural analysis of mAb binding to Protein A in affinity chromatography

G. L. Silva, J. Plewka, R. Tscheließnig, A. Jungbauer, A. C. Dias-Cabral
European Summit of Industrial Biotechnology (ESIB) (2017) Graz, Austria

List of figures

List of tables

List of abbreviations

$A(Q)$	scattering amplitude or angle Q
Bi	Biot number
c	concentration in the pore liquid ($g.L^{-1}$)
C	equilibrium bulk concentration ($g.L^{-1}$)
CBS	consensus binding site
CD	circular dichroism
CIP	cleaning-in-place
C_s	concentration at the particle surface
C_0	initial bulk concentration ($g.L^{-1}$)
DBC	dynamic binding capacity
D_e	effective diffusivity ($cm^2.s^{-1}$)
DNA	Deoxyribonucleic acis
d_p	particle diameter (µm)
D_p	effective diffusivity in the pore ($cm^2.s^{-1}$)
D_s	effective diffusivity in the adsorbed phase ($cm^2.s^{-1}$)
D_0	diffusivity in free solution ($cm^2.s^{-1}$)
EMA	European Medicines Agency
Fab	antigen-binding fragment
Fc	fragment crystallisable region
FDA	Food and Drug Administration
FMC	flow microcalorimetry
HCP	host cell protein
HER2	human epidermal growth factor receptor 2
HPLC	high-performance liquid chromatography
ID	internal diameter (mm)
IgG	immunoglobulin G
ITC	isothermal titration calorimetry
$I(q)$	scattering intensity of angle q
J	mass transfer rate ($g.cm^{-2}.s^{-1}$)

K	thermodynamic equilibrium constant
k_a	on rate constant ($L.g^{-1}.s^{-1}$)
K_A	association constant ($L.g^{-1}$)
k_d	off rate constant (s^{-1})
K_D	dissociation constant ($g.L^{-1}$)
k_f	film mass transfer coefficient ($cm.s^{-1}$)
mAbs	monoclonal antibodies
MALS	multi-angle light scattering
M_w	molecular weight ($g.mol^{-1}$, kDa)
PAT	process analytical technology
PTFE	polytetrafluoroethylene
Q	reaction quotient
Q	scattering vector
q	adsorbed concentration ($g.L^{-1}$)
$\bar{q}$	average concentration in the particle ($g.L^{-1}$)
Q_{ads}	adsorption heat of the molecule to the resin (J)
QbD	quality by design
q_m	maximum adsorbed concentration ($g.L^{-1}$)
R	gas constant ($J.mol^{-1}.K^{-1}$)
Re	Reynolds number
r_p	particle radius (µm)
SAXS	small angle X-ray scattering
Sc	Schmidt number
SEC	size exclusion chromatography
Sh	Sherwood number
SPR	surface plasma resonance
t	time (s)
T	temperature (K)
TAM	thermometric activity monitor
T_H	temperature at $\Delta H^0 = 0$ (K)
T_S	temperature at $\Delta S^0 = 0$ (K)
u	linear velocity ($cm.h^{-1}$)

UV	ultraviolet
v	resin volume (L)
V	bulk liquid volume (L)
v'	reduced linear velocity
δ	stagnant film of thickness
ΔC_p^0	heat capacity ($J.K^{-1}$)
ΔG	Gibbs energy change ($J.mol^{-1}$)
ΔG^0	Gibbs energy change at standard temperature and pressure ($J.mol^{-1}$)
ΔH	enthalpy change ($J.mol^{-1}$)
ΔH_{ads}	adsorption enthalpy of the molecule to the resin ($J.mol^{-1}$)
ΔH^0	enthalpy change at standard temperature and pressure ($J.mol^{-1}$)
ΔS	entropy change ($J.mol^{-1}$)
ΔS^0	entropy change at standard temperature and pressure ($J.mol^{-1}$)
ε	extraparticle porosity
$\overline{\varepsilon}$	agitation power input
ε_p	intraparticle porosity
η	solution viscosity (mPa.s)
λ	ratio between protein radius and pore radius
λ	wave length (nm)
Λ	normalized phase ratio
ρ	solution density ($g.cm^{-3}$)
$\rho(r)$	radial density distribution of distance r
τ_p	tortuosity factor
ϕ	phase ratio (ration between the volume of stationary phase and mobile phase)
ψ_p	diffusional hindrance coefficient

Table of contents

xxx

CHAPTER I - Introduction

1. Downstream processing of monoclonal antibodies

1.1. Monoclonal antibodies

In 1984, the Nobel Prize in Physiology or Medicine was awarded to the immunologists Georges J. F. Köhler and César Milstein for an innovative approach on "the manufacture of predefined specific antibodies by means of permanent tissue culture cell lines" – the hybridoma technique (Köhler & Milstein, 1975).

Antibodies are produced by white blood cells called B-lymphocytes. When the immune system recognizes a substance as foreign (called antigen) the B-lymphocytes are induced to produce antibodies against that specific antigen. In their study, Köhler and Milstein developed a method to fuse in culture antibody-producing B-lymphocytes of a mouse immunized with the targeted antigen with immortal tumor cells from mouse myeloma. The resulting cell line was, and still is, called hybridoma. These cells are therefore immortal (characteristic derived from the tumor cells) and producers of antigen-specific antibodies (derived from the original B-lymphocytes) (Ezzell, 2001; Van Dijk & Van De Winkel, 2001). This was the cornerstone to the manufacturing of monoclonal antibodies (mAbs). Figure I.1 represents the traditional technique to form the hybridoma cell line.

MAbs are produced continuously due to the hybridoma immortal characteristic. However, the greatest challenge in the expression of mAbs from hybridoma is that part of this cell line is of murine origin. This translates in limitations in the therapy, such as reduced serum half-life and a weak immune response, but mostly they can cause a human anti-mouse antibody reaction. In the most extreme cases these allergic reactions can cause kidney failure and, ultimately, death (ElBakri, Nelson, & Abu Odeh, 2010; Ezzell, 2001). The key to overcome this issue is to make the antibody more human though hybridization or humanization techniques. Hybridization techniques involve replacing regions of the murine antibodies (with exception to the Fab regions) with human parts, leading to a chimeric antibody ~66% human and ~33% mouse. Humanization involves selectively replacing the mouse parts with human parts (including the Fab regions) using genetic engineering, leading to an antibody ~90% human. In 2001, Karpas et al. were able to generate a fully human monoclonal antibody "from human myeloma line suitable for hybridoma" (Karpas, Dremucheva, & Czepulkowski, 2001). Since then, the approved human mAbs have already outnumbered the other three mAb types. Figure I.2 shows a representation of the human and mouse parts present in the four types of mAbs (Ezzell, 2001).

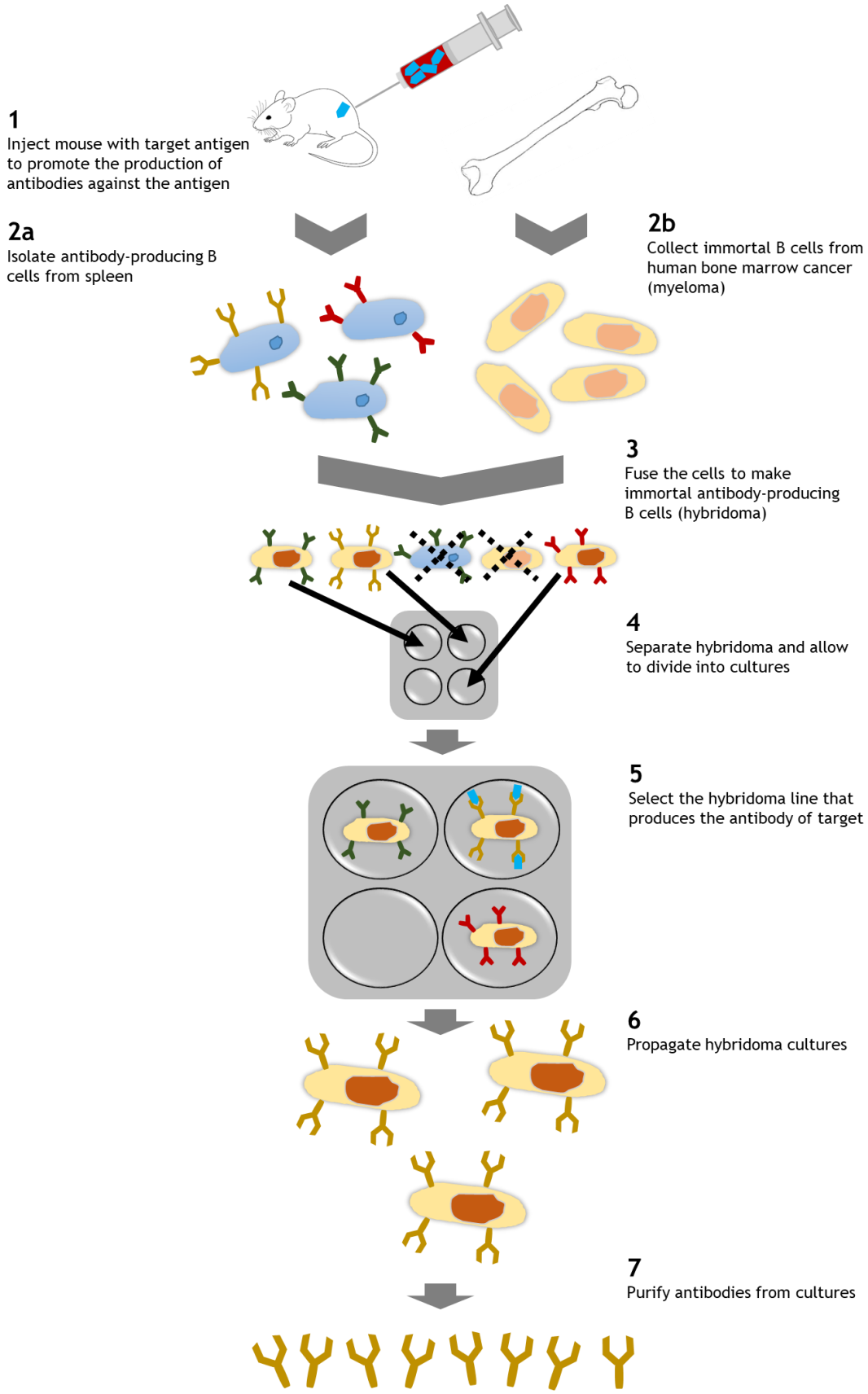

Figure I.1 - Schematic representation of mouse hybridization in the manufacturing of monoclonal antibodies (adapted from Ezzell, 2001).

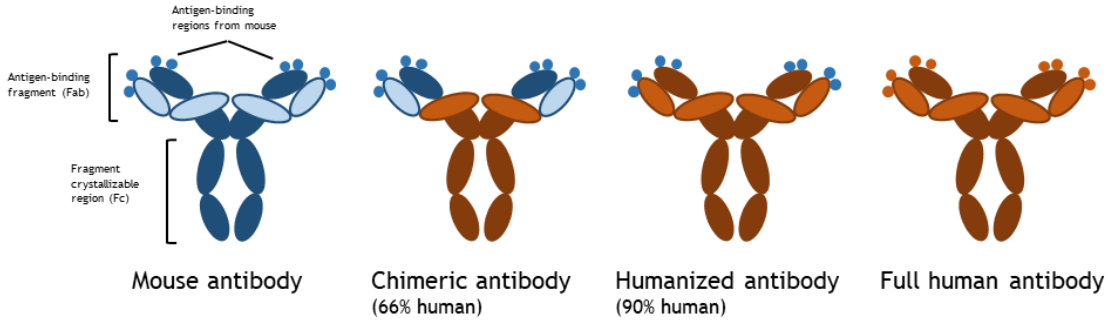

Figure I.2 – Representation of the types of mAbs according to its origin (adapted from Ezzell, 2001).

The first commercialized therapeutic mAb product was Orthoclone OKT3 back in 1986. This mAb was used in the prevention of kidney transplant rejection (Ecker, Jones, & Levine, 2015). Since 1986, the monoclonal antibody market has dramatically increased. However, the predictions were not entirely accurate. In 2001 analysts predicted that 100 mAbs would be on the market by the year 2010 (Ezzell, 2001). However, in 2008, despite nearly 150 human mAbs were entering clinical studies, only 20 had been approved and were on the market (and not only human). As of 2017 there are 50 products that have been approved by both the U.S. Food and Drug Administration (FDA) and the European Medicines Agency (EMA). Table I.1 summarizes the approved mAbs by both agencies along with their therapeutic indications, manufacturing company, expression cell line, and type of mAb (Ecker et al., 2015; Elvin, Couston, & van der Walle, 2013).

In recent years, mAbs cover already a wide range of therapeutic areas, being oncology, autoimmune and inflamm atory diseases the most predominant (Elvin et al., 2013). The antibody market has been rapidly growing. In 2010, the mAb market returned a global sales revenue of 43 billion U.S. dollars (Elvin et al., 2013). In 2013 it reached $75 billion. Also, from the top ten biopharmaceuticals with the most revenue worldwide in 2016, four are mAbs (Morrison & Lähteenmäki, 2017): Humira® (Abbvie) (#1), Rituxan® (Roche/Genentech) (#3), Avastin® (Roche/Genentech) (#5) and Herceptin® (Roche/Genentech) (#6).

Table I.1 - Table of approved mAbs as of 2017 (adapted from (Ecker et al., 2015) and from the Animal Cell Technology Industrial Platform, viewed 19 December 2018, <http://www.actip.org/products/monoclonal-antibodies-approved-by-the-ema-and-fda-for-therapeutic-use/>).

Trade name	International Non-proprietary Name	Company	Target	Type	EMA approval	FDA approval	Cell line	Therapeutic indication(s)
ABthrax®	Raxibacumab	Human Genome Sciences	Bacillus anthracis protective antigen	Human IgG1	Not approved	2012	NS0	Prevention and treatment of inhalation anthrax
Adcetris®	Brentuximab	Seattle Genetics	CD30	Chemeric IgG1	2012	2011	CHO	Hodgkin lymphoma, systemic anaplastic large cell lymphoma
Amjevita®	Adalimumab	Amgen Europe	TNFα	Human IgG1	2017	2016	CHO	Arthritis; rheumatoid arthritis; ulcerative Crohn's disease; psoriasis;
Arzerra®	Ofatumumab	Genmab and GSK	CD20	Human IgG1	2010	2009	NS0	Chronic lymphocytic leukemia
Avastin®	Bevacizumab	Genentech (Roche)	VEGF	Humanized IgG1	2005	2004	CHO	Metastatic colorectal cancer; lung cancer; metastatic breast cancer
Benlysta®	Belimumab	HSG, GSK	BLyS	Human IgG1	2011	2011	NS0	Systemic lupus erythematosus
Bexxar®	Tositumomab	Corixa and GSK	CD20	Murine IgG2a	Not approved	2003	Hybridoma	Non-Hodgkin's lymphoma
Blincyto®	Bevacizumab	Amgen Europe	CD19	BiTEs	2015	2014	CHO	Precursor cell lymphoblastic leukemia-lymphoma
Campath®	Alemtuzumab	Millennium Pharmaceuticals and Genzyme	CD52	Humanized IgG1	2001	2001	CHO	B-cell chronic lymphocytic leukemia

Cimzia®	Certolizumab pegol	UCB	TNFa	Humanized IgG Fab fragment	2009	2008	E. coli	Chron's disease; rheumatoid arthritis
Cinqair™	Reslizumab	Teva Pharmaceuticals Limited	IL-5	Human IgG4/κ	2016	2016	NSO	Asthma
Cosentyx™	Secukinumab	Novartis Europharm	interleukin-17A	Human IgG1/κ	2015	2015	CHO	Arthritis; psoriatic psoriasis; spondylitis; ankylosing
Cyramza	Ramucirumab	Eli Lilly	VEGF	Human IgG1	2014	2014	NS0	Stomach neoplasms
Darzalex®	Daratumumab	Janssen-Cilag	CD38	Human IgG1/κ	2016	2015	CHO	Multiple myeloma
Empliciti	Elotuzumab	Bristol-Myers Squibb	SLAMF7	Human IgG1	2016	2015	NS0	Multiple myeloma
Entyvio®	Vedolizumab	Takeda Pharma	Integrin-α4ß7	HumanizedIgG1	2014	2014	CHO	Colitis; ulcerative Crohn's disease
Erbitux®	Cetuximab	ImClone, Merck Serono and BMS	EGFR	Chimeric IgG1	2004	2004	Sp2/0	Head and neck cancer; colorectal cancer
Gazyvaro®	Obinutuzumab	Roche	CD20	Humanized IgG1	Not approved	2013	CHO	Chronic lymphocytic leukemia
Herceptin®	Trastuzumab	Genentech (Roche)	HER-2	Humanized IgG1	2000	1998	CHO	Breast cancer; metastatic gastric or gastroesophageal junction adenocarcinoma
Humira®	Adalimumab	Abbott	TNFα	Human IgG1	2003	2002	CHO	Rheumatoid arthritis; ankylosing spondylitis; Crohn's disease
Ilaris®	Canakinumab	Novartis	IL-1ß	Human IgG1	2009	2009	Sp2/0	Tumor necrosis factor receptor associated periodic syndrome; familial mediterranean fever

Inflectra	Infliximab	Hospira UK Limited	TNFα	Chimeric human-murine IgG1	2013	2016	Sp2/0-Ag14	Spondylitis; arthritis; rheumatoid colitis; ulcerative arthritis; psoriasis
Kadcyla®	Trastuzumab emtansine	Roche	HER2	Humanized IgG1 as ADC	2013	2013	CHO	Breast cancer
Keytruda®	Pembrolizumab	Merck Sharp & Dohme Limited	PD-1	Human IgG4	2015	2014	CHO	Melanoma
Lartruvo	Olaratumab	Eli Lilly	PDGFR-α	Human IgG1	2016	2016	CHO	Sarcoma
Lemtrada®	Alemtuzumab	Sanofi	CD52	Humanized IgG1	2013	2014	CHO	Multiple sclerosis
Lucentis®	Ranibizumab	Genentech (Roche)	VEGF-A	Humanized IgG1 Fab fragment	2007	2006	E. coli	Neovascular age-related macular degeneration
Nucala	Mepolizumab	GlaxoSmithKline	IL-5	Human IgG1/κ	2015	2015	CHO	Asthma
Opdivo	Nivolumab	Bristol-Myers Squibb Pharma	PD-1	Human IgG4	2015	2015	CHO	Carcinoma; lung carcinoma; renal cell Hodgkin disease melanoma
Orthoclone OKT3®	Muromonab-CD3	Centocor Ortho Biotech (Johnson & Johnson)	CD3	Murine IgG2a	1986	1986	Hybridoma	Transplantation rejection
Perjeta®	Pertuzumab	Roche	HER2	Humanized IgG1	2013	2012	CHO	Breast cancer
Portrazza	Necitumumab	Eli Lilly	EGFR	Human IgG1	2016	2015	NS0	Carcinoma, non-small-cell lung
Praluent	Alirocumab	sanofi-aventis groupe	PCSK9	Human IgG1	2015	2015	CHO	Dyslipidemias
Praxbind®	Idarucizumab	Boehringer Ingelheim International GmbH	dabigatran etexilate	Human FaB	2015	2015	CHO	Hemorrhage

Prolia®	Denosumab	Amgen	RANKL	Human IgG2	2010	2010	CHO	Osteoporosis
Proxinium®	Catumaxomab	Viventia (Eleven Biotherapeutics)	EpCAM	Humanized MAb	2005	2005	CHO	Head and neck cancer
Remicade®	Infliximab	Centocor Ortho Biotech (Johnson & Johnson)	TNFα	Chimeric IgG1	1999	1998	Sp2/0	Crohn's disease; ulcerative colitis; rheumatoid arthritis; psoriatic arthrits
Removab®	Catumaxomab	Fresenius	EpCAM and CD3	Trifunctional MAb IgG2a / IgG2b	2009	Not approved	Mouse hybridoma	Malignant ascites in patients with positive carcinomas
Remsima®	Infliximab	Celltrion Healthcare	TNF-alpha	Chimeric IgG1 Ab	2013	Not approved	CSC-Ps0006	Spondylitis; ankylosing arthritis; rheumatoid colitis; psoriatic psoriasis
ReoPro®	Abciximab	Centocor Ortho Biotech (Johnson & Johnson), Elli Lily	GPIIb/IIIa	Chimeric IgG1 Fab	1995	1994	Sp2/0	High risk angioplasty
Repatha®	Evolocumab	Amgen	LDL-C / PCSK9	Human IgG2	2015	2015	CHO	Dyslipidemias; hypercholesterolemia
Rituxan® MabThera®	Rituximab	Biogen Idec, Genentech (Roche)	CD20	Chimeric IgG1	1998	1997	CHO	Non-Hodgkin's lymphoma; lymphocytic leukemia; rheumatoid arthritis
RoActemra®	Tocilizumab	Chugai (Roche)	IL-6 receptor	Humanized IgG1	2009	2010	CHO	Rheumatoid arthritis
Simponi®	Golimumab	Centocor Ortho Biotech (Johnson & Johnson)	TNFa	Human IgG1	2009	2009	Sp2/0	Rheumatoid arthritis; psoriatic arthritis; ankylosing spondylitis
Simulect®	Basiliximab	Novartis	CD25	Chimeric IgG1	1998	1998	NS0	Reversal of transplantation rejection

Soliris®	Eculizumab	Alexion Pharmaceuticala	Complement C5	Humanized IgG2/4	2007	2007	NS0	Paroxysmal nocturnal hemoglobinuria
Stelara®	Ustekinumab	Centocor Ortho Biotech (Johnson & Johnson)	IL-12 / IL-23	Human IgG1	2009	2009	Sp2/0	Plaque psoriasis
Sylvant®	Siltuximab	Janssen-Cilag International	cCLB8	Chimeric IgG1κ	2014	2014	CHO	Giant lymph node hyperplasia
Synagis®	Palivizumab	MedImmune, Abbott	F-protein of RS virus	Humanized IgG1	1999	1998	NS0	Respiratory syncytial virus
Tysabri®	Natalizumab	Biogen Idec and Elan	VLA-4	Humanized IgG4	2006	2004	Murine myeloma	Multiple sclerosis; Crohn's disease
Vectibix®	Panitumumab	Amgen	EGFR	Human IgG2	2007	2006	CHO	Metastatic colorectal carcinoma
Vervoy®	Ipilimumab	BMS	CTLA-4	Human IgG1	2011	2011	CHO	Melanoma
Xolair®	Omalizumab	Genentech (Roche) and Novartis	IgE	Humanized IgG1	2005	2003	CHO	Asthma
Zevalin®	Ibritumomab tiuxetan	Biogen Idec	CD20	Murine IgG1	2004	2002	CHO	Non-Hodgkin's lymphoma
Zinplava™	Bezlotoxumab	Merck Sharp & Dohme Limited	C. Difficile; toxin B	Human monoclonal antitoxin antibody	2017	2016	CHO	Enterocolitis; pseudomembranous

1.1.1. Trastuzumab

Trastuzumab (Genentech, South San Francisco, CA, USA) was the monoclonal antibody used in the present study. It is a DNA-derived recombinant immunoglobulin G1 (IgG1) of the subclass kappa that binds to the HER2 receptors overexpressed in the breast cancer cells (Goldenberg, 1999). HER2 (also known as Neu, ERBB2) is a proto-oncogene that encodes a transmembrane glycoprotein receptor tyrosine kinase similar to the human epidermal growth factor receptor 2, HER2 (or Erb-B2 receptor tyrosine kinase 2). HER2 is located on the cell surface, interacting with growth factors. An overexpression is correlated with the presence of primary human breast carcinomas (Cho et al., 2003; Goldenberg, 1999) and its amplification serves better as prognostic to lymph-node positives than other factors like hormonal-receptor status (Slamon et al., 1987).

The construction of trastuzumab (Goldenberg, 1999) is based on the humanized antibody humAb4D5 (Carter et al., 1992), which predecessor was the murine mAb mumAb4D5 which directs against the extracellular domain of the human epidermal growth factor receptor 2 (p185HER2), inhibiting the proliferation of tumor cells overexpressing this protein (Carter et al., 1992).

Trastuzumab has been approved in 1998 by the FDA and in 2000 by the EMA, and it is used in treatments for breast cancer, being the 4th largest-selling mAb and the 6th in the biopharmaceutical global market generating a revenue of $6,900 million worldwide (Morrison & Lähteenmäki, 2017) (Table I.2).

Table I.2 – Table of the top 10 biopharmaceuticals by revenue (adapted from (Morrison & Lähteenmäki, 2017)).

Name	Lead company	Molecule type	2016 worldwide sales ($ millions)
Humira	AbbVie	mAb	16,078
Harvoni	Gilead Sciences	Small molecule	9,081
Rituxan (rituximab)	Roche	mAb	7,454
Revlimid	Celgene	Small molecule	6,974
Avastin	Roche	mAb	6,901
Herceptin	Roche	mAb	6,900
Enbrel	Amgen	Protein	6,817
Prevnar 13	Pfizer	Vaccine	5,718
Lantus (insular glargine injection)	Sanofi	Peptide	5,287
Neuplasta (pegfilgrastim)	Amgen	Peptide	4,658

1.2. Protein A chromatography

Protein A chromatography has been optimized over the years and is now the best established technique for antibody capture directly from cell culture supernatant at a pH close to physiological conditions (Bolton, Street, & Mehta, 2016). At these conditions, the antibodies bind reversibly to the Protein A ligands (Shukla, Hubbard, Tressel, Guhan, & Low, 2007). In a single step a high degree of purity and recovery can be achieved (Fahrner et al., 2001; Shukla et al., 2007). In a review paper, Pete Gagnon names three features that contribute to Protein A resins dominance in antibody purification market: induced fit; multi-point attachment and ligand flexibility; and a long track of years of vendor competition to maximize capacity (Gagnon, 2012).

Despite all the advantages of Protein A chromatography, it has also some limitations, starting with the cost of the resin, which is the most expensive material in the purification of mAbs (Z. Liu, Mostafa, & Shukla, 2014). This leads to the search for strategies for column reutilization. Another limitation is the fact that elution needs to be carried at low pH, which also works as a viral inactivation step, but generates aggregates (Kelley, 2009; H. F. Liu, Ma, Winter, & Bayer, 2010; Shukla et al., 2007). Some impurities are removed to some extent from the cell supernatant during the capture, intermediate, and polishing steps, namely host cell protein (HCP), DNA, viruses, endotoxins, and aggregates (H. F. Liu et al., 2010). Others are introduced during the purification process itself and should also be taken into account, such as: leached Protein A, antibody aggregates, buffers, and detergents (H. F. Liu et al., 2010). However, subsequent intermediate and polishing steps will tackle the remainder impurities (Shukla et al., 2007).

Sanitization is a very important step of antibody-Protein A capture step. The cleaning-in-place (CIP) step consists in the use of harsh cleaning agents or detergents for the removal of tightly bound or precipitated contaminants. The use of such agents, like sodium hydroxide (NaOH), can ultimately lead to loss in the binding capacity (Hober, Nord, & Linhult, 2007; M. S. Lin et al., 2007; Linhult et al., 2004; Yang, Biswas, & Chen, 2003) and lifetime (Hahn et al., 2005a; Hale, Drumm, Harrison, & Phillips, 1994; Jiang, Liu, Rubacha, & Shukla, 2009). NaOH at 0.1 up to 0.5 M are the most used column sanitization conditions, being also effective in the inactivation of bacteria, viruses, and endotoxins (Hober et al., 2007).

In the development of a Protein A capture step, one has to take certain factors into consideration such as column dimensions, flow rate, resin cost, and processing time (H. F. Liu et al., 2010). Commercial resins change in their backbone, bead and pore size, and source of Protein A and chain length. The choice of a Protein A resin and its characteristics depends on the application. In early clinical development high dynamic binding capacity has to be considered, and in commercial operations the choice would lie more on a resin with decreased processing time (due to economic reasons) (Ghose, Nagrath, Hubbard, Brooks, & Cramer, 2004; Z. Liu et al., 2014). Considering the costs of Protein A resins, the production rate is an important parameter to take into consideration. High dynamic binding capacities help minimizing the resin volumes needed and the ability to withstand high flow rate helps reducing the cycle times.

1.2.1. Recombinant Protein A resins

Native Protein A is found in the cell wall of *Staphylococcus aureus*. It has 42 kDa and contains five homologous IgG-binding domains; from the N-terminal: E, D, A, B, and C. All these domains have high selectivity and strong affinity to every IgG isotype, with exception to IgG3.

Protein A chromatography is acknowledged as the most costly step in downstream processing, mostly because the resins are not used to their full lifetime extent (Z. Liu et al., 2014). Early generations of Protein A resins contained as a ligand native forms of Staphylococcal Protein A (Pabst, Thai, & Hunter, 2018). In the current resins, manufacturers have made some improvements namely in the binding capacity and alkaline stability.

Through certain point mutations in the Protein A domains alkaline stability was drastically improved, resins now are able to withstand higher sodium hydroxide concentrations for short periods of time for more than 150 CIP cycles without capacity loss (Z. Liu et al., 2014; Pabst et al., 2018).

Increased dy namic binding capacity was achieved by improving static binding capacity by ligand modification with the implementation of repetitive units of Protein A antibody-binding domains (Müller & Vajda, 2016; Roman & Berensmeier, 2014) and with increase in ligand density (McCue, Kemp, Low, & Quiñones-García, 2003). Dynamic binding capacity (DBC) was also increased by reducing mass transfer resistance (Hahn et al., 2005; Hahn, Schlegel, & Jungbauer, 2003; Z. Liu et al., 2014; Perez-Almodovar & Carta, 2009).

Two of the commercially available Protein A resins most used for antibody capture directly from feedstocks are MabSelect SuRe (GE Healthcare) and TOYOPEARL AF-rProtein A HC (Tosoh). In the manufacturing of MabSelect SuRe, the native Protein A B domain was synthetically modified generating the so called Z domain. Each ligand comprises four repetitive units of the Z domain. TOYOPEARL AF-rProtein A HC contains a ligand of six repetitive units of the synthetically engineered Y domain, derived from the native C domain.

1.2.2. IgG-Protein A complex

As mentioned, mAbs are in their great majority full human or humanized IgGs. IgGs are a group of large globular proteins constituted by three subunits: two identical antigen-binding fragments (Fab) and one easily crystallizable fragment (Fc) (Salvalaglio, Zamolo, Busini, Moscatelli, & Cavallotti, 2009; Sandin, Öfverstedt, Wikström, Wrange, & Skoglund, 2004; Saphire et al., 2003). The Fc is connected to the Fab domains by a hinge region that consists of two disulphide bridges between cysteine residues, granting the antibody flexibility depending on the length of the hinge. The light and heavy chains are also connected by a disulphide bridge. This region is primarily where the different IgG subclasses differ (Rayner et al., 2015). The hinge length is connected to the IgG functionality and naturally with their flexibility. Of the four subclasses of IgG, IgG1 is the most abundant in the serum. This subclass corresponds to ~68% of the mAbs in the market, namely because it binds to every class of Fcγ receptor and because of the high specificity and affinity of the antigen to their Fab (Rayner et al., 2015). A representation of an IgG1 can be seen in Figure I.3 (1HZH.pdb).

The antibody binding to Protein A occurs through a hydrophobic region between CH2 and CH3 domains of the Fc known as “consensus binding site” (CBS) through van der Waals and electrostatic interactions in the CH2 domain, and through electrostatic interactions in the CH3 domain (Deisenhofer, 1981; DeLano, Ultsch, de Vos, & Wells, 2000; Gagnon, Nian, Leong, & Hoi, 2015; Salvalaglio et al., 2009; Shukla et al., 2007). Figure I.4 shows a representation of the antibody-binding B-domain of Protein A bound to the Fc region through the hinge between CH2 and CH3 (the crystallographic structure was developed by Deisenhofer, 1FC2.pdb)

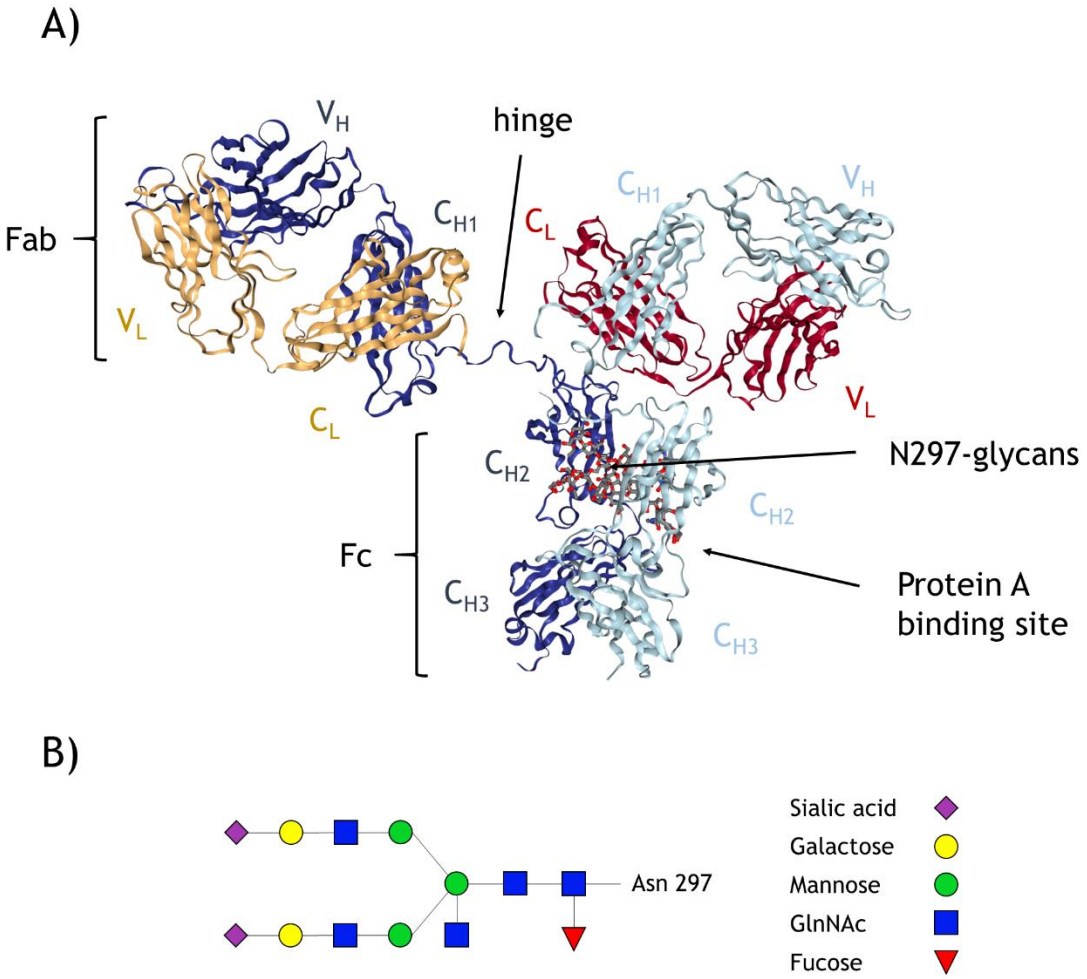

Figure I.3 – A) Crystallographic structure of an IgG1 (1HZH.pdb) showing the fragment crystallizable region (Fc) and the antigen-binding fragment (Fab). The antibody is subdivided into two heavy chains and two light chains, represented with the lower index H and L respectively. The constant and variable regions are also indicated with C and V respectively. Linked to the N-terminus of each of the heavy chains in aspargine 297 are a series of carbohydrates, which have a core common to all human IgG; B) Core of glycans bound to Asn 297 of the heavy chains.

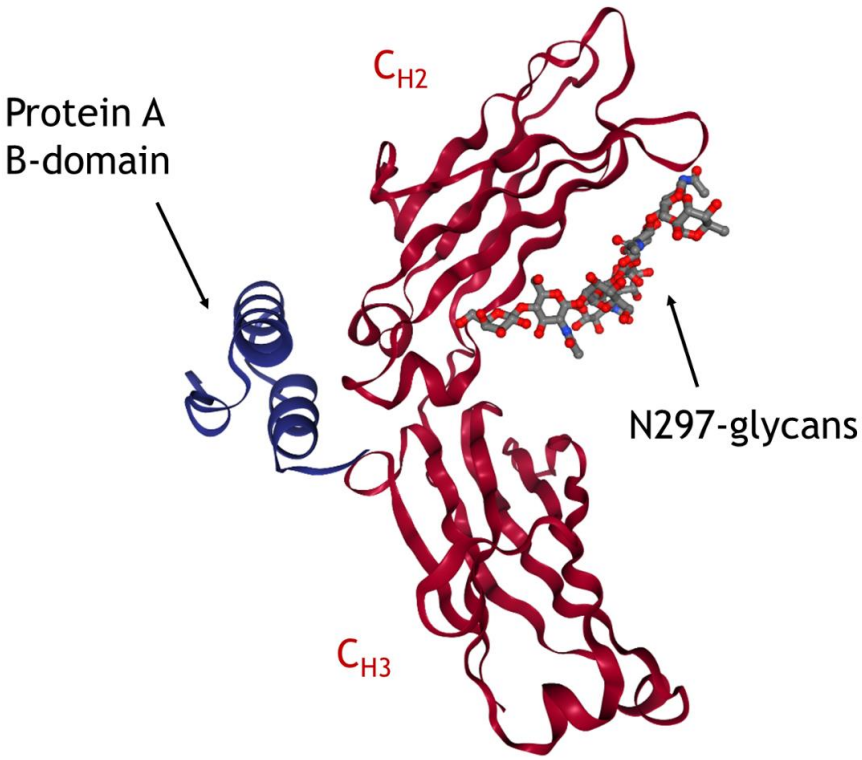

Figure I.4 – Crystallographic representation of the Protein A antibody-binding B-domain to the Fc region in the hinge between CH2 and CH3 (1FC2.pdb).

2. Understanding protein adsorption

The importance of mAbs to the therapeutic market has been increasingly growing (Marichal-Gallardo & Álvarez, 2012; Morrison & Lähteenmäki, 2017) with associated need for the production of high product volumes. Besides, downstream scientists and engineers face a plethora of other technical, economic, and product safety challenges imposed by regulatory agencies. The internationally accepted regulatory approaches for the manufacturing of pharmaceuticals require a control through Quality by Design (QbD) and Process Analytical Technology initiatives (PAT) (Mhatre & Rathore, 2009). These initiatives request a deep understanding of the biomolecule critical quality attributes affecting its safety and efficacy profile as well as a comprehension of the process design space, where the final product meets the necessary criteria for efficiency and safety. These requirements have rendered univariate optimization and trial-and-error-based chromatographic process development largely obsolete (Hanke & Ottens, 2014), calling for the use of mechanistic approaches, derived from fundamental principles and reflecting a higher level of understanding.

Studying preparative chromatography involves a detailed investigation of the physical chemistry fundamentals, considering the equilibrium and the kinetic effects. Most mechanistic approaches describing chromatographic separations consist of two parts: equations describing the fluid flow and mass transfer in the column, and a model to describe the interactions between the sample and the support in the form of adsorption isotherms. Furthermore, for the establishment of consistent models, the biomolecule–resin mechanism of interaction should be understood.

In particle chromatography, protein adsorption to stationary phases is a complex phenomenon that comprises multiple steps and depends on various factors. Giorgio Carta and Alois Jungbauer describe extensively in their book “Protein Chromatography” (Carta & Jungbauer, 2010), in the chapter of Adsorption Equilibria, factors present during protein adsorption that affect prediction theoretical models, namely: 1) heterogeneous distribution of the charged and the hydrophobic groups in the proteins (proteins cannot be considered spherical particles with homogeneous binding character); 2) protein unfolding upon adsorption (the adsorbed molecules become structurally different from molecules in the equilibrium); 3) protein self-association and repulsive interactions; 4) exclusion effects due to resin pore size distribution; 5) diffusional resistance due to limitations associated to the binding kinetics.

In light of these set of factors, it is understandable why predicting protein adsorption in equilibrium is cumbersome and empirical models become useful. The use of hybrid procedures combining modeling with an experimental approach can help predicting key parameters associated with preparative chromatography.

2.1. Isotherms

Resin process performance is determined, as previously mentioned, by equilibrium and kinetics factors. Equilibrium factors, like selectivity and binding capacity, are controlled by the nature, selectivity, and concentration of the binding ligands, by the accessible surface area, and by the nature of the resin backbone. The relationship between a molecule adsorbed to a stationary phase and its concentration in equilibrium with the mobile phase at constant temperature is given by the adsorption isotherm.

The Langmuir isotherm is the most used model to describe antibody adsorption to Protein A resins, even though Protein A resins are of heterogeneous binding nature (Carta & Jungbauer, 2010; Perez-Almodovar & Carta, 2009). In a single component system (and using as example the affinity chromatography system between antibody and Protein A), there is a stoichiometric association of an antibody, A, with the Protein A ligands, B. The formation of the complex AB can be described in equilibrium as follows:

$$A + B \underset{k_d}{\overset{k_a}{\rightleftarrows}} AB \tag{1}$$

where k_a and k_d would respectively represent the on and off rate constants for the binding (association) and desorption (dissociation) rate of antibody to Protein A. The complex formation rate can be described by:

$$\frac{\partial [AB]}{\partial t} = k_a[A][B] - k_d[AB] \tag{2}$$

where t is the time; and the square brackets represent the concentrations of the involved species. The representation of the complex formation rate by the Langmuir kinetic model is given by:

$$\frac{\partial q}{\partial t} = k_a(q_m - q)C - k_d q \tag{3}$$

where q is the amount of adsorbed antibody to the ligands, $i.e.$, the representation of the complex AB, with $[AB] = q$; C is the antibody concentration in equilibrium with the mobile phase, $i.e.$, $[A] = C$; and q_m is the maximum binding capacity of the resin for the antibody, so that the number of free ligands B is given by $[B] = q_m - q$.

In equilibrium, where $\frac{\partial q}{\partial t} = 0$ holds true, Eq. (3) can be rewritten as:

$$q = \frac{q_m C}{\frac{k_d}{k_a} + C} \tag{4}$$

Substituting k_d/k_a with K_D, the equilibrium dissociation constant that is obtained by the ratio between the off and on rate constants, it gives the equation of the Langmuir isotherm:

$$q = \frac{q_m C}{K_D + C} \quad (5)$$

The dissociation constant K_D is given in mg/mL (or mol/L) is the equilibrium concentration at which the surface concentration, q, is half of the maximum binding capacity, q_m. It is the inverse of the affinity constant K_A, which represents the affinity of the resin for the molecule and is expressed in mL/mg (or M^{-1}). The affinity constant of Protein A resins for the Fc part of human IgG1, IgG2, and IgG4 is in the range of 700 g/L or 10^8 M^{-1} (Hober et al., 2007; Jendeberg et al., 1997). With $K_D = \frac{1}{K_A}$, the Langmuir isotherm can be rewritten as:

$$q = \frac{q_m K_A C}{1 + K_A C} \quad (6)$$

Figure I.5 shows representations of typical Langmuir isotherms. It can be seen how different values for the parameters K_D and q_m affect the isotherm behaviour.

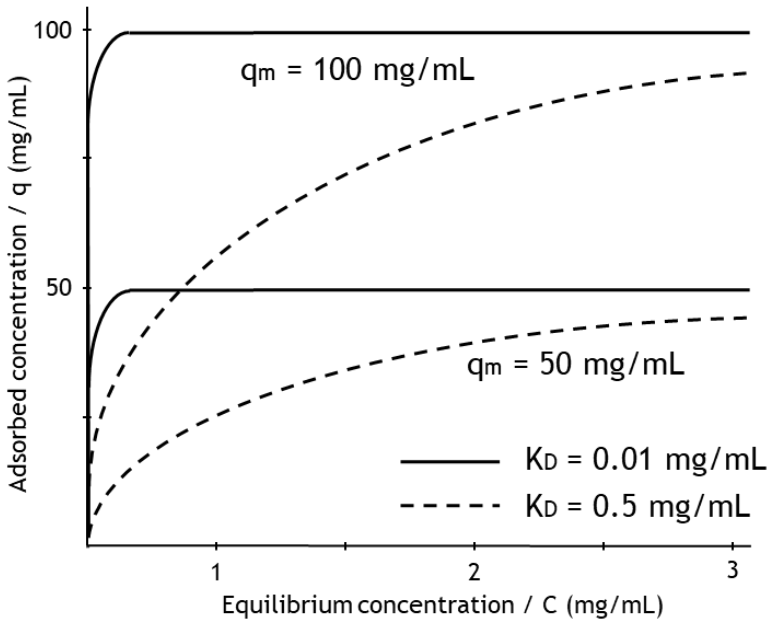

Figure I.5 - Representation of adsorption isotherms and the contribution of its parameters to the adsorption behavior.

As the equilibrium concentration tends to zero $(C \to 0)$, the isotherm approaches its linear region, with:

$$q = q_m K_A C \quad (7)$$

As the equilibrium concentration tends to infinity $(C \to \infty)$, the isotherm approaches the maximum capacity, with:

$$q = q_m \tag{8}$$

The isotherm parameters can be determined by fitting the experimental data of adsorbed concentration at each liquid phase concentration with linearized forms ${}^{q}/_{C}\ vs\ q$ (Scatchard plot, Eq. (9)) or ${}^{C}/_{q}\ vs\ C$ (Eq. (11)) of the Langmuir isotherm:

$$\frac{q}{C} = \frac{q_m}{K_D} - \frac{q}{K_D} \tag{11}$$

$$\frac{C}{q} = \frac{C}{q_m} + \frac{K_D}{q_m} \tag{12}$$

Other isotherm that can be applied to model antibody adsorption to Protein A is the bi-Langmuir isotherm. This model considers energetic heterogeneity of the binding sites and the possibility of interactions between adsorbed species. The general equation for this isotherm is the following:

$$q = \sum_{i=1}^{2} q_{m,i} K_{A,i} C / (1 + K_{A,i} C) \tag{13}$$

2.2. Mass transfer

Mass transfer effects, which are also determinant to resin process performance, control the rate or kinetics factors in adsorption process. These factors are controlled by the particle size, by the pore size, and the porosity or pore network connectivity (Carta, Ubiera, & Pabst, 2005).

Figure. I.6 shows the relationship between the reduced height equivalent to a theoretical plate and the reduced linear velocity v'. The reduced velocity is given by: $v' = v\, d_p / D_0$, where v is the linear velocity, d_p is the particle diameter, and D_0 is the diffusivity in free solution.

In industrial applications, for the processing of biopharmaceuticals, stationary phases usually consist of particles in the size range of 20-100 μm, the diffusivity in free solution is in the order of magnitude of 10^{-7} cm^2/s, and the employed linear velocity is in the range of 100-500 cm/h. Therefore, reduced velocity values would be in a range greater than $v' = 100$, where chromatography is almost only controlled by mass transfer (Carta et al., 2005).

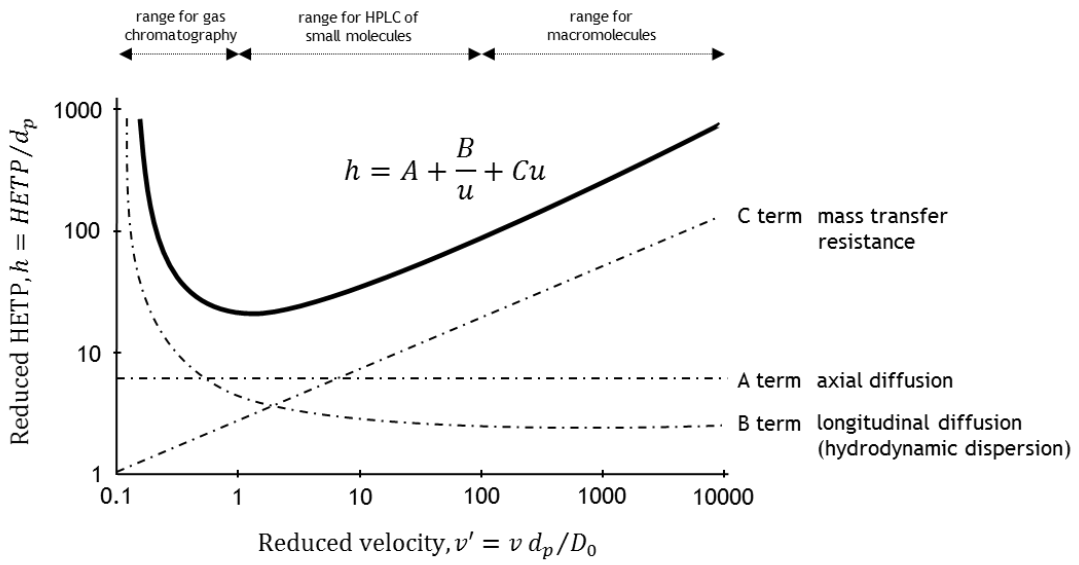

Figure I.6 - Generalized van Deemter equation and plot and the controlling mechanisms in each range.

Mass transfer is an important driving parameter in Protein A chromatography. The rate at which a molecule adsorbs to porous stationary phase packed bed highly depends on the resistances faced along the way. Two types of resistances control overall mass transfer: external transport and intraparticle transport. The external transport in the fluid is associated with the film resistance and dependent on convection, which is controlled by the mobile phase velocity. The intraparticle transport occurs through diffusion which can occur either in the particle pores (pore diffusion – and the driving force being the molecule concentration gradient in the pores liquid) or in the adsorbed phase (solid diffusion - and the driving force being the molecule concentration gradient in the adsorbed phase). In addition, mass transfer through all these transport mechanisms is dependent on the kinetic resistance to binding in the resin surface (Carta et al., 2005).

2.2.1. External transport

The liquid transport over the length of one particle is fast in industrial applications. With typical operating conditions like linear velocity at 150 cm/h in a column packed with beads of the 100 µm range and an extraparticle porosity, ε, of 0.4 (ε ranges from 0.3 to 0.4 in randomly packed beds of spherical particles, being independent of the particle size), the time that fluid takes to convectively go around such particle is approximately 0.1 s, with $t = \frac{\varepsilon d_p}{v}$. Since this process is much faster than protein adsorption, one can consider the protein concentration in the liquid surrounding the particle at each moment as uniform (Carta & Jungbauer, 2010). In this case, the mass transfer rate, J, at the particle surface is driven by the difference between the concentration in the liquid and the concentration adsorbed at the particle surface:

$$J = k_f(C - C_s) \tag{14}$$

where C_s is the concentration at the particle surface, and k_f is the film mass transfer coefficient given by the ratio of the diffusivity in free solution D_0 and the steady state diffusion over a thin stagnant film of thickness δ: $k_f = \frac{D_0}{\delta}$. The diffusivity in free solution for antibodies was estimated from Tyn and Gusek with a value of $D_0 = 3.7 \times 10^{-7}\ cm^2/s$ (Tyn & Gusek, 1990).

In process applications, protein chromatography is driven by laminar flow and the mass transfer coefficient in packed beds can be correlated with engineering parameters such as the Sherwood, Schmidt, and Reynolds numbers, as approached by Wilson and Geankoplis (Wilson & Geankoplis, 1966):

$$Sh = \frac{1.09}{\varepsilon} Re^{0.33} Sc^{0.33} \tag{15}$$

where the Sherwood, Schmidt, and Reynods number are respectively $Sh = \frac{k_f d_p}{D_0} = \frac{d_p}{\delta}$, $Sc = \frac{\eta}{\rho D_0}$, and $Re = \frac{\rho u d_p}{\eta}$, where η is the viscosity, ρ is the solution density, and u is the linear velocity. The Sherwood number is the correlation between convective mass transfer and diffusive mass transfer, or simply the ratio of the particle diameter between the film thickness. The Schmidt number is also a dimensionless parameter that is determined by physical properties. It represents the correlation between the kinematic viscosity (ratio between viscosity and density) of the fluid and mass diffusivity in free solution. The Reynolds number is determined by the flow conditions. With Reynolds number one can determine the proportion of convective flow to turbulent flow over the length of a particle considering a certain linear velocity.

However, for molecules of the colloidal size like therapeutic proteins where external mass transfer is not a driving factor and for the particle sizes employed in industrial chromatography, the external mass transfer coefficient in agitated vessels can be defined as:

$$Sh = 2 + 0.52 \left[\frac{\rho\left(\overline{\varepsilon} d_p^4\right)^{0.33}}{\eta}\right]^{0.52} Sc^{0.33} \tag{16}$$

where $\overline{\varepsilon}$ is the agitation power input per mass of liquid.

2.2.2. Intraparticle transport

As mentioned, intraparticle transport can occur inside the pores or at the surface of the adsorbent, named as pore diffusion and solid diffusion respectively. When pore and solid diffusion are assumed, the mass transfer equation for spherical particles is the following (Carta et al., 2005):

$$\frac{\partial q}{\partial t} = \frac{1}{r^2}\frac{\partial}{\partial r}\left[r^2\left(\varepsilon_p D_p \frac{\partial c}{\partial r} + D_s \frac{\partial q}{\partial t}\right)\right] \tag{17}$$

$$t = 0,\ c = 0,\ q = 0$$

$$r = 0, \frac{\partial C}{\partial r} = 0$$

$$r = r_p, \varepsilon_p D_p \frac{\partial C}{\partial r} + D_s \frac{\partial q}{\partial r} = k_f (C - c) \quad (18)$$

where $\varepsilon_p D_p$ and D_s are the diffusivities in the pore and in the adsorbed phase respectively, r_p is the particle radius, C is the protein concentration in the bulk, and c is the protein concentration in the pore liquid. When $D_s = 0$, the mass transfer is driven uniquely by pore diffusion. When $\varepsilon_p D_p = 0$, it is a solid diffusion controlled process. The diffusivities in the pore and in the adsorbed phase are related with the overall effective pore diffusivity as:

$$D_e = \varepsilon_p D_p + D_s \frac{\partial q}{\partial c} \quad (19)$$

where $\partial q / \partial c$ is the slope of the isotherm in the linear zone.

Pore diffusion reports the transport of the molecules in pores large enough not to have interaction with the solute molecules. The mass transfer rate, J, in the pore liquid is defined in terms of the effective pore diffusivity, D_e, and is given by:

$$J = -D_e \nabla C \quad (20)$$

where ∇C is the solute concentration gradient in the pore liquid. D_e is related to the intraparticle porosity, ε_p, the tortuosity factor, τ_p, and the diffusional hindrance coefficient, ψ_p, and is therefore smaller than the molecule diffusivity in free solution, D_0 (Carta & Jungbauer, 2010):

$$D_e = \frac{\varepsilon_p D_0}{\tau_p} \psi_p \quad (21)$$

The intraparticle porosity is the space of liquid available within the particle. The tortuosity is given by a factor between the effective diffusion path the solute travels along a random orientation of the pores in a bead and a straight-line trajectory to travel along the bead. These two parameters have a certain correlation. In particles with randomly distributed internal structure the larger the $\varepsilon_p$the smaller the τ_p. In protein chromatography, τ_p typically ranges between 1.5 and 4. With tortuosity values larger than 4, pore diffusion becomes very restricted. Values lower than 1.5 are usually associated with pore diffusion no longer controlling mass transfer. The hindrance coefficient, ψ_p, considers the hydrodynamic resistance during the molecule diffusion, and takes into account that the molecules cannot get to a distance any closer to the pore wall than its radius. ψ_p is related to some extent to the ratio between the protein radius and the pore radius: $\lambda = r_{protein}/r_{pore}$. Different equations were developed for large (Brenner & Gaydos, 1977) or small (Anderson & Quinn, 1974) λ values:

$$\psi_p = \left(1 + \frac{9}{8}\lambda\, ln\lambda - 1.539\lambda\right) \text{ for } \lambda < 0.2 \quad (22)$$

$$\psi_p = 0.865(1-\lambda)^2(1 - 2.1044\lambda + 2.089\lambda^3 - 0.984\lambda^5) \text{ for } \lambda > 0.2 \quad (23)$$

Figure I.7, adapted from (Carta & Jungbauer, 2010), plots Eqs. (22) and (23), giving the diffusional hindrance coefficient as a function of the ratio between the protein and the pore radii. As seen, the steric hindrance is decreased by the increase in the ratio between the protein radius and the particle pore radius. To avoid excessive diffusional hindrance, ψ_p has to be greater than 0.5, which means $\lambda <$ 0.125. Therefore, for practical applications in the purification of an antibody (M_w = ~150 kDa) that has a hydrodynamic radius of approximately 5 nm, the average pore radius has to be at least 40 nm.

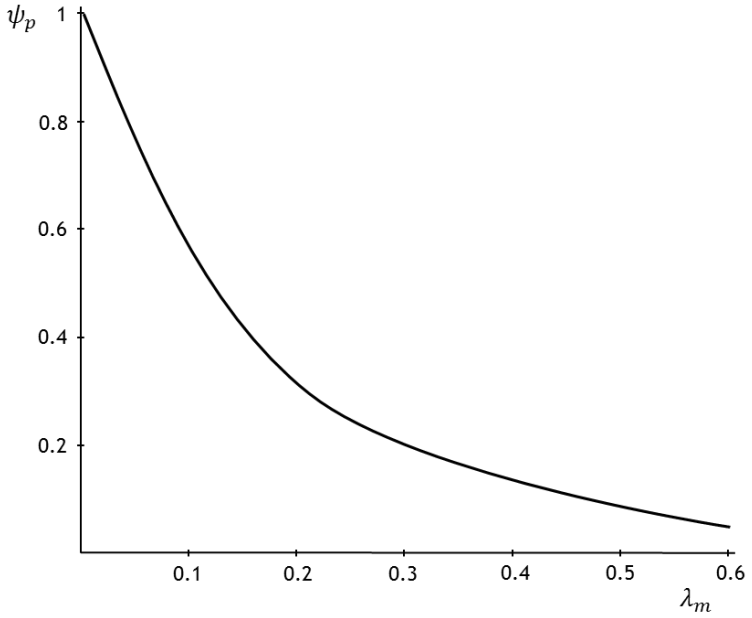

Figure I.7 – Diffusional hindrance coefficient vs. ratio of protein and pore radii.

2.2.3. Antibody transport in Protein A chromatography

Some models have been employed to characterize antibody uptake by Protein A resins of spherical particles in terms of the resistance the antibody faces along the way. Pore diffusion is the dominant intraparticle transport mechanism in the kinetics of antibody binding to Protein A resins (Hahn et al., 2005). This diffusion in the liquid-filled pores is expressed in terms of the pore fluid concentration gradient (Weaver Jr. & Carta, 1996). There is also a certain contribution of the antibody-Protein A complex formation kinetics (Perez-Almodovar & Carta, 2009).

Researchers have demonstrated that various models can predict well mass transfer of antibody in Protein A resins, namely the pore diffusion model, the shrinking core model, and

the heterogeneous binding model (Perez-Almodovar & Carta, 2009). All three consider pore diffusion as the main driving mechanism for mass transfer, but differ in the assumptions for equilibrium and kinetics. Both the pore diffusion model and the shrinking core model consider that the antibody binding sites are homogenous, which in fact is not entirely true. On the other hand, the heterogeneous binding model, as mentioned, is named for assuming the existence of heterogeneous binding sites in Protein A resins. In their studies, Carta and co-workers have found that the first two models lack accuracy to predict adsorption at high antibody concentrations. Only the heterogeneous binding model is capable of describing the overall adsorption kinetic behaviour, both at small time scales (where the other models are also valid) where the antibody binds to the fast (high energy) binding sites and adsorption is dominant, and at longer time scales where the slow (low energy) binding sites are also occupied and mass transfer is dominant (Perez-Almodovar & Carta, 2009a).

2.2.3.1. Pore diffusion model

The pore diffusion model assumes that there is an equilibrium between the adsorbed solute and that in the pore liquid at each radial position of the particle (Weaver Jr. & Carta, 1996). It assumes a Langmuir isotherm type, but neglects the kinetic resistance to binding. Protein uptake kinetics in spherical particles of radius r_p in a closed batch system is described by the following equations and boundary conditions (Perez-Almodovar & Carta, 2009):

$$\varepsilon_p \frac{\partial c}{\partial t} + (1-\varepsilon_p)\frac{\partial q}{\partial t} = \frac{D_e}{r^2}\frac{\partial}{\partial r}\left(r^2 \frac{\partial c}{\partial r}\right) \tag{24}$$

$$t = 0,\ c = 0,\ q = 0$$

$$r = 0,\ \frac{\partial C}{\partial r} = 0$$

$$r = r_p,\ D_e \frac{\partial C}{\partial r} = k_f (C - c)$$

where c is the concentration in the pore liquid.

At initial conditions, the conservation equation is the following:

$$\frac{\partial C}{\partial t} = -\frac{3k_f}{r_p}\frac{v}{V}(C - \mathrm{c}\big|r = r_p) \tag{25}$$

$$t = 0,\ C = C_0$$

where v is the volume of resin, V is the volume of bulk liquid, $\mathrm{c}\big|r = r_p$ is the concentration at the particle surface (where the radial position equals the radius of the particle), and C_0 is the initial concentration in the bulk liquid.

2.2.3.2. Shrinking core model

The shrinking core model assumes a rectangular isotherm, neglects the amount of protein in the interstitial liquid of the bead pores, and also neglects the kinetic resistance to binding (Perez-Almodovar & Carta, 2009; Zandian & Jungbauer, 2009). For rectangular isotherms, like antibody uptake by Protein A resins, batch adsorption in a finite bath can be defined with the batch pore diffusion model. This model was first developed by Teo and Ruthven (Teo & Ruthven, 1986) and then applied by other authors:

$$\frac{C_0}{q}\frac{D_e t}{r_p^2} = \left(1 - \frac{1}{Bi}\right) I_2 - I_1 \tag{26}$$

where Bi is the Biot number, and I_1 and I_2 are simplified adimensional parameters given by:

$$I_1 = \frac{1}{6\lambda\Lambda} ln\left[\frac{\lambda^3+\beta^3}{\lambda^3+1}\left(\frac{\lambda+1}{\lambda+\beta}\right)^3\right] + \frac{1}{\lambda\Lambda\sqrt{3}}\left[\tan^{-1}\left(\frac{2\beta-\lambda}{\lambda\sqrt{3}}\right) - \tan^{-1}\left(\frac{2-\lambda}{\lambda-\sqrt{3}}\right)\right] \tag{27}$$

$$I_2 = \frac{1}{3\Lambda} ln\left(\frac{\lambda^3+\beta^3}{\lambda^3+1}\right) \tag{28}$$

where $\beta = \left(1 - \frac{\bar{q}}{q_{max}}\right)^{1/3}$ and $\lambda = \left(\frac{1}{\Lambda} - 1\right)^3$, and where Λ is the normalized phase ratio given by $\Lambda = \frac{v q_m}{V C_0}$, $\bar{q}$ is the average concentration in the particle, q_m is the maximum binding capacity of the resin, v is the resin volume, V is the mobile phase volume. The Biot number is given by $Bi = \frac{k_f r_p}{D_e}$.

2.2.3.3. Heterogeneous binding model

The heterogeneous binding model assumes that there is a heterogeneous distribution of the binding sites because of the reduced accessibility of the antibody to the binding sites, and considers the kinetic resistance to binding. The binding sites are considered independent, but are assumed to have the same affinity (same K value) for the solute only with fast and slow binding kinetics (Perez-Almodovar & Carta, 2009). This model describes protein uptake by the following equations and boundary conditions:

$$\varepsilon_p \frac{\partial c}{\partial t} + \frac{\partial (q_1+q_2)}{\partial t} = \frac{D_e}{r^2}\frac{\partial}{\partial r}\left(r^2 \frac{\partial c}{\partial r}\right) \tag{29}$$

$$r = 0,\ \frac{\partial C}{\partial r} = 0$$

$$r = r_p,\ D_e \frac{\partial C}{\partial r} = k_f (C - c) \tag{30}$$

$$\frac{\partial q_1}{\partial t} = k_1 \left[(q_{m1} - q_1) C - \frac{q_1}{K_A}\right] \tag{31}$$

$$\frac{\partial q_2}{\partial t} = k_2 \left[(q_{m2} - q_2) C - \frac{q_2}{K_A} \right] \quad (32)$$

where k_1 and k_1 are the binding rate constants for the fast and slow kinetics independent sites, q_1 and q_2 are the surface concentration at those sites respectively, and q_{m1} and q_{m2} are the maximum capacity at those sites, with $q_{m1} + q_{m1} = q_m$.

At initial conditions, the conservation equation is the same as in the pore diffusion model:

$$\frac{\partial C}{\partial t} = -\frac{3k_f}{r_p}\frac{v}{V}\left(C - \mathrm{c}\middle| r = r_p\right) \quad (33)$$

2.3. Thermodynamics

With the constrains from the regulatory agencies like FDA and EMA through Quality by Design (QbD) and Process Analytical Technology (PAT) in the biopharmaceutical manufacturing, there has been an increased need in process and product understanding (Hanke & Ottens, 2014). Mechanistic models and the use of hybrid procedures combining modelling with an experimental approach are on the rise to replace the pure statistical and empirical approaches to accurately predict and optimize those processes, calling, as mentioned, for an improved understanding of the protein–resin interactions.

Thermodynamic analyses of biomolecule adsorption have helped to elucidate complex adsorption mechanisms in liquid chromatography (F.-Y. Lin, Chen, & Hearn, 2002). Thermodynamics gathers complex information about the events at the molecular level that take place in a chromatography column. The methods that are employed to retrieve the thermodynamic quantities associated to a chromatographic process are obtained from batch equilibrium experiments, by analyses of data presented as van't Hoff plots, or from microcalorimetric measurements.

2.3.1. Analysis based on the thermodynamic equilibrium constant

The spontaneity of a process is determined by the Gibbs energy change, ΔG, and is given by the following equation:

$$\Delta G = \Delta G^0 + R\,T\,ln\,Q \quad (34)$$

where Q is the reaction quotient, ΔG^0 the Gibbs energy change at standard temperature and pressure, R is the universal gas constant, and T is the temperature. In equilibrium we have $\Delta G = 0$ and Q becomes K, the thermodynamic equilibrium constant, and thus:

$$\Delta G^0 = -R\,T\,ln\,K \quad (35)$$

In a system at constant temperature and pressure and according to the first law of thermodynamics, the Gibbs energy change is given by (Gibbs, 1873):

$$\Delta G = \Delta H - T\,\Delta S \tag{36}$$

where ΔH is the enthalpy change and ΔS is the entropy change. At standard temperature and pressure conditions:

$$\Delta G^0 = \Delta H^0 - T\,\Delta S^0 \tag{37}$$

According to the second law of thermodynamics, a spontaneous process will return a negative value of ΔG. Gibbs energy is useful because it incorporates both enthalpy and entropy. In some interactions, the enthalpy and entropy contributions reinforce each other. If ΔH is negative and ΔS is positive then ΔG is a negative quantity, and the process is favoured. In other interactions, enthalpy and entropy may have to balance each other out, *i.e.*, that is, ΔH and -TΔS have different signs. In such cases, the spontaneity of the interaction is determined by the magnitudes of ΔH and TΔS. If |ΔH |>>|TΔS |, then the reaction is said to be enthalpy driven because the negative signal of ΔG is predominantly determined by ΔH. Conversely, if |TΔS | >>|ΔH |, then the process is an entropy-driven one.

Combining Eqs (35) and (37):

$$ln\,K = \frac{\Delta H^0}{R\,T} - \frac{\Delta S^0}{R} \tag{38}$$

The value for the thermodynamic equilibrium constant, can be obtained both from the isotherm or with van't Hoff plots. From the van't Hoff equation, a temperature dependence of the retention factor k' can be obtained and the thermodynamic parameters can be calculated from indirect methods. The thermodynamic equilibrium constant K is linearly related to the retention factor through the temperature-independent phase ratio ϕ (i.e., the ratio between the volume of stationary phase and mobile phase): $k' = K\,\phi$. Therefore, when enthalpy and entropy changes are independent from the temperature, they can be obtained by correlating Eq. (38) with the retention factor, giving:

$$ln\,k' = -\frac{\Delta H^0}{R}\frac{1}{T} + \frac{\Delta S^0}{R} + ln(\phi) \tag{39}$$

Csaba Horváth and co-workers determined enthalpy and entropy changes considering their dependence from temperature (Haidacher, Vailaya, & Horváth, 1996). Under that condition, the integrated form of Kirchoff's law is applied to obtain standard enthalpy and entropy, provided that the heat capacity ΔC_p^0 is temperature-independent:

$$\Delta H^0 = \Delta C_p^0 (T - T_H) \tag{40}$$

$$\Delta S^0 = \Delta C_p^0 \, ln\left(\frac{T}{T_S}\right) \tag{41}$$

where T_H and T_S are the temperatures at which ΔH^0 and ΔS^0 are zero, respectively. Therefore, the retention factor can be plotted in terms of temperature dependence through the usually termed *logarithmic* relationship (F.-Y. Lin et al., 2002)

$$ln\, k' = \frac{\Delta C_p^0}{R}\left(\frac{T_H}{T} - ln\frac{T_S}{T} - 1\right) + \, ln(\phi) \tag{42}$$

However, heat capacity as a temperature-independent parameter is a crude assumption. The equation was then formulated to correct for the temperature dependency of ΔC_p^0 (F.-Y. Lin et al., 2002):

$$ln\, k' = a + \frac{b}{T} + \frac{c}{T^2} + \, ln(\phi) \tag{43}$$

The thermodynamic parameters obtained by fitting Eq. (33), often called the *quadratic* relationship, to the experimental chromatographic retention data to be used to determine the thermodynamic quantities by the following relationships:

$$\Delta H^0 = -R\left(b + \frac{2c}{T}\right) \tag{44}$$

$$\Delta S^0 = R\left(a - \frac{c}{T^2}\right) \tag{45}$$

$$\Delta C_p^0 = \frac{2Rc}{T^2} \tag{46}$$

From the aforementioned information we found that thermodynamic quantities associated with the chromatographic process may be obtained from both batch equilibrium experiments and by analyses of data presented as van't Hoff plots (F.-Y. Lin et al., 2002). Nevertheless, the resolution with which variations in thermodynamic behaviour, as a function of protein loading and temperature, can be detected by batch equilibrium experiments is limited, and the indirect method of van't Hoff analysis may be complicated by the presence of multiple sub-processes associated with adsorption.

2.3.2. Microcalorimetric measurements

Unlike other methodologies to assess the thermodynamic parameters associated to adsorption events in liquid chromatography, microcalorimetric techniques do so by direct measurement of the enthalpy (Blaschke, Werner, & Hasse, 2013; F.-Y. Lin et al., 2002). Isothermal titration calorimetry (ITC) is a microcalorimetric technique that probes the interaction mechanisms between molecules and the resin in terms of adsorption enthalpy change (Blaschke et al., 2013). A vessel with the resin in suspension is inserted to a

thermometric activity monitor (TAM) and the protein solution is injected. The TAM measures directly the heat of adsorption of the system and can also detect the heat of dilution that has to be taken into account for proper analysis. The enthalpy change of adsorption can be determined by the following equation:

$$Q_{ads} = v\, q\, \Delta H_{ads} \tag{47}$$

where Q_{ads} is the heat associated to the interaction between the molecule and the resin, v is the volume of the resin, q is the amount of molecule bound per volume of resin, and ΔH_{ads} is the enthalpy change of the adsorption of the molecules to the resin. The resulting ΔH_{ads} is the product of a series of contributions, such as the heat of the interaction itself, the heat of dilution, the heat associated to the desolvation of molecule and resin, and the heat associated to the conformation change or reorientation of the adsorbed molecules on the surface of the resin (Silva, Marques, Thrash, & Dias-Cabral, 2014).

However, ITC is a technique that operates in the static mode, being limited to the thermodynamics attributed to equilibrium and lacking the information associated to mass transfer. It also does not provide insight about the desorption process.

In 1958, Groszek established the flow microcalorimetry (FMC) as a microcalorimetric technique to estimate the heats of wetting of silica gel by a number or organic liquids (Groszek, 1958). He constructed an apparatus (flow microcalorimeter) consisting of a cell of cylindrical volume that could be filled with an adsorbent. Thermocouples were placed surrounding the cell and in contact with the adsorbent and a glass jacket (later replaced with polytetrafluoroethylene (PTFE)) was used for insulation. The main feature of this equipment was the possibility of liquid to flow through the packed column and the wetting temperature is detected by the thermocouples. Years later the company Microscal developed the first commercial flow microcalorimeter. Scientists then started to use it as a tool to investigate the adsorbate-adsorbent phenomena on the fundamental level to obtain the thermodynamic parameters during adsorption and desorption in chromatographic processes (Aguilar, Twarda, Sousa, & Dias-Cabral, 2014; Dias-Cabral, Pinto, & Queiroz, 2002; Groszek, 1998; Raje & Pinto, 1998; Silva et al., 2014; M E Thrash Jr., Phillips, & Pinto, 2005; Marvin E Thrash Jr. & Pinto, 2001; M E Thrash Jr & Pinto, 2002).

The flow microcalorimeter is operated similarly to a liquid chromatography station. The cell is packed with the adsorbent, equilibrated with the running buffer through syringe pumps, and the sample is injected. The resulting heat signal gives valuable information regarding the mass transfer processes and the molecule binding kinetics to the surface of the adsorbent.

The adsorption process consists of multiple steps involved that have thermodynamic significance. There are processes that are source of energy (exothermic processes) and others that require energy to occur (endothermic processes). Examples of endothermic processes are the desolvation (release of water molecules and ions) of the molecule and the adsorbent, the rearrangement of water molecules at the surface, the alteration of molecules conformation,

the reorientation of the molecules at the surface, the repulsive forces between two molecules. The binding itself of the molecule to the adsorbent causes a release of energy, being thus of the exothermic nature. The overall adsorption process is an overlap of these multiple factors. If the resulting enthalpy is negative and $|\Delta H| >> |T\Delta S|$, the overall process is said to be enthalpy driven. If, on the other hand, the endothermic contributors overwhelm the exothermic, the process has to be entropy driven so that Eq. (37) holds true.

FMC is established as a sound and robust online and *in situ* sensor that is employed to retrieve the thermodynamic parameters simulating a liquid chromatography system without being invasive for the molecule nor interfere with the nature of the binding and elution process. Therefore, the gathered data will enable a better understanding of the thermodynamics of the adsorption mechanisms and can be implemented in models that will help to monitor the purification process *in situ* and contribute to its optimization.

2.4. Small angle X-ray scattering

Small angle X-ray scattering (SAXS) is a powerful and robust technique to analyze the three-dimensional (3D) structure of particles of the colloidal size (Bernadó, Mylonas, Petoukhov, Blackledge, & Svergun, 2007; Kikhney & Svergun, 2015). It is a method that has been used to obtain knowledge about the structure of proteins (Mertens & Svergun, 2010), membranes (Zong et al., 2002), polymers (Zong et al., 2002), etc. It has not, however, been much used to study the adsorption phenomena of molecules to adsorbent on a chromatography basis. Unlike other light scattering techniques like X-ray crystallography, SAXS does not require crystallization, nor pre-sample treatment like cryo-electron microscopy.

SAXS consists in the use of a collimated monochromatic X-ray beam that will illuminate a sample loaded in a quartz capillary (Kikhney & Svergun, 2015; Tian, Langkilde, Thorolfsson, Rasmussen, & Vestergaard, 2014). The beam will hit the sample, some light is absorbed and some photons are scattered with an angle 2θ, depending on the sample composition, and will be collected by a detector place at an adjustable distance from the sample (the longer the distance the smaller the angles that can be resolved). The subtraction of the scattering pattern of a reference (the solution buffer) from scattering pattern of the sample will originate the scattering signal of the sample. Figure I.8 shows a schematic representation of SAXS.

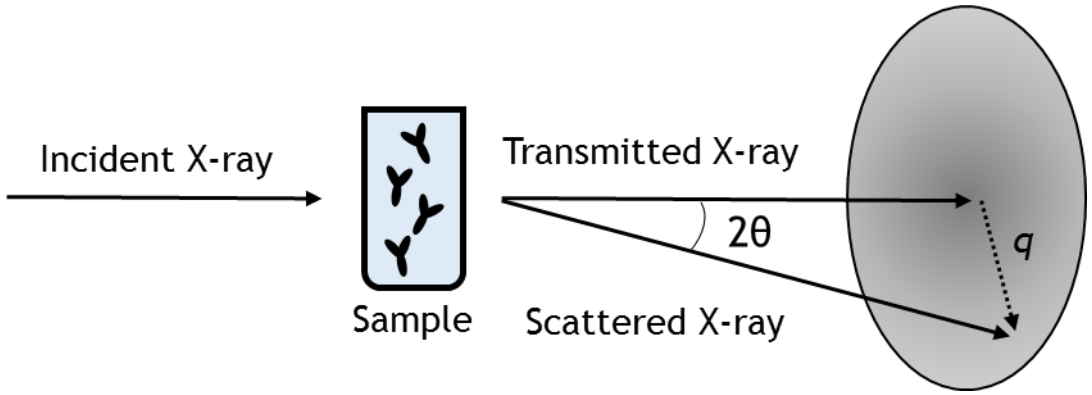

Figure I.8 - Schematic representation of SAXS principle.

The scattering intensity I is the output information and the curves are plotted against the scattering vector q (Kikhney & Svergun, 2015). The characteristic curve of the scattering intensity of a globular protein, plotted in terms of $I(q)\ vs\ q$, is represented in Figure I.9.

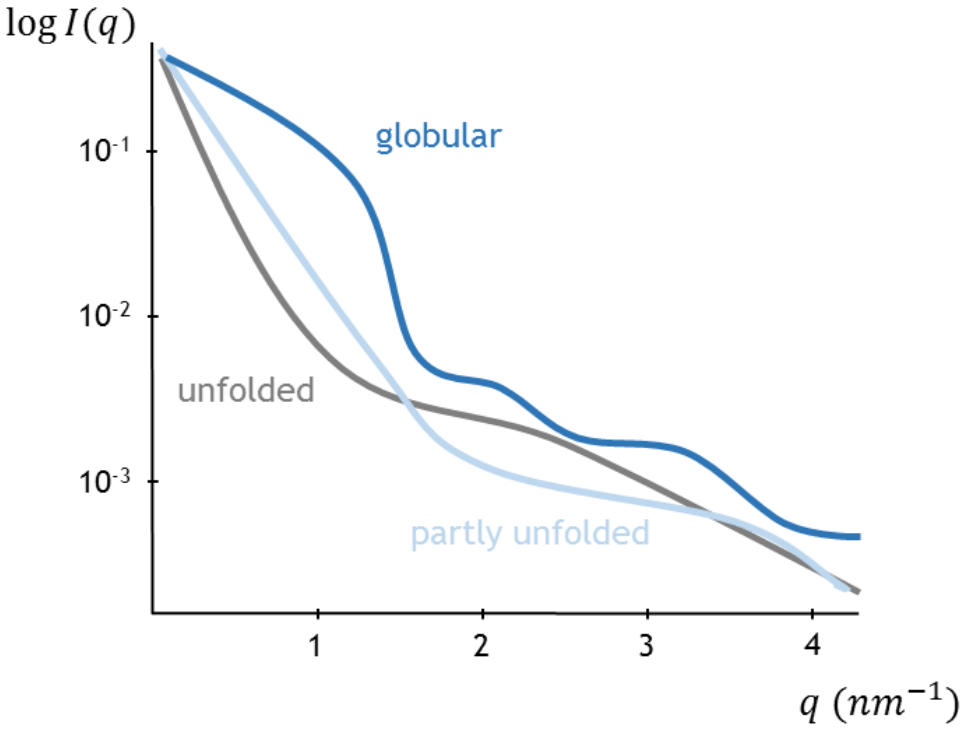

Figure I.9 - Characteristic scattering intensity curve of a globular protein.

This information is retrieved in reciprocal space in terms of q, which is defined as

$$q = 4\pi \frac{\sin\theta}{\lambda} \tag{48}$$

where λ is the wavelength of the X-ray beam.

To translate from the reciprocal space to the real space and have a distribution of the sample size, a Fourier transform has to be applied to the scattering intensity (Kikhney & Svergun, 2015; Mertens & Svergun, 2010):

$$I(q) = \langle I(q) \rangle_\Omega = \langle A(q) A*(q) \rangle_\Omega \tag{49}$$

where the angle brackets represents the spherical average (considering a globular particle), and the scattering amplitude $A(q)$ is the Fourier transform of the excess electron density:

$$A(q) = \Im[\rho(r)] = \int \Delta\rho(r) e^{iqr}\, dr \tag{50}$$

where $\Delta\rho(r) = \rho(r) - \rho_s$, $\rho(r)$ and ρ_s are the electron density of the particle and the solvent respectively, and r is the electron position over the radius of the particle.

Figure I.10 is the real space representation of the scattering intensity plots of Figure I.9, where the zeros of the function represent the longest distance between two scattering points, and the maxima the most represented distance between two scattering points.

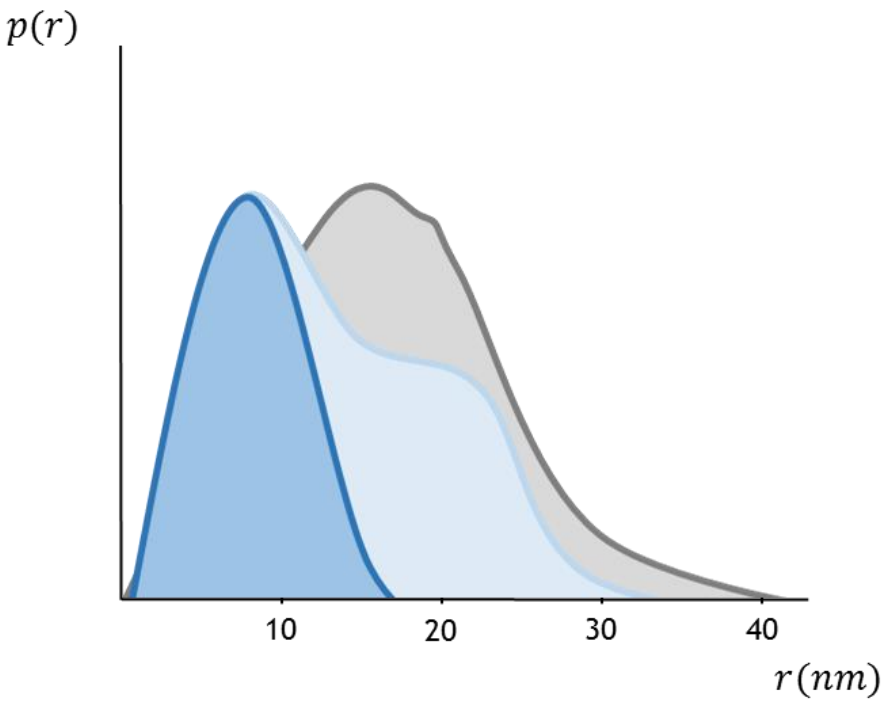

Figure I.10 - Representation in real space of the density distributions from Fig. I.7.

For systems where the scattering is identical for every component, the intensity signal is given by the spherical average of one single particle. For systems where the components do not scatter in an identical manner, the scattering intensity is given by the average of the whole ensemble. Regardless of the type of system, SAXS allows us to obtain certain structural parameters useful to characterize a molecule or a system (the complex protein-ligand in

chromatography), like the molecular weight, the maximum dimension, hydrodynamic radius, radius of gyration, etc (Kikhney & Svergun, 2015; Rambo & Tainer, 2013).

Unlike other sensors employed in chromatography stations, SAXS gathers information in situ, being valuable to the understanding of the evolution of the adsorption layer thickness of protein at the surface of the resin as the process occurs. It is also possible to estimate the stoichiometry of protein to ligand in the case of heterogeneous biding. SAXS is therefore a powerful tool to help monitor the protein-ligand complex formation during a chromatographic step.

3. Objectives

This research thesis has the fundamental goal of studying the biophysical nature of binding of monoclonal antibodies to Protein A resins during the capture step in the downstream processing of these biopharmaceuticals.

Because of the regulatory constraints, pharmaceutical industry is required to monitor and understand every step in the biopharmaceuticals manufacturing pipeline. However, its performance cannot be fully exploited if the process is poorly understood. Being Protein A chromatography a core technology in downstream processing and the most employed unit operation in the capture of antibodies, it is of utmost importance the exhaustive comprehension of the antibody-Protein A complex formation.

In this work we relied on flow microcalorimetry (FMC) and small angle X-ray scattering (SAXS) as *in situ* monitoring techniques to study the antibody-Protein A complex. FMC has thermal sensors implemented in a cylindrical cell mimicking a chromatography column and is able to trace adsorption in terms of the associated enthalpy. SAXS is able to access structural parameters and measure distances and sizes on the nano-scale.

These tools were chosen for their potency, accuracy, and, most of all, for their *in situ* characteristic. In chromatographic applications online sensors are widely implemented (such as UV, pH, and conductivity), however none is known to track binding and elution *in situ*, *i.e.*, within the chromatography column.

In this study, two commercially available Protein A resins will be used: MabSelect SuRe and TOYOPEARL AF-rProtein A HC; and the antibody of interest will be trastuzumab. This work has the aim to study in terms of biophysics the adsorption phenomena involved in the antibody binding to Protein A. Namely, specific goals of this project involve:

- Determining equilibrium and kinetic parameters of antibody adsorption to Protein A resins, such as the affinity constant, the effective diffusivity, and the film mass transfer coefficient;
- Evaluating thermodynamic parameters, such as enthalpy, entropy, and Gibbs energy of adsorption during the establishment of the antibody-Protein A complex;
- Assessing the importance of bead size, intraparticle porosity, and ligand chain length to the binding;
- Visualizing the evolution of the antibody layer thickness with the surface concentration;
- Obtaining an overview of the structural rearrangement of the antibodies at the surface of the Protein A resins;
- Assessing the antibody-ligand stoichiometry at different concentrations in multimeric Protein A chains;
- Understanding the importance of the Protein A chain length and therefore the number of binding sites in the resin capacity.

4. References

Aguilar, P. A., Twarda, A., Sousa, F., & Dias-Cabral, A. C. (2014). Thermodynamic study of the interaction between linear plasmid deoxyribonucleic acid and an anion exchange support under linear and overloaded conditions. Journal of Chromatography A, 1372, 166–173. https://doi.org/10.1016/j.chroma.2014.11.002

Anderson, J. L., & Quinn, J. A. (1974). Restricted Transport in Small Pores. Biophysical Journal, 14(2), 130–150. https://doi.org/10.1016/S0006-3495(74)70005-4

Bernadó, P., Mylonas, E., Petoukhov, M. V., Blackledge, M., & Svergun, D. I. (2007). Structural characterization of flexible proteins using small-angle X-ray scattering. Journal of the American Chemical Society, 129(17), 5656–5664. https://doi.org/10.1021/ja069124n

Blaschke, T., Werner, A., & Hasse, H. (2013). Microcalorimetric study of the adsorption of native and mono-PEGylated bovine serum albumin on anion-exchangers. Journal of Chromatography. A, 1277, 58–68. https://doi.org/10.1016/j.chroma.2012.12.057

Bolton, G. R., Street, B., & Mehta, K. K. (2016). The Role of More than 40 Years of Improvement in Protein A Chromatography in the Growth of the Therapeutic Antibody Industry. Biotechnology Progress, 32(5), 1193–1202. https://doi.org/10.1002/btpr.2324

Brenner, H., & Gaydos, L. J. (1977). The constrained brownian movement of spherical particles in cylindrical pores of comparable radius. Models of the diffusive and convective transport of solute molecules in membranes and porous media. Journal of Colloid And Interface Science, 58(2), 312–356. https://doi.org/10.1016/0021-9797(77)90147-3

Carta, G., & Jungbauer, A. (2010). Protein Chromatography: Process Development and Scale-Up. Weinheim: Wiley-VCH Verlag GmbH & Co. KGaA. https://doi.org/10.1002/9783527630158

Carta, G., Ubiera, A. R., & Pabst, T. M. (2005). Protein mass transfer kinetics in ion exchange media: Measurements and interpretations. Chemical Engineering and Technology, 28(11), 1252–1264. https://doi.org/10.1002/ceat.200500122

Carter, P., Presta, L., Gorman, C. M., Ridgway, J. B., Henner, D., Wong, W. L., … Shepard, H. M. (1992). Humanization of an anti-p185HER2 antibody for human cancer therapy. Proceedings of the National Academy of Sciences, 89(10), 4285–4289. https://doi.org/10.1073/pnas.89.10.4285

Cho, H.-S., Mason, K., Ramyar, K. X., Stanley, A. M., Gabelli, S. B., Denney Jr, D. W., & Leahy, D. J. (2003). Structure of the extracellular region of HER2alone and in complex with the Herceptin Fab. Nature, 421, 756–760. https://doi.org/10.1038/nature01423.Published

Deisenhofer, J. (1981). Crystallographic refinement and atomic models of a human Fc fragment and its complex with fragment B of Protein A from Staphylococcus aureus at 2.9-and 2.8-A resolution. Biochemistry, 20, 2361–2370. https://doi.org/10.1021/bi00512a001

DeLano, W. L., Ultsch, M. H., de Vos, A. M., & Wells, J. A. (2000). Convergent solutions to binding at a protein-protein interface. Science, 287(5456), 1279–1283. https://doi.org/10.1126/science.287.5456.1279

Dias-Cabral, A. C., Pinto, N. G., & Queiroz, J. A. (2002). Studies on hydrophobic interaction adsorption of bovine serum albumin on polypropylene glycol – sepharose under overloaded conditions. Separation Science and Technology, 37(7), 1505–1520. https://doi.org/10.1081/SS-120002734

Ecker, D. M., Jones, S. D., & Levine, H. L. (2015). The therapeutic monoclonal antibody market. MAbs, 7(1), 9–14. https://doi.org/10.4161/19420862.2015.989042

ElBakri, A., Nelson, P. N., & Abu Odeh, R. O. (2010). The state of antibody therapy. Human Immunology, 71(12), 1243–1250. https://doi.org/10.1016/j.humimm.2010.09.007

Elvin, J. G., Couston, R. G., & van der Walle, C. F. (2013). Therapeutic antibodies: market considerations, disease targets and bioprocessing. International Journal of Pharmaceutics, 440(1), 83–98. https://doi.org/10.1016/j.ijpharm.2011.12.039

Ezzell, C. (2001). Magic bullets fly again. Scientific American, 285(4), 35–41. https://doi.org/10.1038/scientificamerican1001-34

Fahrner, R. L., Knudsen, H. L., Basey, C. D., Galan, W., Feuerhelm, D., Vanderlaan, M., & Blank, G. S. (2001). Industrial purification of pharmaceutical antibodies: development, operation, and validation of chromatography processes. Biotechnology and Genetic Engineering Reviews, 18(1), 301–327. https://doi.org/10.1080/02648725.2001.10648017

Gagnon, P. (2012). Technology trends in antibody purification. Journal of Chromatography A, 1221, 57–70. https://doi.org/10.1016/j.chroma.2011.10.034

Gagnon, P., Nian, R., Leong, D., & Hoi, A. (2015). Transient conformational modification of immunoglobulin G during purification by protein A affinity chromatography. Journal of Chromatography A, 1395, 136–142. https://doi.org/10.1016/j.chroma.2015.03.080

Ghose, S., Allen, M., Hubbard, B., Brooks, C., & Cramer, S. M. (2005). Antibody variable region interactions with protein A: Implications for the development of generic purification processes. Biotechnology and Bioengineering, 92, 665–673. https://doi.org/10.1002/bit.20729

Ghose, S., Nagrath, D., Hubbard, B., Brooks, C., & Cramer, S. M. (2004). Use and optimization of a dual-flowrate loading strategy to maximize throughput in protein-A affinity chromatography. Biotechnology Progress, 20, 830–840. https://doi.org/10.1021/bp0342654

Gibbs, J. W. (1873). Graphical Methods in the Thermodynamics of Fluids. In Transactions of the Connecticut Academy of Arts and Sciences (pp. 309–342).

Goldenberg, M. M. (1999). Trastuzumab, a recombinant DNA-derived humanized monoclonal antibody, a novel agent for the treatment of metastatic breast cancer. Clinical Therapeutics, 21(2), 309–318. https://doi.org/10.1016/S0149-2918(00)88288-0

Groszek, A. J. (1958). A Calorimeter for Determination of Heats of Wetting. Nature, 182(4643), 1152–1153. https://doi.org/10.1038/1821152a0

Groszek, A. J. (1998). Flow adsorption microcalorimetry. Thermochimica Acta, 312(1971), 133–143. https://doi.org/10.1016/S0040-6031(97)00447-4

Hahn, R., Bauerhansl, P., Shimahara, K., Wizniewski, C., Tscheliessnig, A., & Jungbauer, A. (2005). Comparison of protein A affinity sorbents: II. Mass transfer properties. Journal of Chromatography A, 1093, 98–110. https://doi.org/10.1016/j.chroma.2005.07.050

Hahn, R., Schlegel, R., & Jungbauer, A. (2003). Comparison of protein A affinity sorbents. Journal of Chromatography B, 790, 35–51. https://doi.org/10.1016/S1570-0232(03)00092-8

Haidacher, D., Vailaya, A., & Horváth, C. (1996). Temperature effects in hydrophobic interaction chromatography. Proceedings of the National Academy of Sciences of the United States of America, 93(6), 2290–2295. https://doi.org/10.1073/pnas.93.6.2290

Hale, G., Drumm, A., Harrison, P., & Phillips, J. (1994). Repeated cleaning of protein A affinity column with sodium hydroxide. Journal of Immunological Methods, 171, 15–21. https://doi.org/10.1016/0022-1759(94)90223-2

Hanke, A. T., & Ottens, M. (2014). Purifying biopharmaceuticals: knowledge-based chromatographic process development. Trends in Biotechnology, 32(4), 210–220. https://doi.org/10.1016/j.tibtech.2014.02.001

Hober, S., Nord, K., & Linhult, M. (2007). Protein A chromatography for antibody purification. Journal of Chromatography B, 848, 40–47. https://doi.org/10.1016/j.jchromb.2006.09.030

Jendeberg, L., Nilsson, P., Larsson, A., Denker, P., Uhlén, M., Nilsson, B., & Nygren, P. Å. (1997). Engineering of Fc1 and Fc3 from human immunoglobulin G to analyse subclass specificity for staphylococcal protein A. Journal of Immunological Methods, 201(1), 25–34. https://doi.org/10.1016/S0022-1759(96)00215-3

Jiang, C., Liu, J., Rubacha, M., & Shukla, A. A. (2009). A mechanistic study of Protein A chromatography resin lifetime. Journal of Chromatography A, 1216, 5849–5855. https://doi.org/10.1016/j.chroma.2009.06.013

Karpas, A., Dremucheva, A., & Czepulkowski, B. H. (2001). A human myeloma cell line suitable for the generation of human monoclonal antibodies. Proceedings of the National Academy of Sciences, 98(4), 1799–1804. https://doi.org/10.1073/pnas.98.4.1799

Katiyar, A., Thiel, S. W., Guliants, V. V., & Pinto, N. G. (2010). Investigation of the mechanism of protein adsorption on ordered mesoporous silica using flow microcalorimetry. Journal of Chromatography A, 1217(10), 1583–1588. https://doi.org/10.1016/j.chroma.2009.12.058

Kelley, B. (2009). Industrialization of mAb production tehcnology: the bioprocessing industry at a crossroads. MAbs, 1(5), 443–452. https://doi.org/10.4161/mabs.1.5.9448

Kikhney, A. G., & Svergun, D. I. (2015). A practical guide to small angle X-ray scattering (SAXS) of flexible and intrinsically disordered proteins. FEBS Letters, 589(19PartA), 2570–2577. https://doi.org/10.1016/j.febslet.2015.08.027

Köhler, G., & Milstein, C. (1975). Continuous cultures of fused cells secreting antibody of predefined specificity. Nature, 256(5517), 495–497. https://doi.org/10.1038/256495a0

Li, R., Dowd, V., Stewart, D. J., Burton, S. J., & Lowe, C. R. (1998). Design, synthesis, and application of a Protein A mimetic. Nature Biotechnology, 16(2), 190–195. https://doi.org/10.1038/nbt0298-190

Lin, F.-Y., Chen, W.-Y., & Hearn, M. T. W. (2002). Thermodynamic analysis of the interaction between proteins and solid surfaces: application to liquid chromatography. Journal of Molecular Recognition, 15(2), 55–93. https://doi.org/10.1002/jmr.564

Lin, M. S., Chiu, H. M., Fan, F. J., Tsai, H. T., Wang, S. S. S., Chang, Y., & Chen, W. Y. (2007). Kinetics and enthalpy measurements of interaction between B-amyloid and liposomes by surface plasmon resonance and isothermal titration microcalorimetry. Colloids and Surfaces B: Biointerfaces, 58(2), 231–236. https://doi.org/10.1016/j.colsurfb.2007.03.014

Linhult, M., Gülich, S., Gräslund, T., Simon, A., Karlsson, M., Sjöberg, A., … Hober, S. (2004). Improving the Tolerance of a Protein A Analogue to Repeated Alkaline Exposures Using a Bypass Mutagenesis Approach. Proteins: Structure, Function, and Bioinformatics, 55, 407–416. https://doi.org/10.1002/prot.10616

Liu, H. F., Ma, J., Winter, C., & Bayer, R. (2010). Recovery and purification process development for monoclonal antibody production. MAbs, 2(5), 480–499. https://doi.org/10.4161/mabs.2.5.12645

Liu, Z., Mostafa, S. S., & Shukla, A. A. (2014). A comparison of Protein A chromatographic stationary phases: Performance characteristics for monoclonal antibody purification. Biotechnology and Applied Biochemistry, 62(1), 37–47. https://doi.org/10.1002/bab.1243

Marichal-Gallardo, P. A., & Álvarez, M. M. (2012). State-of-the-art in downstream processing of monoclonal antibodies: Process trends in design and validation. Biotechnology Progress, 28(4), 899–916. https://doi.org/10.1002/btpr.1567

McCue, J. T., Kemp, G., Low, D., & Quiñones-García, I. (2003). Evaluation of protein-A chromatography media. Journal of Chromatography A, 989(1), 139–153. https://doi.org/10.1016/S0021-9673(03)00005-0

Mertens, H. D. T., & Svergun, D. I. (2010). Structural characterization of proteins and complexes using small-angle X-ray solution scattering. J Struct Biol, 172(1), 128–141. https://doi.org/10.1016/j.jsb.2010.06.012

Mhatre, R., & Rathore, A. S. (2009). Quality by design: an overview of the basic concepts. In Quality by Design for Biopharmaceuticals: Principles and Case Studies (pp. 1–8). John Wiley & Sons, Inc.

Morrison, C., & Lähteenmäki, R. (2017). Public biotech in 2016 - The numbers. Nature Biotechnology, 35, 623–629. https://doi.org/10.1038/nbt.3917

Müller, E., & Vajda, J. (2016). Routes to improve binding capacities of affinity resins demonstrated for Protein A chromatography. Journal of Chromatography B, 1021, 159–168. https://doi.org/10.1016/j.jchromb.2016.01.036

Pabst, T. M., Thai, J., & Hunter, A. K. (2018). Evaluation of recent Protein A stationary phase innovations for capture of biotherapeutics. Journal of Chromatography A, 1554, 45–60. https://doi.org/10.1016/j.chroma.2018.03.060

Perez-Almodovar, E. X., & Carta, G. (2009). IgG adsorption on a new protein A adsorbent based on macroporous hydrophilic polymers. I. Adsorption equilibrium and kinetics. Journal of Chromatography A, 1216, 8339–8347. https://doi.org/10.1016/j.chroma.2009.09.017

Raje, P., & Pinto, N. G. (1998). Importance of heat of adsorption in modeling protein equilibria for overloaded chromatography. Journal of Chromatography A, 796(1), 141–156. https://doi.org/10.1016/S0021-9673(97)01071-6

Rambo, R. P., & Tainer, J. A. (2013). Accurate assessment of mass, models and resolution by small-angle scattering. Nature, 496(7446), 477–481. https://doi.org/10.1038/nature12070.Accurate

Rayner, L. E., Hui, G. K., Gor, J., Heenan, R. K., Dalby, P. A., & Perkins, S. J. (2015). The Solution Structures of Two Human IgG1 Antibodies Show Conformational Stability and Accommodate Their C1q and FcγR Ligands. The Journal of Biological Chemistry, 290(13), 8420–8438.

https://doi.org/10.1074/jbc.M114.631002

Roman, M. F. Von, & Berensmeier, S. (2014). Improving the binding capacities of protein A chromatographic materials by means of ligand polymerization. Journal of Chromatography A, 1347, 80–86.
https://doi.org/10.1016/j.chroma.2014.04.063

Rosa, S. A. S. L., da Silva, C. L., Aires-Barros, M. R., Dias-Cabral, A. C., & Azevedo, A. M. (2018). Thermodynamics of the adsorption of monoclonal antibodies in phenylboronate chromatography: Affinity versus multimodal interactions. Journal of Chromatography A, 1569, 118–127.
https://doi.org/10.1016/j.chroma.2018.07.050

Salvalaglio, M., Zamolo, L., Busini, V., Moscatelli, D., & Cavallotti, C. (2009). Molecular modeling of Protein A affinity chromatography. Journal of Chromatography A, 1216, 8678–8686.
https://doi.org/10.1016/j.chroma.2009.04.035

Sandin, S., Öfverstedt, L.-G., Wikström, A.-C., Wrange, Ö., & Skoglund, U. (2004). Structure and Flexibility of Individual Immunoglobulin G Molecules in Solution. Structure, 12, 409–415.
https://doi.org/10.1016/j.str.2004.02.011

Saphire, E. O., Stanfield, R., Crispin, M. D. M., Morris, G., Zwick, M. B., Pantophlet, R. A., … Burton, D. R. (2003). Crystal structure of an intact human IgG: antibody asymmetry, flexibility, and a guide for HIV-l vaccine design. In Glycobiology and Medicine (pp. 55–66). New York: Plenum Publishers.

Shukla, A. A., Hubbard, B., Tressel, T., Guhan, S., & Low, D. (2007). Downstream processing of monoclonal antibodies-Application of platform approaches. Journal of Chromatography B, 848(1), 28–39.
https://doi.org/10.1016/j.jchromb.2006.09.026

Silva, G. L., Marques, F. S., Thrash, M. E., & Dias-Cabral, A. C. (2014). Enthalpy contributions to adsorption of highly charged lysozyme onto a cation-exchanger under linear and overloaded conditions. Journal of Chromatography A, 1352, 46–54.
https://doi.org/10.1016/j.chroma.2014.05.049

Slamon, D. J., Clark, G. M., Wong, S. G., Levin, W. J., Ullrich, A., & McGuire, W. L. (1987). Human Breast Cancer: Corelation of Relapse and Survival with Aplification of the HER-2/neu Oncogene. Science, 235, 177–182.
https://doi.org/10.1126/science.3798106

Suzuki, M. (1990). Adsorption engineering. Reactive Polymers (Vol. 14). Tokyo and Amsterdam: Kodansha Ltd. and Elsevier Science Publishers B.V.

Teo, W. K., & Ruthven, D. M. (1986). Adsorption of water from aqueous ethanol using 3-A molecular sieves. Industrial & Engineering Chemistry Process Design and Development, 25(1), 17–21.
https://doi.org/10.1021/i200032a003

Thrash Jr., M. E., Phillips, J. M., & Pinto, N. G. (2005). An Analysis of the Interactions of BSA with an Anion-Exchange Surface Under Linear and Non-Linear Conditions. Adsorption, 10, 299–307. https://doi.org/10.1007/s10450-005-4815-0

Thrash Jr., M. E., & Pinto, N. G. (2001). Flow microcalorimetric measurements for bovine serum albumin on reversed-phase and anion-exchange supports under overloaded conditions. Journal of Chromatography A, 908, 293–299. https://doi.org/10.1016/S0021-9673(00)01034-7

Thrash Jr, M. E., & Pinto, N. G. (2002). Characterization of enthalpic events in overloaded ion-exchange chromatography. Journal of Chromatography A, 944(1–2), 61–68. https://doi.org/10.1016/S0021-9673(01)01340-1

Tian, X., Langkilde, A. E., Thorolfsson, M., Rasmussen, H. B., & Vestergaard, B. (2014). Small-Angle X-ray Scattering Screening Complements Conventional Biophysical Analysis: Comparative Structural and Biophysical Analysis of Monoclonal Antibodies IgG1, IgG2, and IgG4. Journal of Pharmaceutical Sciences, 103(6), 1701–1710. https://doi.org/10.1002/jps.23964

Tyn, M. T., & Gusek, T. W. (1990). Prediction of diffusion coefficients of proteins. Biotechnology and Bioengineering, 35(4), 327–338. https://doi.org/10.1002/bit.260350402

Van Dijk, M. A., & Van De Winkel, J. G. J. (2001). Human antibodies as next generation therapeutics. Current Opinion in Chemical Biology, 5(4), 368–374. https://doi.org/10.1016/S1367-5931(00)00216-7

Weaver Jr., L. E., & Carta, G. (1996). Protein Adsorption on Cation Exchangers: Comparison of Macroporous and Gel-Composite Media. Biotechnology Progress, 12, 342–355. https://doi.org/10.1021/bp960021q

Wilson, E. J., & Geankoplis, C. J. (1966). Liquid Mass Transfer at Very Low Reynolds Numbers in Packed Beds. Industrial & Engineering Chemistry Fundamentals, 5(1), 9–14. https://doi.org/10.1021/i160017a002

Yang, L., Biswas, M. E., & Chen, P. (2003). Study of binding between protein A and immunoglobulin G using a surface tension probe. Biophysical Journal, 84(1), 509–522. https://doi.org/10.1016/S0006-3495(03)74870-X

Zandian, M., & Jungbauer, A. (2009). Engineering properties of a camelid antibody affinity sorbent for Immunoglobulin G purification. Journal of Chromatography A, 1216(29), 5548–5556. https://doi.org/10.1016/j.chroma.2009.05.051

Zong, X., Kim, K., Fang, D., Ran, S., Hsiao, B. S., & Chu, B. (2002). Structure and process relationship of electrospun bioabsorbable nanofiber membranes. Polymer, 43, 4403–4412. https://doi.org/10.1016/S0032-3861(02)00275-6

CHAPTER II - Publications

Results

The high demand of large amounts of pure and safe mAbs has resulted in more extensive and thorough research on the topic of purification of these products. For the purification capture step, Protein A chromatography resins have been fully exploited because of their robustness and selectiveness for most of the antibody isoforms. With a long track of years of research on this topic, the cornerstones for Protein A chromatography have already been laid, namely in terms of resins binding capacity, affinity, stability, and life time. Nevertheless, aspects like the structural organization of the antibodies upon binding, antibody to ligand stoichiometry, ligand orientation and accessibility still require deeper investigation and lack valuable input.

This research resulted in a contribution for a slightly better understanding of antibody-ligand binding from a structural and thermodynamic point of view, with the publication of three scientific articles. Considering that the two commercial Protein A resins used (GE's MabSelect SuRe and Tosoh's TOYOPEARL AF-rProtein A HC) differ both in the backbone composition and in the number of the Protein A ligand binding sites, the focus of the publications was in evaluating the differences in the antibody binding between the two resins.

More specifically, the evolution of the antibody adsorption layer thickness was monitored during the chromatographic step. This is an important parameter because it allows to have an idea on the binding orientation of the antibodies and on the attachment orientation of the Protein A to the backbone, and ultimately provide some input to the effective pore size, which could sterically influence the migration of subsequent molecules. At this point, the thermodynamic investigation provided information about the presence of reorganization processes involved after adsorption. The kinetics studies showed that the antibody uptake is dependent on the equilibration time and follows heterogeneous binding at high concentrations due to the fact that the resins have multiple potential binding sites per ligand. Finally, the evaluation of antibody to ligand stoichiometry confirmed that in fact multimeric Protein A ligands can bind more than one antibody molecule depending on the concentration and that there are preferred binding orientations.

Below are listed the main findings of each individual scientific publication within the framework of this thesis:

Publication I – "Antibody adsorption in Protein A affinity chromatography – In situ measurement of nanoscale structure by small angle X-ray scattering"

In this publication we intended to characterize structural changes occurring during the Protein A capture step of an antibody. We wanted to see how the adsorption layer thickness would evolve from loading to elution. In addition, we wanted to extract the system's structural

parameters from the scattering profiles, such as the correlation length and the system dimensionality.

SEM images from MabSelect SuRe beads were acquired and we created a model to characterize the internal structure of the agarose backbone with infinitely long cross-linked cylinders of characteristic thickness subdivided in two types: strands and junctions, with a junction being the cross-link of two or more strands.

We found that the average radius of the agarose fibres was 12 nm, while upon loading with antibody the thickness would increase 5.5 nm and 10.4 nm for strands and junctions respectively, with layer regeneration after elution. Given the fact that the antibody has a hydrodynamic diameter of 11.5 nm, we believe that we are probing the thickness and not the length of the antibody, suggesting that the Protein A chain would not be in a fully stretched position but more on a tilted orientation.

We hypothesized that on average 1.2 antibody molecules would bind to the Protein A tetrameric chain, and they would bind preferably to the outermost domains.

Publication II - "Antibody binding heterogeneity of Protein A resins"

In this publication we intended to characterize the antibody binding to two Protein A resins (MabSelect SuRe and TOYOPEARL AF-rProtein A HC) of different chain length, particle size, porosity, and backbone in terms of adsorption energy and uptake kinetics.

The isothermal adsorption profile showed high affinity with a rectangular profile, typical for Protein A chromatography, of both resins to the antibody. At higher equilibrium concentrations, two steps are seen as opposed to a classic Langmuir isotherm. Given the fact that these synthetically engineered resins have multiple antibody binding sites in each chain (MabSelect SuRe has a tetrameric Protein A chain and TOYOPEARL AF-rProtein A HC has a hexameric Protein A chain), binding is of the heterogeneous nature with high and low energy binding sites.

Antibody uptake kinetics follows the shrinking core model at low equilibrium times, consistent with what is expected in Protein A affinity chromatography. However, during longer equilibrium the shrinking core model fails to predict adsorption, presenting lower diffusivity. We believe that as the ultimate capacity is attained, steric effects derived from already bound molecules may influence binding of subsequent antibody molecules to the other binding domains of the same Protein A chain.

Microcalorimetry showed that antibody adsorption is an overall exothermic process which can be subdivided in two sub-steps in terms of the process associated energy. The first moment represent antibody binding to high energy Protein A sites. The second is associated to the energy associated to antibody reorganization in the ligand. The evolution of enthalpy as function of antibody surface concentration also indicates the heterogeneity of binding sites

Publication III - "The pearl necklace model in Protein A chromatography – molecular mechanisms at the resin interface"

In this publication we intended to characterize antibody binding to MabSelect SuRe resin in terms of stoichiometry of antibody to Protein A chain, binding orientation, and preferred binding site in the chain.

SAXS was used to assess the radial density distributions from the antibody-Protein A complex at different equilibrium and surface concentration and compare them to the radial density distributions computed from crystallographic structures of the antibody and Protein A domains.

We rendered different binding orientations and stoichiometry and saw that at low isotherm concentrations the most probable stoichiometry is 1:1 with the antibody bound to one of the outermost Protein A domains of the tetrameric chain. At intermediate concentrations in a 1:1 stoichiometry the innermost domain is the most probable binding site to the antibody. At saturation, the outermost ligand becomes favoured again.

The binding of two antibody molecules to one single Protein A chain (2:1 stoichiometry) becomes probable at high concentrations (biologically there would be a mixture of 1:1 and 2:1 configurations). In this case the antibody molecules would have a greater probability to be bound to the two outermost Protein A domains. These findings may support the idea that the steric hindrance from the agarose would be greater than the hindrance from the proximity of another antibody molecule.

3:1 stoichiometry configuration was also tested. There is a better match at higher concentrations than at low, however the results are not strong enough to argue in favour of this possibility. The steric effects are too high and the configurations are densely packed. We would need to consider true molecular dynamic simulations to account for those factors.

The possibility of 2:1, and to some extent also 3:1, configurations helps to strengthen the heterogeneous binding nature of this Protein A resin. In every scenario, the best fits were obtained with the Protein A chain in a hook-like conformation as opposed to a fully stretched position.

1. Publication I

Antibody Adsorption in Protein-A Affinity Chromatography – In-Situ Measurement of Nanoscale Structure by Small-Angle X-ray Scattering

Jacek Plewka,[1,2] | Gonçalo L. Silva,[1,3,4] | Rupert Tscheließnig,[2,3] | Harald Rennhofer,[2] | Cristina Dias-Cabral,[3,4] | Alois Jungbauer,[1,5] | Helga C. Lichtenegger,[1,2]

[1]Austrian Centre of Industrial Biotechnology, Muthgasse 18, 1190 Vienna, Austria
[2]Department of Material Science and Process Engineering, University of Natural Resources and Life Sciences, Peter-Jordan Strasse 82, 1190 Vienna, Austria
[3]CICS-UBI – Health Sciences Research Centre, University of Beira Interior, Av. Infante D. Henrique, 6201-001 Covilhã, Portugal
[4]Department of Chemistry, University of Beira Interior, R. Marquês d'Ávila e Bolama, 6201-001 Covilhã, Portugal
[5]Department of Biotechnology, University of Natural Resources and Life Sciences, Muthgasse 18, 1190 Vienna, Austria

Correspoding author

Helga Lichtenegger: Institute of Physics and Materials Science, Peter-Jordan-Straße 82, 1190 Vienna, Austria
Email: helga.lichtenegger@boku.ac.at

Funding information

Austrian Research Promotion Agency FFG – grant number 824186
Fundação para a Ciência e Tecnologia in Portugal – grant number SFRH/BD/104498/2014

Abstract

Protein-A chromatography is the most widely used chromatography step in downstream processing of antibodies. A deeper understanding of the influence of the surface topology on a molecular/nanoscale level on adsorption is essential for further improvement. It is not clear if the binding is homogenous throughout the entire bead network. We followed the protein absorption process and observed the formation of a protein layer on fibers of chromatography resin in a time-resolved manner in nanoscale. To characterize the changes in the antibody-protein-A ligand complex, small angle X-ray scattering was employed using a miniaturized, X-ray-transparent chromatography column packed with a MabSelect SuRe resin. Antibody-free MabSelect SuRe resin fiber had an average radius of 12 nm and the protein layer thickness resulting from antibody adsorption was 5.5 and 10.4 nm for fiber and junctions respectively under applied native conditions. We hypothesize that an average of 1.2 antibodies were adsorbed per protein-A ligand tetramer bound to the outermost units. In contrast to previous studies, it was therefore possible for the first time to directly correlate the nanostructure changes inside the column, which is otherwise a black box, with the adsorption and elution process.

Keywords

Agarose; immunoglobulin; protein-A chromatography; protein layer thickness; small angle X-ray scattering

Acknowledgments

This work has been supported by the Federal Ministry for Digital and Economic Affairs (bmwd), the Federal Ministry for Transport, Innovation and Technology (bmvit), the Styrian Business Promotion Agency SFG, the Standortagentur Tirol, Government of Lower Austria and ZIT - Technology Agency of the City of Vienna through the COMET-Funding Program managed by the Austrian Research Promotion Agency FFG. The funding agencies had no influence on the conduct of this research.

This work was carried out in cooperation with Boehringer Ingelheim RCV, Process Science, and Novartis/Sandoz.

G.L.S. acknowledges his doctoral fellowship SFRH/BD/104498/2014 to Fundação para a Ciência e Tecnologia in Portugal.

Special thanks to D. Irrasch for manufacturing the parts needed for the SAXS column as well as to dr. Pernot from BM29 and dr. Hermida Merino from BM26 for assisting with synchrotron experiments.

Conflict of interest statement

There is no conflict of interest.

1.1. Introduction

Although protein-A affinity chromatography is the most commonly employed method for the purification of antibodies, the adsorption process on the nanoscale is yet not well understood. Previous models rely on the crystal structure of the protein-antibody complex (Deisenhofer, 1981; Graille et al., 2000; Deis et al., 2015; Sauer-Eriksson et al., 1995), or the amount of adsorbed antibody from bulk solution (Ghose et al., 2007). However, direct information about the structural changes inside the column during the adsorption process requires a method capable of following the process in-situ and on the nanoscale length. This is a challenging task, since the investigation has to be performed in a time resolved way and under native process conditions. Despite great progress in understanding the nature of interactions between antibody and affinity resins during the purification step, previous investigations heavily depended on empirical methods such as comparison of the sensors signals before and after chromatography column (Iyer et al., 1999; Orellana et al., 2009; Gerontas et al., 2013; Mallik & Hage, 2006). This leaves the structural changes inside the chromatography column, where the actual process happens, unclear, thus creating "missing link".

Full-length protein-A from Staphylococcus aureus is composed of five homologous binding domains (Lofdahl et al., 1983); however, to improve its selectivity and alkaline stability, protein-A ligands used in chromatography are made from engineered domains (most popularly derived from the B-domains or the C-domain) (Muller & Vajda, 2016) immobilized on chromatographic supports, such as agarose or hydroxylated methacrylic polymer (Boschetti & Jungbauer, 2000).

Protein layer thickness refers to the amount of protein adsorbed at a solid surface and its positioning toward it, and has been the subject of numerous studies in the last five decades (Rabe et al., 2011; Vogler, 2012). However, for more complex systems, such as protein-A chromatography resin, in which antibody is adsorbed to the surface via ligand-mediated interactions, the applicable research methods are greatly limited. Mazzer et al. (Mazzer et al., 2017) proposed neutron reflectivity measurements to probe the protein-A–antibody complex arrangement at the solid-liquid interface. However, they immobilized protein-A ligands on the silicon surface, compromising the native state of the chromatography bead backbone and performed the experiment in batch mode. Also other methods used for the structural determination of protein-surface interactions require a sample pretreatment resulting in non-native process conditions as described in the review by Rabe et al. (Rabe et al., 2011).

In the present study, we followed antibody layer formation in situ and their adsorption and desorption kinetics on a protein-A chromatography resin during a typical purification run. We used MabSelect SuRe (GE Healthcare), a popular protein-A chromatography resin, as the model system and small angle X-ray scattering (SAXS) as the probing method. Cross-linked, porous agarose beads 85 µm in diameter are characterized by a rigid, high-flow backbone matrix and a tetrameric ligand of synthetically engineered B-domains, called Z-domain, able of binding up to immobilized via short linkers (Ghose et al., 2014; Wolfram Research 2018). From

equilibrium binding capacity and ligand density it was derived that on average 3.3 antibody molecules are bound to one MabSelect SuRe protein A ligand (Ghose et al., 2007; Jungbauer & Hahn, 2004).

SAXS is a powerful technique for probing the structural properties of materials on the nanoscale and ideally suitable for non-destructive in-solution experiments. The technique is based on elastic scattering of X-ray photons by electrons, which provides information about fluctuations in electron density within illuminated sample volumes. The use of brilliant synchrotron radiation facilities allows time-resolved studies on versatile materials, making it an excellent tool for investigating the development of protein layer thickness and its kinetics under native chromatography conditions (Blanchet & Svergun, 2013). SAXS is routinely applied to study conformational changes to the proteins directly after elution from the column in HPLC-SAXS modes (Brookes et al., 2013) like HIC-SAXS (Kulsing et al., 2016), SEC-SAXS (Ryan et al., 2018; O'Brien et al., 2018)as well as to study structure of porous materials often with the combination of other structural characterization methods like Scanning Electron Microscopy (SEM) (de Coelho Escobar & dos Santos, 2014). However, the method to follow the adsorption process in-situ in the column by SAXS opens up a new avenue to deeper investigation of all modes of chromatography.

1.2. Methods and methods

1.2.1. Materials

For protein-A chromatography, an agarose-based resin (MabSelect™ SuRe™, GE Healthcare) was used. The model protein used for this investigation was 13 mg/mL Herceptin® (Trastuzumab – humanized IgG1) solution from Roche dialyzed into running buffer (0.01 mM phosphate buffer with 150 mM NaCl, pH 7.4). The quality of the antibody solution was assessed on SEC column (Supplementary Fig.II.S.1). No dimerization of protein solution was observed. Sodium phosphate dibasic, sodium dihydrogen phosphate, sodium chloride, and glycine-HCl were purchased from Merck Millipore.

1.2.2. Chromatography column for in situ small angle X-ray scattering

A miniature chromatography column was built in our laboratory for simultaneous chromatography runs and in situ characterization by SAXS (Fig. II.1.1). The column resembled a conventional HPLC column, a cylinder filled with a stationary phase closed with a frit at the bottom. A capillary (Hilgenberg GmbH – mark tube from quartz glass) with 1.5 mm diameter and 10-µm thick glass walls to reduce the absorbance of X-rays was glued into a metal housing for protection. A gap in the metal housing allowed undisturbed passing of photons. The SAXS column was connected to an ÄKTAprime plus chromatography system via HPLC connectors for flow-through experiments and placed in the incident X-ray beam for in situ measurements. A

280 nm UV signal was collected downstream of the column. The resulting UV chromatographs were time-corrected based on the additional volume between the column and UV sensor.

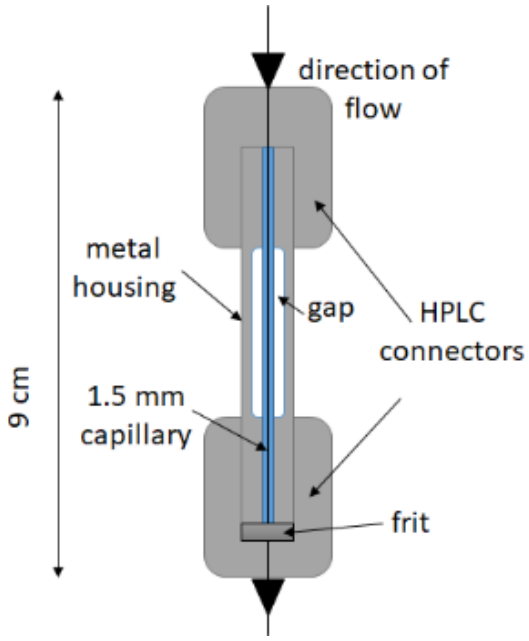

Figure II.1.1 – Schematic of a SAXS column.

1.2.3. Protein-A chromatography run

The chromatography run included equilibration of the SAXS column with running buffer (0.01 mM phosphate buffer with 150 mM NaCl, pH 7.4), injection of 4 mg of monoclonal antibody standard solution from the loop to oversaturate the column, washing off unbound free antibodies, and a subsequent elution step with 0.1 M glycine buffer (pH 3.5). A constant flow rate of 0.1 mL/min was applied throughout chromatography run. Both conductivity and UV 280 nm signal were collected (Supplementary Table II.S.1).

1.2.4. In situ X-ray characterization

In situ on-line characterization of the protein-A chromatography process by SAXS was performed at the European Synchrotron (ESRF, Grenoble, France), beamlines BM26B (Portale et al., 2013) and BM29 (Pernot et al., 2013). Scattering images with an exposure of 1 s were collected every second throughout the protein-A chromatography purification process using a 2D detector (Pilatus 1M) at a photon energy of 12 keV (λ=1.033 Å) and sample to detector distance of 5 m. The 2D images were further processed using an ESRF integrated data reduction system to obtain plots of the intensity dependence on scattering vector q, defined as $q = 4\pi \sin(\theta)/\lambda$, where 2θ is the scattering angle. The q range used for data evaluation was trimmed to 0.03 to 1.83 nm^{-1} to exclude noisy data. Subsequent data processing and model fitting was performed in Mathematica 11.2 (Wolfram Research 2018). Measurements were

repeated several time to ensure reliable results, in particular since the signal from the resin was superimposed on the signal from the protein layer. The same data features were reproducibly found throughout all scattering measurements, thus allowing the extraction of subtle changes. From all measurements performed, only one typical set is presented in this manuscript. Results from multiple experiments are available in the Supplementary (Supplementary Fig. II.S.2).

1.2.5. Scanning electron microscopy of agarose

In order to visualize the inner structure of the agarose network in MabSelect SuRe resin, a modified drying protocol was applied (Nweke et al., 2017). Agarose beads were transferred into 2.3 M sucrose solution, which worked as a cryo-protectant, and flash-frozen using liquid nitrogen. A solid bead drop was then cut using an MT-990 Motorized Precision Microtome from RMC Boeckeler equipped with a tungsten carbide knife. The 30-µm-thick bead slices were collected and dehydrated in graded ethanol series prior to drying with CO_2 solution using a Critical Point Dryer Leica EM CPD030. The resulting dried agarose bead slices were transferred to an aluminum slab and sputter coated with an Au layer approximately 4 nm thick prior to visualization using the Scanning Electron Microscope Quanta™ 250 FEG from FEI under high vacuum conditions.

1.3. Results and Discussion

1.3.1. Protein-A chromatography and in situ small angle X-ray scattering

Protein-A chromatography was performed with a miniature column built in our laboratory for simultaneous chromatography runs and in situ characterization by SAXS. A flow experiment was chosen over regular batch study, as it ensures a constant amount of resin within the illuminated volume of X-ray beam throughout the chromatography run. Such approach guarantees that the observed changes in the scattering profiles are exclusively caused by introduced protein or its interactions with chromatography resin. Moreover, flow experiments allow studying not only adsorption phenomenon like in batch mode, but also the desorption strengthening our understanding on the whole process. Scattering profiles representing structural changes inside the chromatography column were recorded every second in situ throughout the protein-A chromatography run using SAXS. The product was characterized by a UV sensor further downstream in order to correlate the chromatogram with the SAXS results. To ensure protein saturation of the resin binding sites within the SAXS column, the capacity of the resin at given conditions and flow rate was exceeded, which was represented as a sharp peak in the UV data phase called “wash” (Fig. II.1.2A). Note that the amount of protein absorption achieved in this way may be different from the maximal possible amount that is calculated from the isotherm at equilibrium conditions, but corresponds to the maximum under the given circumstances, as it would occur in an industrial process. Free, unbound antibodies

present in the column were washed off using running buffer to ensure that only bound protein and the resin contributed to the scattering profile at this stage of the protein-A run. Elution of the bound protein from the protein-A resin was achieved by lowering the pH on the column to disrupt the affinity of antibodies towards protein-A ligands.

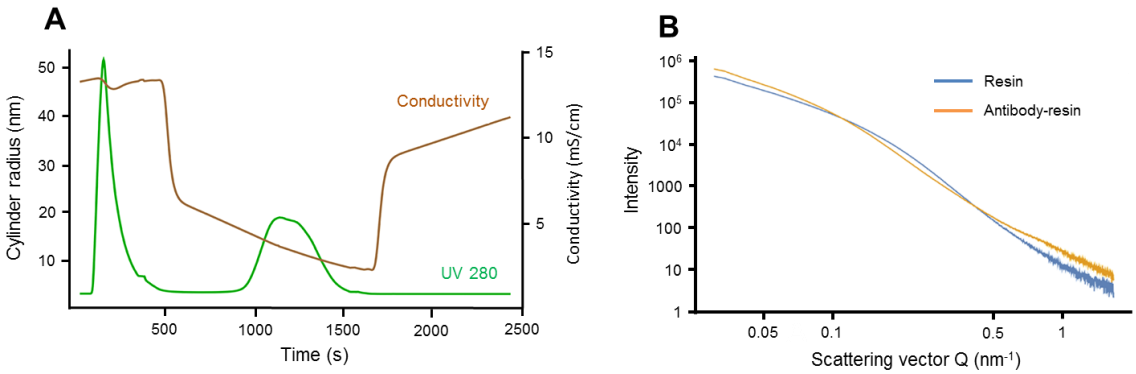

Figure II.1.2 - A: Chromatograph of the 280 nm UV signal (green) and conductivity (brown) for the protein-A run. B: Scattering profiles for antibody-free MabSelect SuRe resin (blue) and saturated resin (orange). The transition of the shoulder visible at q=0.2 nm^{-1} for antibody-free resin to saturated resin is highlighted by the arrow. Additionally, regions for dimensionality and Porod fits are indicated.

In Figure II.1.2B, representative SAXS curves (the same for multiple performed experiments) are shown for the antibody-free MabSelect SuRe taken from the "injection" or "regeneration" phase and the corresponding saturated resin from the "wash" and "elution" phases before the elution peak. The shoulder present at q = 0.2 nm^{-1} representing resin feature (blue curve) clearly moves to a smaller q during saturation (orange curve), indicating an increase in the analyzed system size according to the reciprocal nature of Bragg's law. Furthermore, the intensity at the higher q (q = 0.6 nm^{-1}) becomes stronger during protein loading. Antibodies have a radius of gyration of roughly 5 nm (Pilz et al., 1980), which leads to a SAXS signal in this region. Therefore, we attribute this part of the SAXS curve to the presence of antibodies and denote it in the figure as an antibody peak. In contrast, the shoulder at the lower q is also present without protein and attributed to the resin (with and without bound protein).

1.3.2. Small angle X-ray scattering parameters reflecting protein adsorption

In addition to the qualitative changes in the SAXS curve upon protein adsorption and elution, quantitative parameters have to be extracted from different parts of the SAXS curve to follow the structural changes during purification.

1.3.2.1. Dimensionality

At very low q, decay of the SAXS curve is given by the dimensionality of the scatterer: $I(q) \sim q^{-D}$, where *D* corresponds to 0 for spheres, 1 for rod-like scatterers, and 2 for plate-like scatterers. In a double logarithmic plot, *D* is given by the slope of the curve (Fig. II.1.2B). The slope changes from 1.6 in the antibody-free resin to 2 in the saturated resin, which corresponds to a change from slender to thicker fibers and is in good agreement with the actual structure of MabSelect SuRe.

1.3.2.2. Correlation length estimate

The parameter that qualitatively describes structural changes as an estimate of the intensity-averaged electron density fluctuations throughout illuminated sample volume is l_{CH}* (Eq. 1)

$$l_{CH}{}^{*} = \frac{\pi}{Q} \cdot \int_{q_{min}}^{q_{max}} I(q) \cdot q \cdot dq, \qquad \text{where} \qquad Q = \int_{q_{min}}^{q_{max}} I(q) \cdot q^2 \cdot dq \qquad (1)$$

where $l_{CH}{}^{*}$ is the mean correlation length estimate and Q is the invariant.

Unlike the radius of gyration determination, which requires fitting according to Guinier's approximation, the correlation length is calculated based on the integral of the scattering profile and thus is less sensitive to noisy data (O. Glatter, 1982; Ehmann et al., 2015). Moreover, in contrast to the Guinier approximation, evaluation of the correlation length does not require the sample to be dilute.

1.3.2.3. Fractal dimension and surface roughness

The higher q portion of the scattering curve ($Q(r)$ >>1) is generally determined by Porod's law, according to which the scattered X-ray intensity decreases with q^{-4} for smooth 3D objects, but the exponent can also deviate from 4 in the case of a volume or surface fractal. The antibody-free resin has an exponent close to 4, which then approaches 3.5 during protein adsorption. Surface fractals have values between 3 and 4, which clearly indicate increased surface roughness. The q region used for Porod fitting is shown in Supplementary Figure II.S.3.

1.3.3. Time evolution of small angle X-ray scattering parameters

All of the above SAXS parameters were quantitatively evaluated at each time point during a protein-A chromatography run using Mathematica software (Wolfram Research 2018) and could be exactly correlated with the purification steps by simultaneous UV analysis (Fig. II.1.3). Both SAXS parameters and UV signal clearly responded to the process of loading antibody solution on the column and reached a plateau as soon as the resin was saturated. Since the amount of the chromatographic resin within a column is constant in time, all the changes in fitted SAXS parameters have to be caused by loaded and discharged protein solution or its

interactions with the resin. This assumption is also validated by the fact that all of mentioned parameters come back to their initial values after the protein elution.

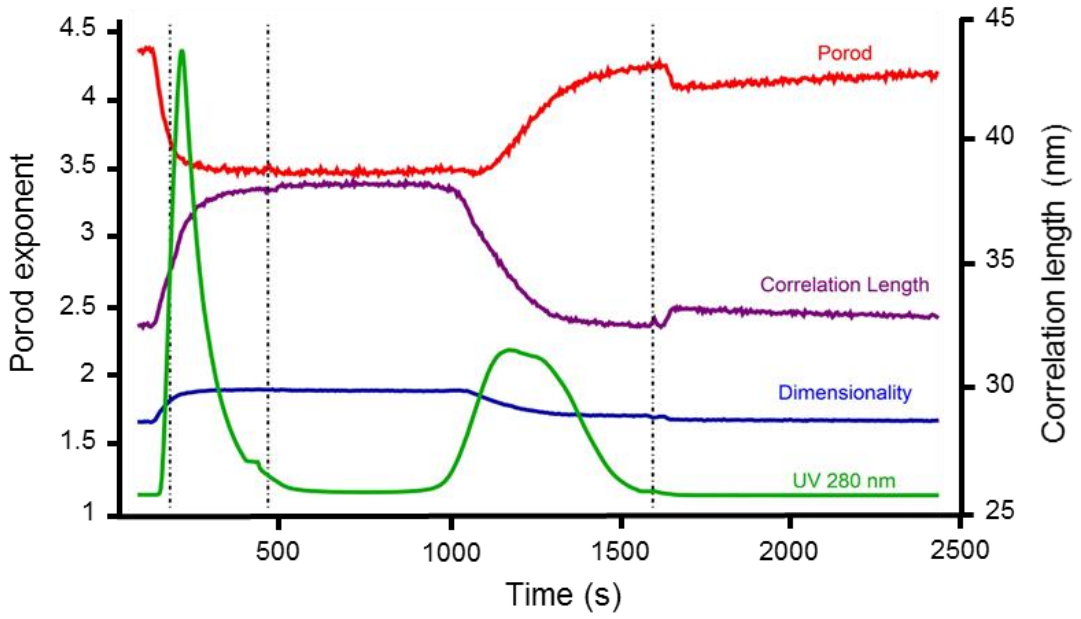

Figure II.1.3 - Comparison of overall fitting parameters for the SAXS time series overlaid on top of the UV signal.

The saturated resin SAXS signal after the "wash" phase is characterized by plumper resin fibers (higher dimensionality) with longer correlation length (larger l_{CH}^{*}). Notably, the dimensionality and correlation length, although extracted from different features of the SAXS curve, proceed in parallel throughout the chromatography process, confirming the evolution from slender to plumper fibers via adsorption of protein. Therefore, the development of l_{CH}^{*} is attributed to the presence of an antibody layer on top of the chromatographic resin.

The fractal dimension sharply decreases after injection, which corresponds to an increasing surface roughness in the saturated resin, and reaches a plateau in parallel with the other parameters. After elution of the bound antibodies from the SAXS column, all parameters gradually returned to their initial values. The final scattering profile after regeneration of the MabSelect SuRe resin with the running buffer resulted in a signal identical to the initial signal (x^2 = 0.01), indicating that the system fully recovered and was ready for the next chromatographic run.

Therefore, we have shown with a simple fitting routine that we can follow the protein-A purification process in situ using SAXS as a probing method. Moreover, the method allowed us to identify and initially characterize structural changes in the system due to adsorption and also desorption phenomena using the "model-free" approach that is independent of the detailed structure of the analyzed system and requires no data modeling.

Note, that due to the relatively low concentration of monoclonal antibodies in the bulk solution (and the low x-ray contrast of protein with respect to water), the main signal comes from the resin in the beam and the monoclonal antibodies tightly packed to it. It contributes

to the scattering profiles so much that it completely overshines the signal from the freely floating monoclonal antibodies (see also Supplementary Fig. II.S.4).

1.3.4. Protein layer thickness

As the analysis of general SAXS parameters allows us to follow adsorption processes in a time-resolved manner by applying a simple fitting routine, quantitative information on layer thickness and its development depend on the resin structure and, therefore, requires the use of a structural model. Thus, we studied the morphology of the virgin resin using scanning electron microscopy (SEM). Images were recorded on cryo-cut beads clearly showing the agarose internal network (Fig. II.1.4A).

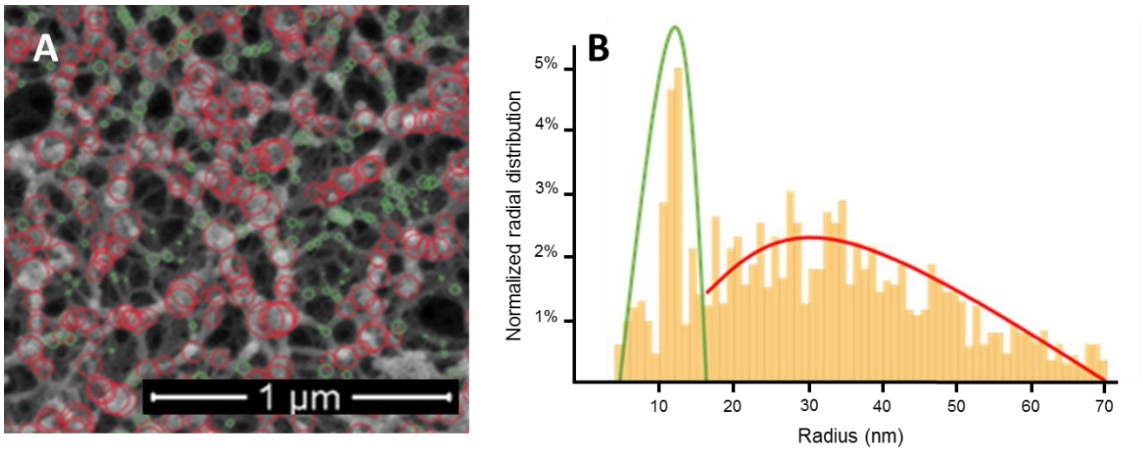

Figure II.1.4 - A: An overlay of Euclidean circles representing the feature diameters within the first plane of the MabSelect SuRe internal agarose network over a SEM picture. Green circles represent radii between 3 and 15 nm, red circles represent radii of 15 to 70 nm. B: A histogram of normalized radii distribution from the semi-automated feature detection algorithm. Green peak is attributed mean fiber thickness, the red peak to junctions between strands.

1.3.4.1. Structural analysis of resin

For further analysis, a semi-automated algorithm for SEM image processing was applied to obtain a general overview of size distribution within the internal structure of the MabSelect SuRe agarose network. First, the SEM image from MabSelect SuRe was binarized and processed (erosion, Gaussian filters) to visualize the strands and junctions in the first plane of the picture.

Next, circles were automatically assigned for the binarized features with diameters corresponding to the locally longest Euclidean distances between “no data” points. The histogram of all radii within an analyzed image (Fig. II.1.4B) represents the normalized distribution of all feature radii between 3 and 70 nm (1 nm bin width). Roughly two populations were identified: the peak at ~11 nm attributed to the mean fiber thickness, and the broader peak centered at ~30 nm attributed to junctions between strands. The results are biased by the applied analytical method and some of the values may be overpopulated due to the irregularity in their shape.

1.3.4.2. Broken rod model

The internal structure of the MabSelect SuRe agarose backbone can be approximated by the so-called broken rod model based on a system consisting of long agarose fibers approximated with infinitely long cylinders characterized by the cross-sectional radius R_1 and cross-linked junctions with radius R_2 (Fig. II.1.5). The scattered intensity is then given by $I(q)$ (Eq. 2).

$$I(q) \sim \sum_{i=1}^{2} k_i / q \left[\frac{J_1(qR_i)}{qR_i}\right]^2 \quad (2)$$

where k_i denotes the relative weights of cylinder radii R_1 and R_2, and $J_1(x)$ is the Bessel function of the first kind for infinitely long cylinders ($L>>R$). Assuming a distribution of R_1 and R_2 about a mean value, we obtain Eq. 3.

$$I(q) \sim \sum_{i=1}^{2} k_i / q \int_0^{\infty} \left[\frac{J_1(qx)}{qx}\right]^2 \cdot G(x)_i dx \quad (3)$$

where $G(x)$ is the normal distribution of each radius separately as determined in Eq. 4:

$$G(x)_i = \frac{1}{\sqrt{2\pi\sigma_i^2}} \cdot e^{-\frac{(x-\mu_i)^2}{2\sigma_i^2}} \quad (4)$$

where μ_i is the mean of the distribution and σ_i^2 is the variance.

Although the broken rod model is certainly idealized, it has already been applied successfully to analyze the gelation process of polysaccharide gels, such as alginate (Yuguchi et al., 2016; Yuguchi et al., 2000; Stokke et al., 2000) or sorbitol (Maeda et al., 1999), to obtain insight into the kinetics of gel formation and structural information about fiber diameter throughout the process. The model assumes that infinitely long agarose strands of characteristic diameter are interconnected, creating nodes of different thickness denoted as junctions and, therefore, approximated as two populations of rigid cylinders (Fig. II.1.5). Similar models built on polydisperse cylinders were also used for other agarose-based chromatographic materials characterization using small angle neutron scattering (Koshari et al., 2018). The broken rod model, however, demonstrated a superior fit to experimental data (Fig. II.1.6A) (a comparison to other models is shown in the supplementary information, Supplementary Table II.S.2 and Supplementary Fig. II.S.5).

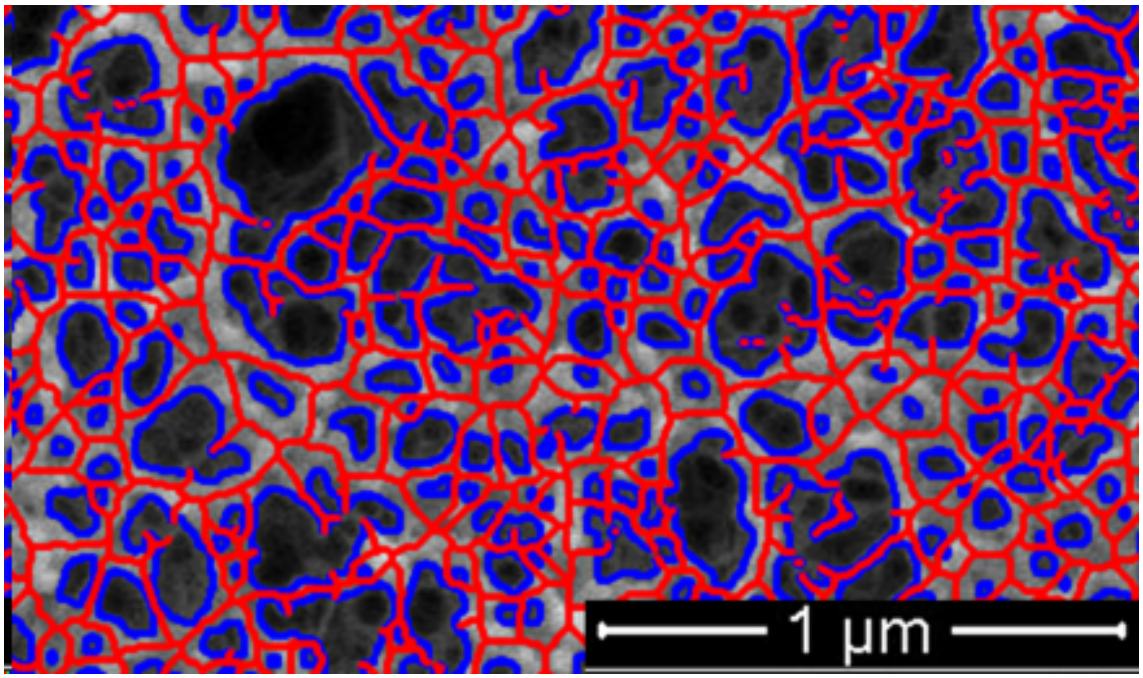

Figure II.1.5 - Visual representation of the broken rod model for an agarose network with infinitely long fibers cross-linked to create junctions. Red, center of agarose fibers in the first plane; blue, edges of fibers.

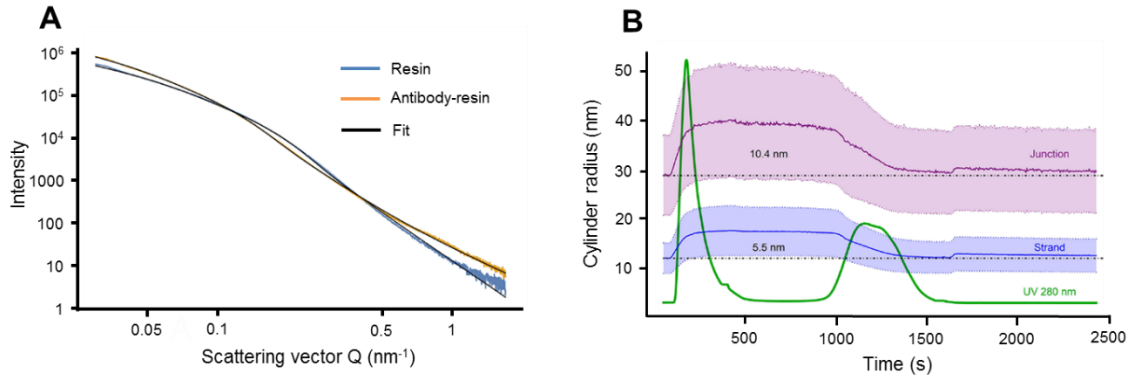

Figure II.1.6 - A: Fit of broken rod model (black) to corresponding scattering profiles. Due to good agreement between data and fit it lays directly on top of the data points. B: Evolution of the radii of strands (blue) and junctions (purple) with their corresponding size distribution during a protein-A chromatography run.

1.3.4.3. Protein layer thickness

The broken rod model was used to quantitatively evaluate the evolution of resin strand and junction thickness during adsorption and desorption in the chromatography run. According to the broken rod model, the antibody-free MabSelect SuRe resin is characterized by an average cylinder radius of 11.8 and 28.6 nm for agarose strands and junctions, respectively for all performed measurements, which is in a good agreement with both the literature (Nweke et al., 2017) and visual examination of SEM micrographs (Fig. II.1.4A). Upon saturation of the chromatographic resin with an antibody solution, as indicated by the first peak in the UV

spectrum (Fig. II.1.2A), the agarose strand radius increased 250 s after the protein injection, and then plateaued until protein elution. The difference in the values between antibody-free and saturated agarose strands of 5.5 nm (Table II.1.1) was attributed to so-called protein layer thickness, an important mechanistic parameter that could potentially indicate a change in the conformation of the adsorbed protein or in the protein orientation within the layer. The resulting protein layer thickness for junctions was calculated as being almost twice as long. The difference in protein layer thickness for strands and junctions could be explained by a steric hindrance effect in which cross-linked strands block certain positions of the antibody-protein-A complex, promoting antibody binding to protein-A ligand units further away from the surface of junctions. As presented in Fig. II.1.6B, values for the strand and junction radii gradually return to their initial values due to subsequent elution steps. Therefore, performing measurements in flow instead of batch mode, we not only assessed native process conditions, but also examined both adsorption and desorption structural changes on nanometer scale.

Table II.1.1 - Comparison of the radii of strands and junctions according to the broken rod model and resulting protein layer thickness.

	Strand radius ± distribution, nm	**Junction radius ± distribution, nm**
Antibody-free resin	11.8±3.1	28.7±8.1
Saturated MabSelect SuRe resin	17.3±5.0	39.1±11.2
Resulting protein layer thickness	5.5±5.9	10.4±13.8

The broken rod model readily provides insight into the protein layer thickness and its kinetics in the MabSelect SuRe resin system. The model also allows speculation about the structural changes within a very complex system. We suggest the following structural interpretation of the protein layer thickness results (Fig. II.1.7). Agarose strands (11 nm mean radius) are grafted with protein-A tetramer ligands, which have a length of approximately 10 nm when stretched (single unit of *Staphylococcus aureus* protein-A has a length of 3 nm, PDB:1BDD (Gouda et al., 1992)). According to the broken rod model, the radius of antibody-free MabSelect SuRe strands is 11.8 ± 3.1 nm; thus, protein-A ligands contribute only slightly, if at all, to the strand thickness derived from the SAXS scattering profile. A possible explanation would be a relatively low spatial grafting density of protein-A ligands on top of the agarose strand surface. Moreover, a high degree of ligand flexibility can smear the protein-A contribution to the resulting SAXS scattering profiles. When saturated, the MabSelect SuRe strand radius increases to 17.3 ± 5.0 nm. The resulting protein layer thickness is caused by the attachment of antibody moieties to protein-A ligand units via Fc-mediated binding, which stiffens their structure. Knowing the amount of protein adsorbed (the elution peak area from the chromatograph), the binding capacity is calculated to be ~35 mg of antibodies per milliliter

of MabSelect SuRe resin. Taking into account molecular weights of 150 and 26.7 kDa for monoclonal antibody and protein-A ligand, respectively, we estimate 1.2 molecules of antibodies bound to each protein-A ligand tetramer (taking 5.6 mg of protein-A ligand per milliliter of MabSelect SuRe resin) (Hans J. Johansson, 2009; Weinberg et al., 2017). Therefore, we conclude that there are 10 possible binding configurations for one or two antibodies in complex with protein-A ligand, which explains the slightly greater distribution of sizes for agarose strands when saturated with antibodies. The resulting protein layer thickness of 5.5 ± 5.9 nm is well below the average diameter of IgG1 protein (11.5 nm, PDB: 1HZH) (Saphire et al., 2001).

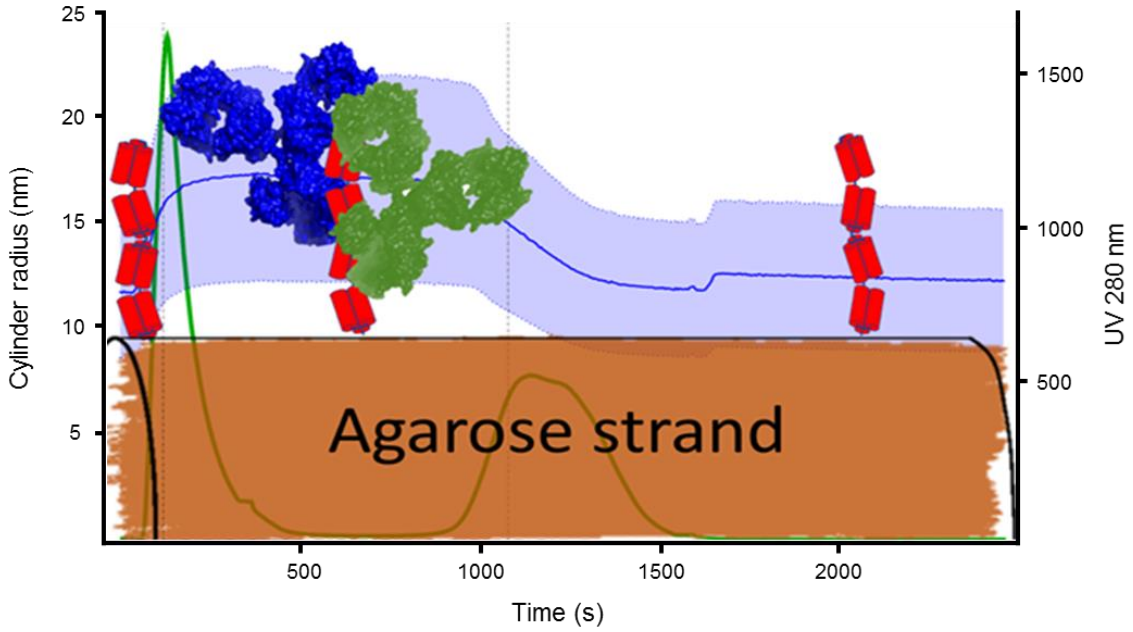

Figure II.1.7 - Structural interpretation of protein layer thickness development throughout the protein-A chromatography run. Protein-A ligand tetramers (in red) are attached to the agarose strand (orange). All entities are in scale to facilitate size comparison.

The distribution indicates that there are places on agarose strands at which no protein is present, up to a protein layer thickness of approximately 12 nm, matching the width of IgG. Potentially, the above consideration would suggest that antibodies are positioned in proximity to and facing the agarose fiber surface, so that we are probing the thickness and not the length of the antibody. However, the significant size distribution of protein layer thickness derived from the additive nature of combining distributions ($(\sigma_z)^2 = (\sigma_1)^2 + (\sigma_2)^2$) would also allow other configurations with antibodies positioned side-on close to the surface, but tilted, though there is a lower probability of their occurrence. To position antibody parallel to an agarose strand in proximity of the surface, the antibody-protein-A complex has to possess high bending and rotation freedom, which would only be possible if the antibody is bound to the outermost units of a protein-A ligand tetramer. Similar observations were made using neutron reflectivity to measure protein-A-antibody complex distance on a silica surface (Mazzer et al., 2017); Mazzer

et al. suggested that two IgG molecules are bound to a protein-A tetramer ligand with "a somewhat skewed orientation and close proximity to the silica surface". They also concluded that antibody was bound to the protein-A ligand tetramer domain in a side-on to tilted orientation further from the silica interface. Having similar conclusions to ours, Mazzer's work strengthens our reasoning, especially as they worked in the idealized and therefore easier to characterize environment in batch mode with protein-A ligands immobilized on silicon wafer instead of native chromatography resin under flow conditions.

The nature of junctions is harder to decipher, as they are less consistent in shape and size and we do not know if the protein-A ligand grafting density is the same as for strands. Thus, junctions have a considerable size distribution of 28.7 ± 8.1 nm, which is even higher when junction ligands are saturated with antibodies (39.1 ± 11.2 nm). Therefore, the protein layer thickness for a junction is 10.4 ± 13.8 nm, approximately twice as thick as strands. The above data are suggestive of a different profile of the antibody-protein-A ligand complex structure for many ligands available on the surface of junctions compared to those on strands. Some of the ligand units may not be available for antibody binding due to a steric hindrance effect of cross-linking strands blocking likely more energetically favorable binding sites, which would explain different sizes and the substantial size distribution of junction protein layer thickness.

A small angle scattering investigation on the similar agarose-based chromatography resin was reported by Koshari et al. (Koshari et al., 2018), where they investigated among others SP Sepharose FF resin using neutrons. SP Sepharose FF is a cation exchanger resin based on 4% cross-linked agarose like the backbone of MabSelect SuRe resin, therefore one would expect similar scattering profiles and subsequent structural parameters for both of them. However, both the applied methodology and results show significant discrepancies between our work and Koshari's. Koshari used polydisperse cylinder model resulting in mean cylinder radii of around 1 nm reasoning it to be a rigid single or double helices from agarose within strand, whereas with the broken rod model we obtained a strand radius of almost 12 nm, which is in hand with literature and SEM investigation. Moreover, within the broken rod model we assumed not only infinitely long cylinders instead of artificially setting them to 1000 nm in length, but also used two populations of cylinders to account for junctions which played important role in the architecture of cross-linked agarose beads. This resulted in a better fit of the model to the data as visually compared to fits reported in Koshari's paper and more consistent results of strands and junctions' radii. It should be noted, however, that Koshari et al. did their study with SANS, while ours was performed with SAXS; therefore, the different size of the observed resin fibrils/strands might be due to the different contrast for neutrons and x-rays, in particular since they used D_2O as a solvent, thus potentially enhancing the contrast between individual fibrils (single or double helices) within a single resin strand.

Irrespective of the applied model, the agarose network with its stands and junctions exhibit a quite distinctive surface topology with two different adsorption sites showing layers of different thickness. The developed methodology could be applied to any other

chromatography method such as ion-exchange, hydrophobic interaction or multimodal chromatography with agarose backbone.

1.4. Conclusions

Using a simple fitting routine without any further modeling can follow the structural changes occurring in situ in a miniaturized chromatography column. An entire chromatography run from equilibration, through loading and washing, to elution can be observed in-situ under native conditions using SAXS as a probing method. Moreover, based on the SEM micrographs, we created a model allowing us to characterize the internal structure of the MabSelect SuRe agarose network with infinitely long cross-linked cylinders of characteristic thickness representing strands and junctions within the system. We monitored the development of the radii of these cylinders throughout a protein-A chromatography run and found that the agarose strands have an average radius of 11.8 nm, while upon saturation with antibodies the difference was identified as the protein layer thickness (5.5 nm and 10.4 nm for strands and junctions respectively). Based on the information on the system's components and parameters, we hypothesize that an average 1.2 antibodies are bound to each protein-A ligand tetramer. Most likely, they are bound to the outermost units within tetramer ligands from the agarose surface and the whole complex is parallel to the surface in its proximity, where we probed the antibody thickness in side-on or tilted orientation.

1.5 References

Blanchet, C. E., & Svergun, D. I. (2013). Small-Angle X-Ray Scattering on Biological Macromolecules and Nanocomposites in Solution. In Annual Review of Physical Chemistry, Vol 64, ed. M. A. Johnson and T. J. Martinez. Palo Alto: Annual Reviews.

Boschetti, E., & Jungbauer, A. (2000). Separation of antibodies by liquid chromatography. Vol. 2.

Brookes, E., Perez, J., Cardinali, B., Profumo, A., Vachette, P., & Rocco., M. (2013). Fibrinogen species as resolved by HPLC-SAXS data processing within the UltraScan Solution Modeler (US-SOMO) enhanced SAS module. J Appl Crystallogr 46 (6):1823-33.

de Coelho Escobar, C., & dos Santos., J. H. (2014). Effect of the sol-gel route on the textural characteristics of silica imprinted with Rhodamine B. J Sep Sci 37 (7):868-75.

Deis, L. N., Wu, Q., Wang, Y., Qi, Y., Daniels, K. G., Zhou, P., & Oas., T. G. (2015). Suppression of conformational heterogeneity at a protein-protein interface. Proceedings of the National Academy of Sciences-Biological Sciences 112 (29):9028-33.

Deisenhofer, J. (1981). Crystallographic refinement and atomic models of a human Fc fragment and its complex with fragment B of protein A from Staphylococcus aureus at 2.9- and 2.8-A resolution. Biochemistry 20 (9):2361-70.

Ehmann, H. M. A., Werzer, O., Pachmajer, S., Mohan, T., Amenitsch, H., Resel, R., Kornherr, A., Stana-Kleinschek, K., Kontturi, E., & Spirk., S. (2015). Surface-Sensitive Approach to Interpreting Supramolecular Rearrangements in Cellulose by Synchrotron Grazing Incidence Small-Angle X-ray Scattering. Acs Macro Letters 4 (7):713-6.

Gerontas, S., Shapiro, M. S., & Bracewell., D. G (2013). Chromatography modelling to describe protein adsorption at bead level. Journal of Chromatography A 1284:44-52.

Ghose, S., Hubbard, B., & Cramer., S. M. (2007). Binding capacity differences for antibodies and Fc-fusion proteins on protein A chromatographic materials. Biotechnology and Bioengineering 96 (4):768-79.

Ghose, S., Zhang, J., Conley, L., Caple, R., Williams, K. P. & Cecchini., D. (2014). Maximizing Binding Capacity for Protein A Chromatography. Biotechnology Progress 30 (6):1335-40.

Gouda, H., Torigoe, H., Saito, A., Sato, M., Arata, Y., & Shimada., I. (1992). 3-Dimensional solution structure of the B-domain of Staphylococcal Protein-A – Comparisons of the solution and crystal structures. Biochemistry 31 (40):9665-72.

Graille, M., Stura, E. A., Corper, A. L., Sutton, B. J., Taussig, M. J., Charbonnier, J. B., & Silverman., G. J. (2000). Crystal structure of a Staphylococcus aureus protein A domain complexed with the Fab fragment of a human IgM antibody: structural basis for recognition of B-cell receptors and superantigen activity. Proceedings of the National Academy of Sciences of the United States of America-Biological Sciences 97 (10):5399-404.

Guenet, J.-M. (1992). Thermoreversible Gelation of Polymers and Biopolymers. London: Academic Press.

Johansson, H. J., Ljunglöf, A., & Palmgren, R. (2009). Affinity chromatography matrix. ed. O. A. G. H. B.-S. Ab.

Iyer, H., Tapper, S., Lester, P., Wolk, B. & van Reis., R. (1999). Use of the steric mass action model in ion-exchange chromatographic process development. Journal of Chromatography A 832 (1):1-9.

Jungbauer, A., & Hahn, R. (2004). Engineering protein A affinity chromatography. Current opinion in drug discovery & development 7 (2):248-56.

Koshari, S. H. S., Wagner, N. J. & Lenhoff., A. M. (2018). Effects of Resin Architecture and Protein Size on Nanoscale Protein Distribution in Ion-Exchange Media. Langmuir 34 (2):673-84.

Kulsing, C., Komaromy, A. Z., Boysen, R. I. & Hearn., M. T. (2016). On-line determination by small angle X-ray scattering of the shape of hen egg white lysozyme immediately following elution from a hydrophobic interaction chromatography column. Analyst 141 (20):5810-4.

Lofdahl, S., Guss, B., Uhlen, M., Philipson, L. & Lindberg., M. (1983). "Gene for Staphylococcal Protein-A." Proceedings of the National Academy of Sciences of the United States of America-Biological Sciences 80 (3):697-701.

Maeda, H., Yuguchi, Y., Kitamura, S., Urakawa, H., Kajiwara, K., Richtering, W., Fuchs, T., & Burchard, W. (1999). Structural aspect of gelation in schizophyllan/sorbitol aqueous solution. Polymer Journal 31 (6):530-4.

Mallik, R., & Hage., D. S. (2006). Affinity monolith chromatography. Journal of Separation Science 29 (12):1686-704.

Mazzer, A. R., Clifton, L. A., Perevozchikova, T., Butler, P. D., Roberts, C. J., & Bracewell, D. G. (2017). Neutron reflectivity measurement of protein A-antibody complex at the solid-liquid interface. Journal of Chromatography A 1499:118-31.

Muller, E., & Vajda, J. (2016). Routes to improve binding capacities of affinity resins demonstrated for Protein A chromatography. Journal of Chromatography B-Analytical Technologies in the Biomedical and Life Sciences 1021:159-68.

Nweke, M. C., M. Turmaine, R. G. McCartney, and D. G. Bracewell. 2017. Drying techniques for the visualization of agarose-based chromatography media by scanning electron microscopy. Biotechnology Journal 12 (3):5.

O'Brien, D. P., Brier, S., Ladant, D., Durand, D., Chenal, A., & Vachette, P. (2018). SEC-SAXS and HDX-MS: A powerful combination. The case of the calcium-binding domain of a bacterial toxin. Biotechnology and Applied Biochemistry 65 (1):62-8.

Glatter O, & Kratky O. (1982). Small Angle X-ray Scattering. London: Academin Press.

Orellana, C. A., Shene, C., & Asenjo, J. A. (2009). Mathematical modeling of elution curves for a protein mixture in ion exchange chromatography applied to high protein concentration. Biotechnology and Bioengineering 104 (3):572-81.

Pernot, P., Round, A., Barrett, R., Antolinos, A. D., Gobbo, A., Gordon, E., Huet, J., Kieffer, J., Lentini, M., Mattenet, M., Morawe, C., Mueller-Dieckmann, C., Ohlsson, S., Schmid, W., Surr, J., Theveneau, P., Zerrad, L., & McSweeney S. (2013). Upgraded ESRF BM29

beamline for SAXS on macromolecules in solution. Journal of Synchrotron Radiation 20:660-4.

Pilz, I., Schwarz, E., Durchschein, W., Licht, A., & M. Sela, M. (1980). Effect of cleaving interchain disulfide bridges on the radius of gyration and maximum length of anti-poly(D-Alanyl) antibodies before and after reaction with tetraalanine hapten. Proceedings of the National Academy of Sciences of the United States of America-Biological Sciences 77 (1):117-21.

Portale, G., Cavallo, D., Alfonso, G. C., Hermida-Merino, D., van Drongelen, M., Balzano, L., Peters, G. W. M., Goossens, J. G. P., & Bras. W. (2013). Polymer crystallization studies under processing-relevant conditions at the SAXS/WAXS DUBBLE beamline at the ESRF. Journal of Applied Crystallography 46:1681-9.

Rabe, M., Verdes, D., & Seeger S. (2011). Understanding protein adsorption phenomena at solid surfaces. Advances in Colloid and Interface Science 162 (1-2):87-106.

Ryan, T. M., Trewhella, J., Murphy, J.M., Keown, J. R., Casey, L., Pearce, F. G., Goldstone, D. C., Chen, K., Luo, Z., Kobe, B., McDevitt, C. A., Watkin, S. A., Hawley, A. M., Mudie, S. T., Boban, V. S., & Kirby, N. (2018). An optimized SEC-SAXS system enabling high X-ray dose for rapid SAXS assessment with correlated UV measurements for biomolecular structure analysis. Journal of Applied Crystallography 51 (1):97-111.

Saphire, E. O., Parren, P., Pantophlet, R., Zwick, M. B., Morris, G. M., Rudd, P. M., Dwek, R. A., Stanfield, R. L., Burton, D. R., & Wilson, I. A. (2001). Crystal structure of a neutralizing human IgG against HIV-1: A template for vaccine design. Science 293 (5532):1155-9.

Sauer-Eriksson, A. E., Kleywegt, G. J., Uhlen, M., & Jones, T. A. (1995). Crystal structure of the C2 fragment of streptococcal protein G in complex with the Fc domain of human IgG. Structure 3 (3):265-78.

Stokke, B. T., Draget, K. I., Smidsrod, O., Yuguchi, Y., Urakawa, H., & Kajiwara, K. (2000). Small-angle X-ray scattering and rheological characterization of alginate gels. 1. Ca-alginate gels. Macromolecules 33 (5):1853-63.

Vogler, E. A. (2012). Protein adsorption in three dimensions. Biomaterials 33 (5):1201-37.

Weinberg, J., Zhang, S., Crews, G., Healy, E., Carta, G., & Przybycien, T. (2017). Polyclonal and monoclonal IgG binding on protein A resins-Evidence of competitive binding effects. Biotechnol Bioeng 114 (8):1803-12.

Wolfram Research, Inc. 2018. Mathematica. Champaign, Illinois: Wolfram Research, Inc.

Yuguchi, Y., Hasegawa, A., Padol, A. M., Draget, K. I., & Stokke, B. T. (2016). Local structure of Ca2+ induced hydrogels of alginate-oligoguluronate blends determined by small-angle-X-ray scattering. Carbohydrate Polymers 152:532-40.

Yuguchi, Y., Urakawa, H., Kajiwara, K., Draget, K. I., & Stokke., B. T. (2000). Small-angle X-ray scattering and rheological characterization of alginate gels. 2. Time-resolved studies on ionotropic gels. Journal of Molecular Structure 554 (1):21-34.

1.6 Supplementary Information

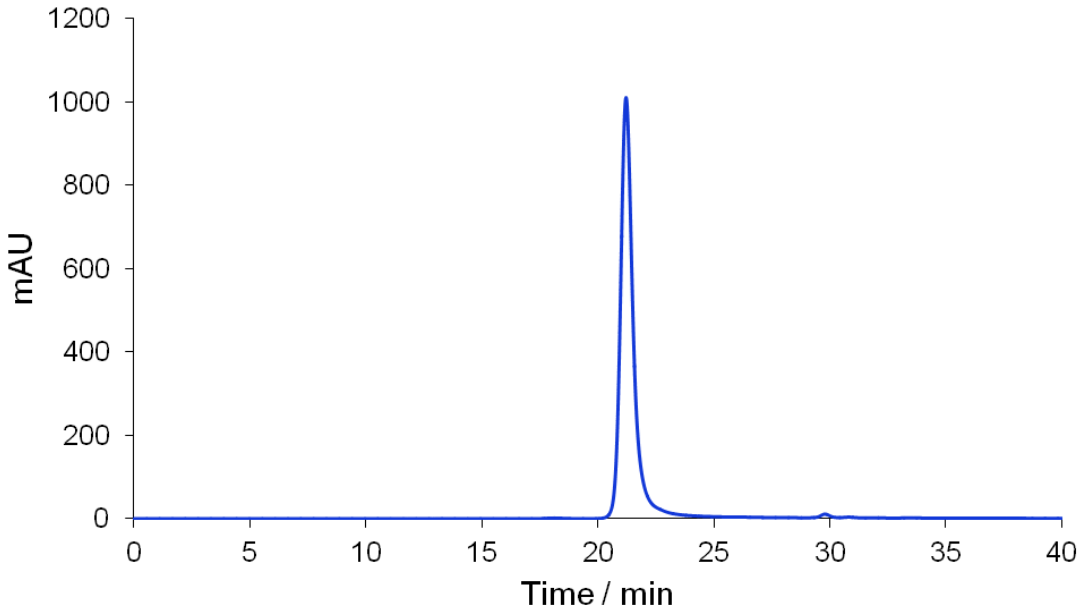

Figure II.S.1 - Size exclusion chromatography of Herceptin solution showing single peak, which indicates that used antibody solution was monomeric.

Table II.S.1 - A default program for protein-A chromatography runs. CV stands for column volume, %B means percentage of elution buffer in the flow. Scattering profiles were collected every second throughout the run. Change to A and B means rapid flush of the pump with corresponding buffer A- running buffer, B- elution buffer. It was implemented into the system due to low flow rates that prevent fast exchange of the pump volume.

	cv	volume [mL]	time [s]	accumulative time [s]	%B
equilibration	4	0.8	4	0	0
loading		0.25	1.25	4	0
washing	4	0.8	4	5.25	0
change to B	5	1	5	9.25	100
elution	15	3	15	14.25	100
change to A			0.1	29.25	0
equilibration	15	3	15	29.35	0
end				44.35	0
				2661	

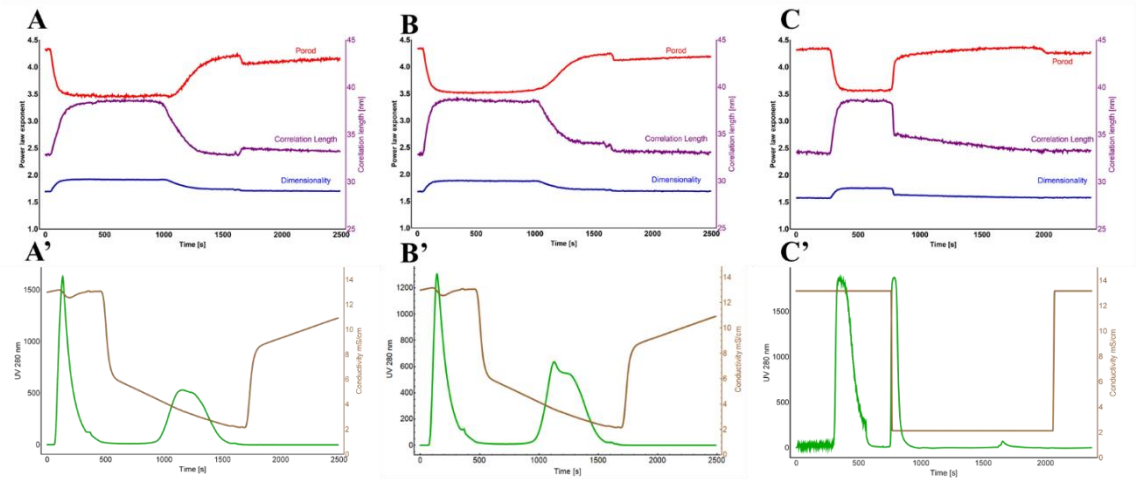

Figure II.S.2 - Comparison of protein-A runs A,B from BM26B beamline and C from BM29 at ESRF, France. Top panel presents fitting parameters like Porod exponent (red), correlation length (purple) and dimensionality (blue), whereas bottom panel shows corresponding UV 280 nm signal (green) and conductivity (brown). Note, that different chromatography system used at BM29 resulted in different spreading of the features in chromatograph, but similar values for Power law fitting.

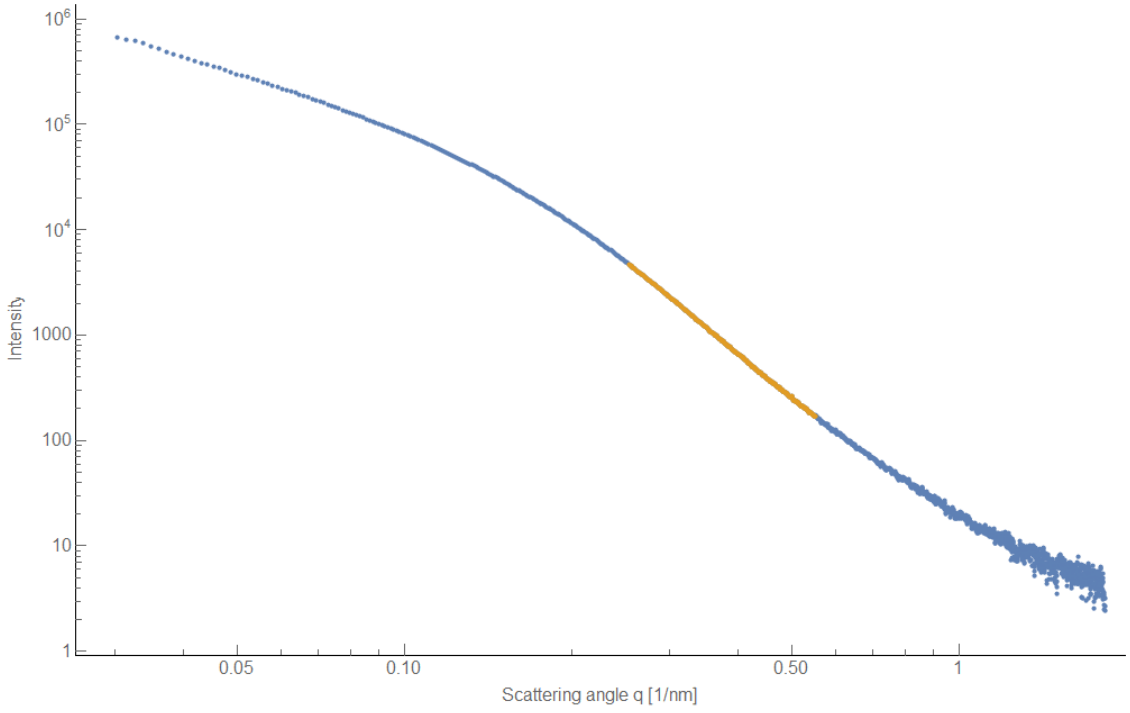

Figure II.S.3 - Scattering profile for antibody-free MabSelect SuRe resin in blue, region where Porod was fitted in orange.

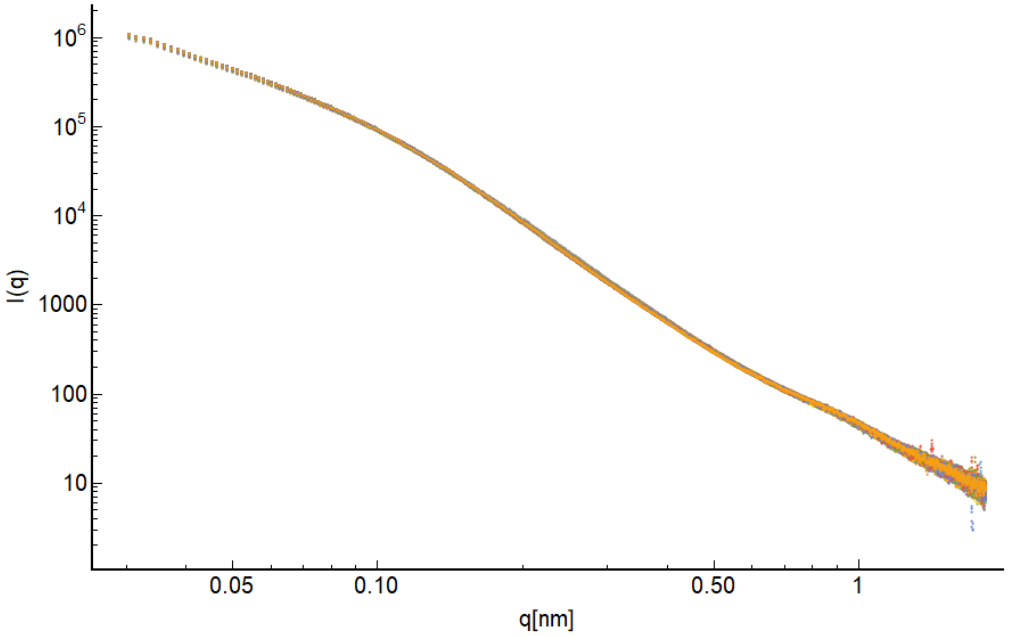

Figure II.S.4 - Overlay of scattering profiles from 125s to 1000 s every 10 s. The peak for the overload in UV is visible at 132s. No difference is seen between the scattering patterns during overloading, which indicates that freely floating monoclonal antibodies are not visible in our SAXS signal due to the low concentration in bulk solution.

Table II.S.2 - Summary of data modelling with various models representing Chi^2 analysis and resulting radii.

	Antibody-free MabSelect			Saturated MabSelect SuRe		
	radius 1	radius 2	chi^2	radius 1	radius 2	chi^2
Broken rod	11.8	28.7	53.3	17.3	39.1	2.2
two 1000 nm cylinders with distribution	7.1	32.8	168	337.3	59.8	537.8
single 1000 nm cylinder with distribution	15	-	164.6	185.2	-	816.7

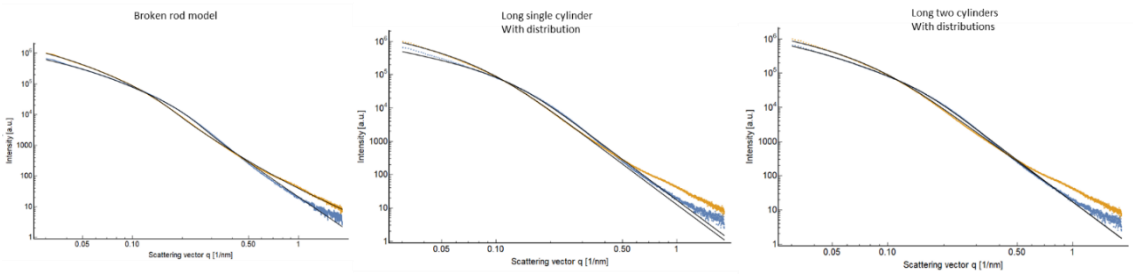

Figure II.S.5 - Comparison of different model fits (in black) to Antibody-free (blue) and Saturated (orange) MabSelect SuRe resin scattering profiles.

2. Publication II

Antibody binding heterogeneity of Protein A resins

Gonçalo Fradique Lopes da Silva,[1,2,3] | Jacek Plewka,[3,4] | Rupert Tscheließnig,[3,5] | Helga Lichtenegger,[3,4] | Alois Jungbauer,[3,5] | Ana Cristina Mendes Dias-Cabral,[1,2]

[1]CICS-UBI – Health Sciences Research Centre, University of Beira Interior, Av. Infante D. Henrique, 6201-001 Covilhã, Portugal
[2]Department of Chemistry, University of Beira Interior, R. Marquês d'Ávila e Bolama, 6201-001 Covilhã, Portugal
[3]Austrian Centre of Industrial Biotechnology, Muthgasse 18, 1190 Vienna, Austria
[4]Department of Material Science and Process Engineering, University of Natural Resources and Life Sciences, Peter-Jordan Strasse 82, 1190 Vienna, Austria
[5]Department of Biotechnology, University of Natural Resources and Life Sciences, Muthgasse 18, 1190 Vienna, Austria

Corresponding author

Cristina Dias-Cabral: CICS-UBI – Health Sciences Research Centre, University of Beira Interior, Av. Infante D. Henrique, 6201-001 Covilhã, Portugal;
Email: ccabral@fcsaude.ubi.pt

Funding information

Austrian Research Promotion Agency FFG – grant number 824186
Fundação para a Ciência e Tecnologia in Portugal – grant number SFRH/BD/104498/2014

Abstract

Protein A affinity chromatography is a core unit operation in antibody manufacturing. Nevertheless, there is not enough understanding of in-column antibody adsorption in the Protein A capture step. This work aims to investigate in situ the establishment of an antibody (trastuzumab) layer during Protein A chromatography both in terms of energetic contributions and uptake kinetics. Flow microcalorimetry is employed as a technique with an in situ operating detector which provides understanding on the thermodynamics of the adsorption process. In addition, the antibody uptake rate is also investigated in order to establish a correlation between its diffusion on the stationary phase and the associated thermodynamics. Two resins with different particle sizes, intraparticle porosities, and Protein A ligand structure were studied: the synthetically engineered B-domain tetrameric MabSelect SuRe and synthetically engineered C-domain hexameric TOYOPEARL AF-rProtein A HC. The uptake rate follows a pore diffusion model at low equilibrium time, showing a slower diffusivity after a certain time because of the heterogenous binding nature of these two resins. In addition, the microcalorimetric studies show that adsorption enthalpy is highly favourable at low isotherm concentrations and evolves towards an equilibrium with the increasing of surface concentration. These data suggest that the relationship between adsorption enthalpy and the establishment of the antibody layer in the Protein A chain is consistent with heterogeneous adsorption.

Keywords

Monoclonal antibodies, affinity chromatography, Protein A, adsorption enthalpy, flow microcalorimetry, uptake kinetics

Acknowledgements

This work has been supported by the Federal Ministry of Science, Research and Economy (BMWFW), the Federal Ministry of Traffic, Innovation and Technology (bmvit), the Styrian Business Promotion Agency SFG, the Standortagentur Tirol, the Government of Lower Austria and ZIT - Technology Agency of the City of Vienna through the COMET-Funding Program managed by the Austrian Research Promotion Agency FFG.

This work was carried out in cooperation with Boehringer Ingelheim RCV, Process Science, and Novartis/Sandoz.

G.L.S. acknowledges his doctoral fellowship SFRH/BD/104498/2014 to Fundação para a Ciência e Tecnologia in Portugal.

Conflict of interest statement

There is no conflict of interest.

2.1. Introduction

Monoclonal antibodies are an ever-growing market, representing already nearly half of the total sales of biopharmaceuticals (Ecker, Jones, & Levine, 2015; Morrison & Lähteenmäki, 2017). Protein A affinity chromatography is by far the most important and most frequently applied chromatography step in manufacturing biopharmaceuticals, being a core technology in downstearm processing of antibodies, Fc fusion proteins and antibody fragments (Shukla, Hubbard, Tressel, Guhan, & Low, 2007). The method is popular due to its high selectivity, high capacity, and robustness (Hober, Nord, & Linhult, 2007; Shukla et al., 2007). Several decades of development maturated the available materials and protocols. Originally, wild type Staphylococcal protein A composed of five different antibody-binding domains (A, B, C, D, E) was immobilized and used for affinity capture (Boyle, 1990; Uhlén et al., 1984). Currently, also engineered variants are available, with improved alkaline stability. Two of the most popular ones are the tetrametric Z form derived from the B-domain, and the hexameric Y-domain, a mutant from the C-domain. Each domain consists of three α-helices, which bind to the CH2 region in the Fc part of the antibody (DeLano, Ultsch, de Vos, & Wells, 2000; Salvalaglio, Zamolo, Busini, Moscatelli, & Cavallotti, 2009).

At ligand saturation, 2-3 of these binding sites or domains are occupied (Ghose, Hubbard, & Cramer, 2007). Attempts have been made with molecular dynamics simulation to understand the steric hindrance, as accessibility of the sites affects the antibody binding process/kinetics (Salvalaglio et al., 2009; Yu et al., 2016). It has been proposed that mainly interactions of hydrophobic nature, salt bridges and hydrogen bonding contribute to binding to Protein A (Ghose, Allen, Hubbard, Brooks, & Cramer, 2005; Li, Dowd, Stewart, Burton, & Lowe, 1998). There are also reports stating that the antibody undergoes a slight conformational change during the interaction with the Protein A ligand (Gagnon, Nian, Leong, & Hoi, 2015; Mazzer, Perraud, Halley, O'Hara, & Bracewell, 2015). Thus, it is clear that several sub-processes are involved in antibodies binding to Protein A ligands (Lin, Chen, & Hearn, 2002). Besides the adsorption process itself, which may involve desolvation of both protein and ligand before the favourable interaction, conformational changes also have an effect in binding.

Thermodynamic analyses of biomolecule adsorption have been facilitating the elucidation of complex adsorption mechanisms. Often neglected, enthalpy was proven to be highly dependent on the loading/saturation of the surface. It has also been observed that after adsorption on ion exchange and hydrophobic interaction chromatography, protein rearranges at the surface and a strong entropic contribution, depending on the system, may be involved (Lin et al., 2002; Ueberbacher, Rodler, Hahn, & Jungbauer, 2010).

To provide insight into the thermodynamic properties of adsorption processes, microcalorimetric methods have been proven to be reliable methodologies. Mainly two techniques have been used for this purpose: isothermal titration calorimetry (ITC) and flow microcalorimetry (FMC). The adsorption enthalpy, measured by ITC offers an excellent insight into the binding strength, however further information cannot be inferred. FMC on the other

hand, is able, to some extent, to dissect the sub-processes involved in the interaction between the biomolecule and the resin and as a consequence to discriminate between different energy sources. The technique has been used, with good results, to study the adsorption thermodynamics of biomolecules on ion exchange (Silva, Marques, Thrash, & Dias-Cabral, 2014), hydrophobic interaction (Aguilar, Twarda, Sousa, & Dias-Cabral, 2014) and mixed-mode chromatography (Rosa, da Silva, Aires-Barros, Dias-Cabral, & Azevedo, 2018). Flow microcalorimetry simulates lab-scale chromatography and implies that the system is in equilibrium. The adsorption process, the rearrangement of water molecules, the alteration of protein conformation, the reorientation of the protein molecules at the surface, the desolvation of proteins and ions are some of the major contributors to the heat exchange associated with the overall adsorption process. These different energy sources can be dissected and accounted for (Lin et al., 2002). The fact that flow microcalorimetry considers mass transfer implications for simulating a dynamic chromatography system allows it to be on the cutting-edge of online and in situ monitoring of an adsorptive process. With the use of flow microcalorimetry we are one step closer to understanding how the adsorption enthalpy changes with the loading concentration and how thermodynamics of these processes are influenced by the type of resin, both under linear and overloaded conditions.

Combining together the data provided by FMC, equilibrium binding (adsorption isotherm), and uptake kinetics, the antibody-Protein A binding process is characterized. We have selected two of the most important commercially available Protein A chromatography media: MabSelect SuRe and TOYOPEARL AF-rProtein A HC to determine the thermodynamic parameters for antibody-Protein A interaction. Mabselect SuRe is an alkaline stable tetramer and TOYOPEARL AF-rProtein A HC an alkaline stable hexamer. The ligands are immobilized on crosslinked agarose (MabSelect SuRe) or a methacrylate polymer bead (TOYOPEARL). In addition to the different ligand structure, these two resins differ in average particle size; MabSelect SuRe 85 μm and TOYOPEARL AF-rProtein A HC 45 μm, which has a great influence in the uptake kinetics (Tao, Perez-Almodovar, Carta, Ferreira, & Robbins, 2011). The antibody binding kinetics to the Protein A ligands is reported as diffusional mass transfer controlled (Hahn et al., 2005). The formation of antibody-Protein A complex and the displacement kinetics is limited by pore diffusion (Perez-Almodovar & Carta, 2009; Tao et al., 2011).

2.2. Materials and Methods

2.2.1. Materials

The monoclonal antibody trastuzumab was purchased from Roche (Basel, Switzerland) (Lot. B1050B07). All the following reagents were purchased from MilliporeSigma (Burlington, MA, USA): sodium phosphate dibasic (Na2HPO.2H2O) (Lot.K450726804049), sodium dihydrogen phosphate (NaH2PO.2H2O), (Lot.K93717142706), glycine (C2H5NO2) (Lot.VP614601407), and sodium chloride (NaCl) (Lot.K48705904713).

2.2.2. Adsorption isotherms

The adsorption isotherms were measured by mass balance determination after 24 hours incubation of antibody in MabSelect SuRe (GE Healthcare, Uppsala, Sweden) (Lot. 10247535) and TOYOPEARL AF-rProtein A HC-650F (Tosoh, Tokyo, Japan) (Lot. 65RPHFA02Y) resins. The incubation was conducted in a 96-multi well plate (Greiner, Kremsmünster, Austria). The resin volume was 0.025 mL and the volume of a protein stock was adjusted with Na-phosphate buffer 0.02 M + NaCl 0.15 M at pH 7.4 in each well to reach the concentration range 0.01-10 $mg.mL^{-1}$ in a final bulk volume of 0.25 mL. The samples were incubated for 24 h in a thermomixer (Thermo Fisher Scientific, Waltham, MA, USA) at 20 ºC and 900 rpm. After incubation, the supernatant was filtered with HPLC-grade Millex-GV syringe filter (PVDF membrane pore size: 0.22 µm) (MilliporeSigma) and the equilibrium bulk protein concentration was measured at Abs 280 nm using a UV plate reader (Tecan, Männedorf, Switzerland).

2.2.3. Batch uptake kinetics

The antibody uptake as function of time by MabSelect SuRe and TOYOPEARL AF-rProtein A HC was obtained in agitated vessels. A slurry of 50% resin was prepared in Na-phosphate buffer 0.02 M + NaCl 0.15 M at pH 7.4 and 0.25 mL of slurry added to every vessel. Two initial protein phase concentrations were studied: C_0 = 0.75 $mg.mL^{-1}$ and C_0 = 1.5 $mg.mL^{-1}$. The solution volume was respectively 20 mL and 10 mL. The suspensions were recirculated for 24 h at 200 rpm and the bulk protein concentration was measured by recirculating the sample through the U9-L UV monitor of an ÄKTA Pure (GE Healthcare).

2.2.4. Flow Microcalorimetry

The heat exchange experiments of antibody adsorption on Protein A resins were conducted in a flow microcalorimeter (Microscal FMC 4 Vi, Microscal Limited, London, UK). The microcalorimeter contains a 0.171 mL cell that was packed as a standard chromatography column with the MabSelect SuRe and TOOYPEARL AF-rProtein A HC resins in Na-phosphate buffer 0.02 M + NaCl 0.15 M at pH 7.4 (running buffer). The cell is coupled with two thermistors sensitive enough to detect the power change (µW) occurring during the adsorption process. The operating temperature was 25±1 ºC. The system was equilibrated with running buffer at 1.5 $mL.h^{-1}$ during 10 CV. The antibody feed concentrations ranged from 1 to 30 $mg.mL^{-1}$, resulting in loadings up to 27 $mg.mL^{-1}$ packed bed for MabSelect SuRe and up to 17 $mg.mL^{-1}$ for TOYOPEARL AF-rProtein A HC. The injection volume was 0.1 mL in every experiment. During the process the thermistors detect a change in potential, convert it into power and transmit it to the software (CALDOS 4, Microscal Limited) which records the thermogram signal along the time span of the process (the calorimeter is operated in the heat conduction mode). After injection and binding, a washing step is carried with high salt buffer (Na-phosphate buffer 0.02

M + NaCl 2 M pH 7.4), followed by elution at low pH (glycine 0.1 M pH 3.0). The sanitization process was carried with NaOH 0.1 M, followed by ultrapure water and ethanol 20%.

2.2.5. HPLC analysis

Antibody concentration was measured using a CIM® n-Protein A monolith disk (BIA Separations, Ajdovščina, Slovenia), 12.0 mm ID × 3.0 mm, in a HPLC system (Shimadzu LC-2010A HT, Kyoto, Japan). The system was equilibrated with Na-phosphate buffer 0.03 M + NaCl 1 M pH 7.5 during 10 CV. The injection volume was 0.1 mL and elution was carried with HCl pH 2 in a step gradient during 20 CV.

2.3. Results and Discussion

2.3.1. Langmuir adsorption isotherms

The adsorption isotherms for the two Protein A affinity resins (MabSelect SuRe and TOYOPEARL AF-rProtein A HC) are shown in Figure II.2.1. The Langmuir equation was used to fit the experimental data. It describes the protein adsorbed to the resin, q, in equilibrium with the solution concentration, C, and is given by:

$$q = \frac{q_m C}{K_D + C} \quad (1)$$

where q_m gives the maximum adsorbed capacity and K_D is the dissociation constant.

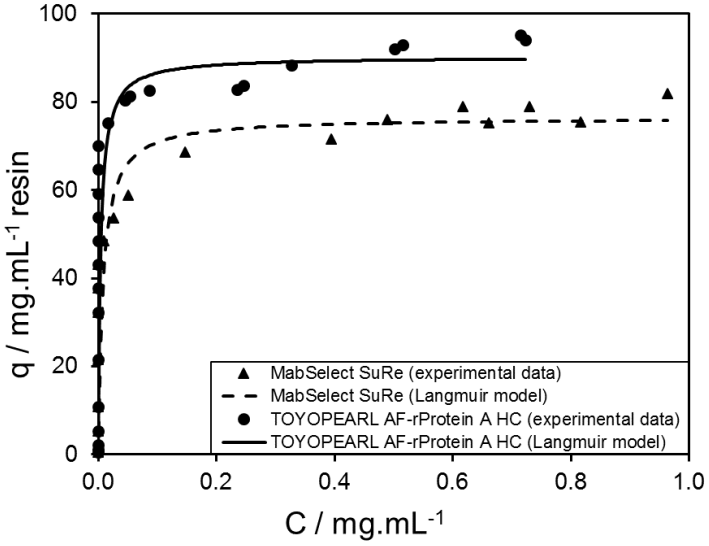

Figure II.2.1 - Adsorption isotherms of antibody in Na-phosphate buffer 0.02 M + NaCl 0.15 M at pH 7.4 on the resins MabSelect SuRe (full triangles) and TOYOPEARL AF-rProtein A HC (full circles). Incubation of 0.01-10 mg.mL^{-1} antibody in a bulk volume of 0.25 mL with 10% resin for 24 h at 250 rpm. Data were fitted with Langmuir model for MabSelect SuRe (dashed line) and TOYOPEARL AF-rProtein A HC (full line).

The isotherms show highly favourable adsorption, as expected for Protein A affinity chromatography (Hahn et al., 2005; Müller & Vajda, 2016). Both Langmuir fits present a rectangular shape that levels between 0.2 and 0.4 mg.mL^{-1} equilibrium concentration depending on the resin. The isotherms are highly favorable, with TOYOPEARL AF-rProtein A HC presenting a higher equilibrium binding capacity (q_m = 96 mg.mL^{-1} packed bed) and higher affinity (with and K_D = 0.0042 mg.mL^{-1}) than MabSelect SuRe (q_m = 79 mg.mL^{-1} packed bed and K_D = 0.0079 mg.mL^{-1}). The isotherm data denotes a second increase in q values for equilibrium concentrations higher than 0.3 mg.mL^{-1}, which is more clearly seen in the TOYOPEARL AF-rProtein A HC isotherm. This behavior in the isotherm was also seen in a recent study by Pabst et al. (Pabst, Thai, & Hunter, 2018). It is well described that the Langmuir isotherm assumes monolayer coverage and energetic equivalence of all the binding sites (Bellot & Condoret, 1993; Carta & Jungbauer, 2010). Nonetheless, this isotherm has been used to model antibody adsorption to Protein A chromatography resins (Hahn, Schlegel, & Jungbauer, 2003; Pabst et al., 2018; Perez-Almodovar & Carta, 2009), known for their heterogeneous binding characteristic due to the multimeric chains, with high energy (also called fast) and low energy (also called slow) binding sites (Ljungquist, Jansson, Moks, & Uhlén, 1989; Pabst et al., 2018; Perez-Almodovar & Carta, 2009). Therefore, antibody binding to more than one domain of the Protein A chain is possible (Ghose et al., 2007; Ljungquist et al., 1989; Perez-Almodovar & Carta, 2009). Thus, the slight deviation from the Langmuir model seen in the isotherm (Fig. II.2.1) and in Pabst et al. work (Pabst et al., 2018) at high concentrations could be associated to the heterogeneity of the multimeric Protein A ligand, which in the present study is more visible in presence of TOYOPEARL AF-rProtein A HC resin as it has a hexamer structure compared to the tetramer of Mabselect SuRe.

2.3.2. Batch uptake kinetics – shrinking core model

For rectangular isotherms, like in the antibody uptake by Protein A resins, batch adsorption in a finite bath can be defined with the shrinking core model, which considers pore diffusion as the dominant transport mechanism.

Pore diffusion in chromatography media is usually defined through the effective diffusivity, D_e (Carta & Jungbauer, 2010), which is highly dependent on tortuosity (molecule path is longer than a straight trajectory), steric hindrance (associated with the ratio of molecule to pore size), and matrix porosity (Carta & Jungbauer, 2010). MabSelect SuRe shows a greater effective diffusivity than TOYOPEARL AF-rProtein A HC for both C_0, as seen in Table II.2.1, where the parameters fitted by the shrinking core model for both resins can be found. In spite of the larger particle size of MabSelect SuRe (Ø = 85 µm), these greater D_e values can be related to the larger intraparticle porosity (ε_p = 0.76) compared to TOYOPEARL AF-rProtein A HC (Ø = 45 µm and ε_p = 0.36) (Pabst et al., 2018; Perez-Almodovar & Carta, 2009).

Table II.2.1 - Summary of the fitted parameters of the pore diffusion model of antibody uptake kinetics by MabSelect SuRe and TOYOPEARL AF-rProtein A HC.

Parameters	MabSelect SuRe		TOYOPEARL AF-rProtein A HC	
C_0 (mg.mL^{-1})	0.72	1.40	0.74	1.37
q_{max} (mg.mL^{-1} resin)	55.7	53.4	77.5	75.4
D_e (cm^2.s^{-1})	3.3×10^{-8}	3.3×10^{-8}	1.7×10^{-8}	1.2×10^{-8}
k_f	1.25×10^{-3}	1.25×10^{-3}	2.37×10^{-3}	2.37×10^{-3}

The shrinking core model was first developed by Teo and Ruthven (Teo & Ruthven, 1986) and then applied by other authors (Perez-Almodovar & Carta, 2009; Zandian & Jungbauer, 2009), and the general equation is as follows:

$$\frac{C_0}{q}\frac{D_e t}{r_p^2} = \left(1 - \frac{1}{Bi}\right) I_2 - I_1 \tag{2}$$

where C_0 is the initial protein concentration in the mobile phase, D_e is the effective diffusivity, t is the time, q is the adsorbed protein, r_p is the particle radius, Bi is the Biot number, and I_1 and I_2 are simplified dimensionless parameters given by:

$$I_1 = \frac{1}{6\lambda\Lambda}\ln\left[\frac{\lambda^3+\beta^3}{\lambda^3+1}\left(\frac{\lambda+1}{\lambda+\beta}\right)^3\right] + \frac{1}{\lambda\Lambda\sqrt{3}}\left[\tan^{-1}\left(\frac{2\beta-\lambda}{\lambda\sqrt{3}}\right) - \tan^{-1}\left(\frac{2-\lambda}{\lambda-\sqrt{3}}\right)\right] \tag{3}$$

$$I_2 = \frac{1}{3\Lambda}\ln\left(\frac{\lambda^3+\beta^3}{\lambda^3+1}\right) \tag{4}$$

where $\beta = \left(1 - \frac{\bar{q}}{q_{max}}\right)^{1/3}$ and $\lambda = \left(\frac{1}{\Lambda} - 1\right)^3$, and where Λ is the normalized phase ratio given by $\Lambda = \frac{vq_{max}}{VC_0}$, $\bar{q}$ is the average concentration in the particle, q_{max} is the maximum binding capacity of the resin, v is the resin volume, V is the mobile phase volume. The Biot number is given by $Bi = \frac{k_f r_p}{D_e}$, where k_f is the film mass transfer coefficient.

Antibody uptake kinetics by MabSelect SuRe and TOYOPEARL AF-rProtein A HC was measured at different initial concentrations (C_0 = 0.75 mg.mL^{-1} and C_0 = 1.5 mg.mL^{-1}). The data were plotted in terms of the adsorbed concentration and the dimensionless solution concentration over time and is shown in Figs. II.2.2A and II.2.2B. The represented solid lines show the uptake prediction based on the application of the aforementioned shrinking core model. This model considers a single type of adsorption site with infinite affinity, where the molecule is first adsorbed at the surface and then the front migrates towards a protein-free centre of the particle. Steric hindrance in this pore diffusion-controlled process is caused by the bound antibodies at the pore entrance, leading to a slower migration front towards the

centre of the pore (Perez-Almodovar & Carta, 2009). For both resins it can be seen that the model predicts well the uptake rate at early equilibration time but the rate slows down as the ultimate capacity is attained. The same behavior was found by Carta and co-workers when modeling antibody adsorption to Protein A by the shrinking core model (Perez-Almodovar & Carta, 2009). In addition to this model, Carta's group also employed other models driven by pore diffusion to analyse the adsorption process, namely the pore diffusion model, and the heterogeneous binding model. The models differ on the kinetic resistance considerations and the accessibility of the pores. The authors found that despite all three models being able to correctly predict antibody binding at low concentrations, the first two returned some deviations at high concentrations. Only the heterogeneous binding model was able to adjust precisely, suggesting that it is unlikely that all the binding sites are homogeneous. There is a distribution between the aforementioned fast and slow binding sites. Therefore, only the kinetic filling of the high affinity sites may be well represented by the shrinking core model (Hahn et al., 2005; Perez-Almodovar & Carta, 2009).

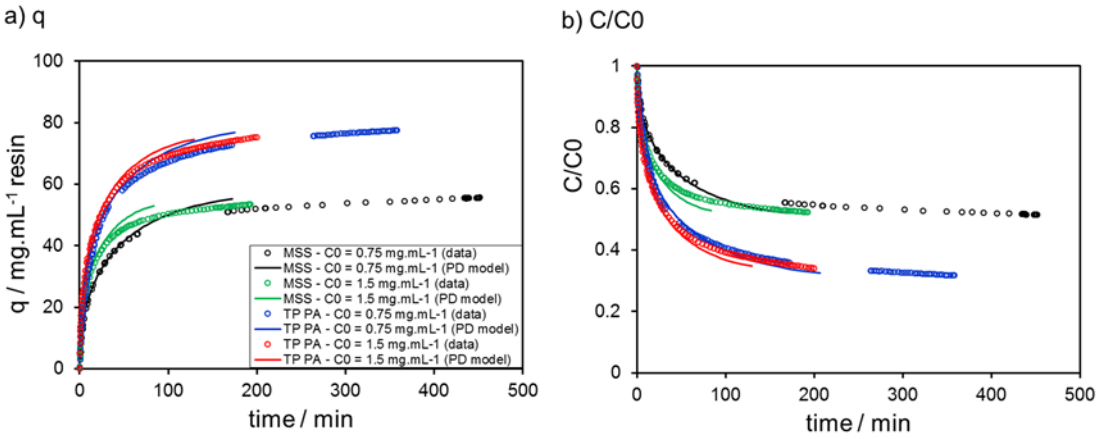

Figure II.2.2 - Batch adsorption kinetics of antibody at C_0 = 0.75 mg.mL^{-1} and C_0 = 1.5 mg.mL^{-1} in Na-phosphate buffer 0.02 M + NaCl 0.15 M at pH 7.4 on the resins MabSelect SuRe (MSS) and TOYOPEARL AF-rProtein A HC (TP PA); a) adsorbed concentration, q, over time; b) dimensionless solution concentration, C/C_0, over time. Solid lines represent the uptake prediction based on the shrinking core model.

2.3.3. Adsorption heat profile

By reproducing lab-scale conditions of a regular chromatography system, flow microcalorimetry is a powerful tool to characterize a chromatographic process with respect to the associated thermodynamics. We have already successfully investigated the energy profile in the purification of other biomolecules, namely lysozyme (Silva et al., 2014), plasmid DNA (Aguilar et al., 2014) and mAbs (Rosa, da Silva, Aires-Barros, Dias-Cabral, & Azevedo, 2018), and concluded that biomolecule purification in liquid chromatography is a complex process that should be carefully interpreted. The adsorption of a biomolecule to a ligand in a chromatographic process has different characteristics from a batch process both in terms of mass transfer properties and associated energy. It has been described that there are multiple

factors and subprocesses influencing protein adsorption in chromatography with both favorable and unfavorable contributions to the process. All these contributions have a thermodynamic significance regardless of their source. The possibly existing subprocesses underlying the interaction between a protein and the resin may involve, depending on the type of interaction (F.-Y. Lin et al., 2002): 1) dehydration and/or removal of the electric double layer of the biomolecule and sorbent; 2) interactions between the biomolecule and the sorbent; 3) structural rearrangement of the biomolecule upon adsorption; 4) rearrangement of the excluded water or ion molecules in bulk solution. Protein and surface desolvation are the major contributors for entropy increase and for endothermic energy. The release of co-ions and dehydration is usually more prominent in ion exchange. In Protein A affinity chromatography, as previously mentioned, protein-ligand binding is a result of different types of interactions, namely interactions of hydrophobic nature, van der Waals forces, and hydrogen bonding (Ghose, Allen, Hubbard, Brooks, & Cramer, 2005; Li, Dowd, Stewart, Burton, & Lowe, 1998). The occurrence of interactions of exothermal nature contribute majorly to the adsorptive process enthalpy (Katiyar, Thiel, Guliants, & Pinto, 2010). Antibodies bind to Protein A at neutral conditions, under which the highly conserved histidyl residue at the Protein A binding site interacts with the uncharged CH2-CH3 Fc region in the antibody (Ghose et al., 2005). Therefore, endothermic desolvation heats are not likely to be very prominent, which is attested by the obtained thermograms (Figs. II.2.3 and II.2.4).

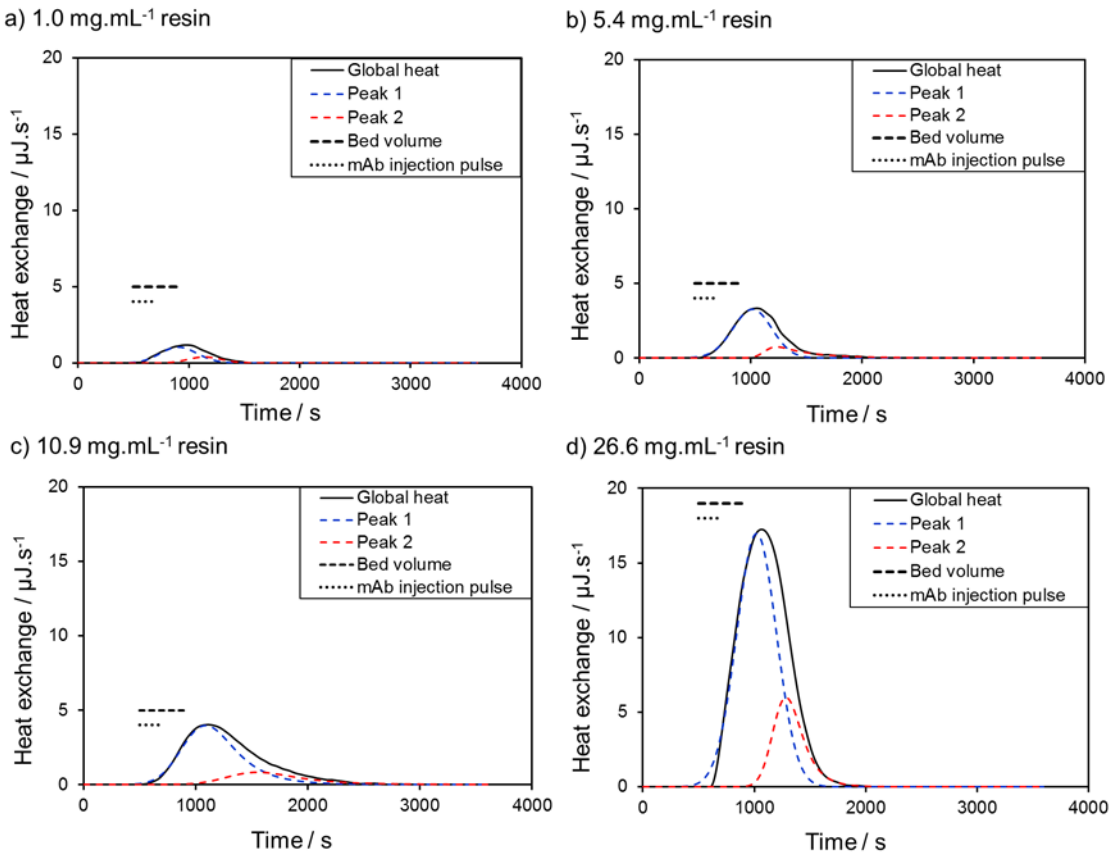

Figure II.2.3 - Heat exchange profile of antibody adsorption on MabSelect SuRe at concentrations in the linear range of the isotherm for different surface concentrations: a) 1.0 mg.mL^{-1} resin; b) 5.4 mg.mL^{-1} resin; c) 10.9 mg.mL^{-1} resin; and d) 26.6 mg.mL^{-1} resin. Equilibrium with Na-phosphate buffer 0.02 M + NaCl 0.15 M at pH 7.4 and 0.01 mL antibody injection prepared in the same buffer; flow rate was 1.5 mL.h^{-1}. Peak deconvolution was done with EMG functions using PaeakFit v4 software, with the first peak shown in a blue dashed curve, the second peak in a red dashed curve, and the overall net heat in a black full curve. The bed volume starting in the first moment of contact between the antibody and the adsorbent is shown in a black dashed line, and the antibody injection pulsed is shown in a black dotted line.

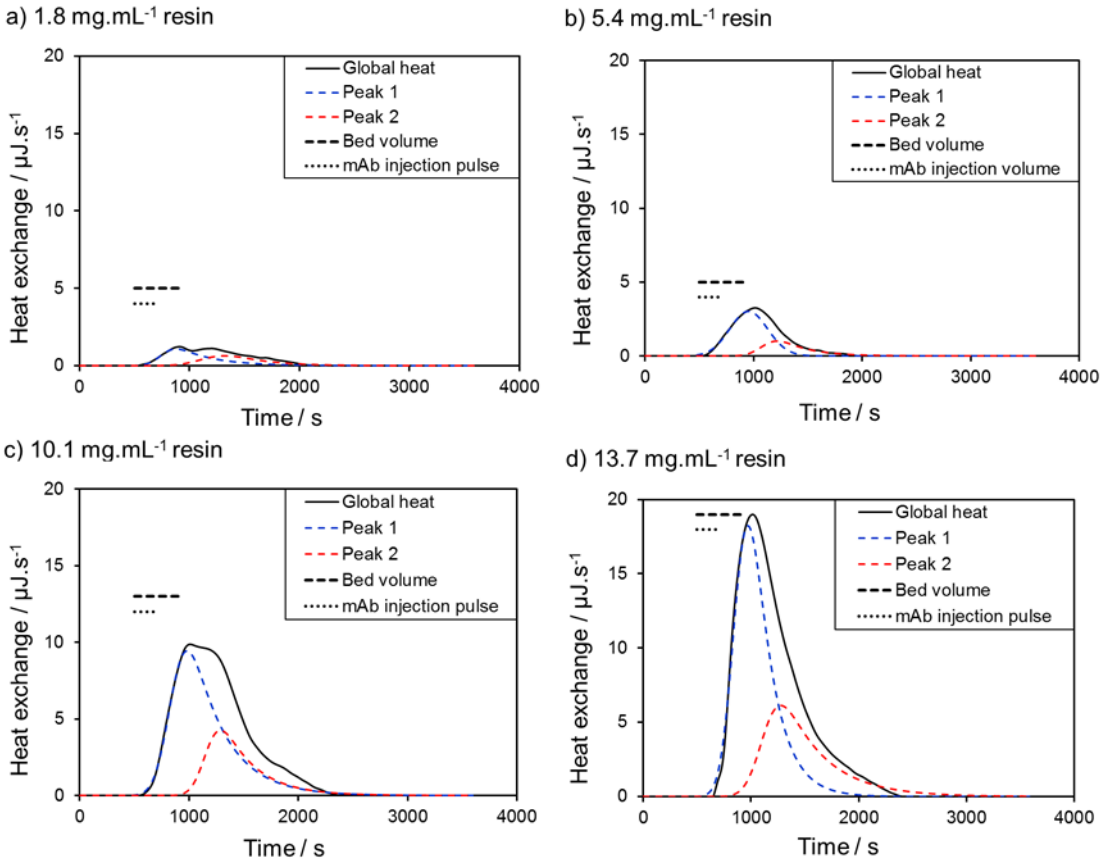

Figure II.2.4 - Heat exchange profile of antibody adsorption on TOYOPEARL AF-rProtein A HC at concentrations in the linear range of the isotherm for different surface concentrations: a) 1.8 mg.mL^{-1} resin; b) 5.4 mg.mL^{-1} resin; c) 10.1 mg.mL^{-1} resin; and d) 13.7 mg.mL^{-1} resin. Equilibrium with Na-phosphate buffer 0.02 M + NaCl 0.15 M at pH 7.4 and 0.01 mL antibody injection prepared in the same buffer; flow rate was 1.5 mL.h^{-1}. Peak deconvolution was done with EMG functions using PaeakFit v4 software, with the first peak shown in a blue dashed curve, the second peak in a red dashed curve, and the overall net heat in a black full curve. The bed volume starting in the first moment of contact between the antibody and the adsorbent is shown in a black dashed line, and the antibody injection pulsed is shown in a black dotted line.

The measured heat exchange profiles are shown in Figure II.2.3A-D (MabSelect SuRe) and Figure II.2.4 A-D (TOYOPEARL AF-rProtein A HC). A black dashed bar indicating the bed volume is shown in every graph (0.171 mL, corresponding to 6.8 min of residence time at the operation volumetric flow rate of 1.5 mL.h^{-1}) starting at the moment that the migration front of the injection pulse first enters the bed. It is also shown a black dotted bar indicating the

injection pulse (0.1 mL). In every experiment, the signal presents a maximal energy release followed by a tailed heat dissipation until zero. Because of the associated tailing, the signal was deconvoluted in two peaks to discriminate between the different substeps occurring during the adsorption process. PeakFIT software (Systat Software, Inc., Chicago, IL, USA) was used for this purpose and the Exponentially Modified Gaussian function was applied.

The antibody adsorption to both resins has an overall exothermic heat exchange profile characteristic of the type of interactions present. The signals start with a shallow release of energy as the antibody sample reaches the column. The first exotherm peaks at the time the injection pulse completes the first column volume. The second peak starts at the time the first peaks, so it is mostly generated after the end of the antibody pulse. For both resins, the magnitude of the signals increases with the increase of the loading and the first exotherm translates an event with a greater release of energy than the second exotherm.

All the microcalorimetry measurements were conducted in the linear range of the isotherm and at 6.8 min residence time. According to the shrinking core model, when the antibodies in a sample reach the adsorbent they bind to the first Protein A ligands at the surface of the beads with the subsequent molecules binding to the inner ligands until reaching the centre of the particle. In a recent study we concluded that in the linear range of the isotherm, the antibodies would bind preferably to the outermost domains in an average stoichiometry of 1:1 or lower (Silva et al., 2019). Therefore, the reorientation/rearrangement of the molecules upon binding is more favorable than multilayer formation. The energy for this rearrangement would be given by the decrease of enthalpy from the first to the second observed exothermic event (Suzuki, 1990). All these changes are energetically significant and help explaining tailing beyond residence time towards the establishment of a favorable arrangement of the adsorbed antibody molecules at the surface. It is also observed that the tailing profile in TOYOPEARL AF-rProtein A HC is longer than in MabSelect SuRe, in accordance with the lower effective diffusivity results from the uptake studies and the differences in the Protein A ligand size.

In conclusion, the first exotherm results from the first contact of the antibodies with the ligand and the second exotherm could result from the rearrangement of the adsorbed molecule within the same ligand. Also, as mentioned, having multiple binding sites per Protein A ligand is a source of heterogeneous binding, with high and low energy sites. So, the binding of antibody is likely a stochastic phenomenon in which the distribution of the binding energy determines the probability of concomitant binding events (Silva et al., 2019).

2.3.4. Adsorption enthalpy

The adsorption enthalpy of a given process is determined by the ratio between energy (integration of the heat exchange curve) and mole of adsorbed product.

$$\Delta H_{ads} = \frac{Q_{ads}}{vq} \tag{5}$$

where Q_{ads} represents the net heat of adsorption, v the resin volume, and q the adsorbed protein amount per sorbent volume.

The Gibbs free energy, ΔG, at any moment of the association/dissociation process is given by:

$$\Delta G = \Delta G^0 + RTlnQ \quad (6)$$

where ΔG^0 represents the standard Gibbs energy, R is the universal gas constant (8.314 $J.K^{-1}.mol^{-1}$), T is the temperature in Kelvin, and Q the reaction quotient defined as the ratio between the complex protein-ligand concentration and the product of the protein concentration and ligand concentration. When the system is in equilibrium, Q can be defined as K, the reaction equilibrium constant, and $\Delta G = 0$, giving:

$$\Delta G^0 = -RTlnK \quad (7)$$

The change in the standard Gibbs free energy of an adsorptive process that can be reversible is given by:

$$\Delta G^0 = \Delta H^0 - T\Delta S^0 \quad (8)$$

where ΔH^0 represents the change in standard enthalpy ($J.mol^{-1}$), and ΔS^0 the change in standard entropy ($J.K^{-1}.mol^{-1}$) of the process. Combining Eqs. (7) and (8), it is possible to calculate the change in standard entropy for the reaction. K can be extrapolated from q/C for infinite dilution, according to Eq. (9):

$$K = \lim_{C \to 0} \frac{q}{C} \quad (9)$$

Figures II.2.5A and II.2.5B show the antibody adsorption enthalpy for a range of surface concentration. The enthalpy values were calculated integrating the heat signals from Figures II.2.3 and II.2.4 dividing by the respective molar amount of adsorbed antibody. Blue crosses and green full circles represent the enthalpy derived from the first and second peak respectively, and the red full triangles the net enthalpy of the whole adsorptive interaction.

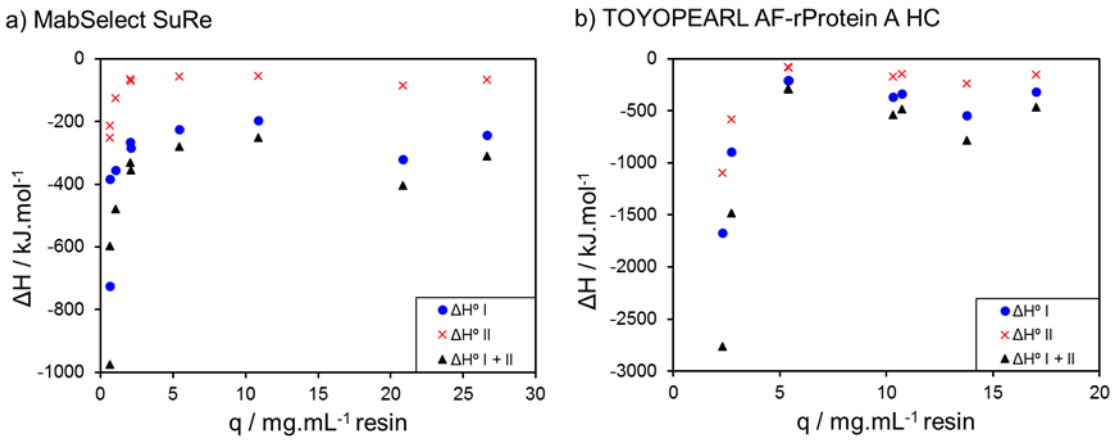

Figure II.2.5 - Enthalpy of adsorption of antibody over surface concentration on a) MabSelect SuRe and b) TOYOPEARL AF-rProtein A HC. Enthalpy values were determined by integrating the heat profile curves from Figs. II.2.3 and II.2.4 and normalized for the adsorbed moles of antibody. The enthalpy associated to the first peak is shown in blue full circles, the enthalpy derived from the second peak in red crosses, and the overall adsorption enthalpy in full black triangles.

From Eqs. (7) and (9) the Gibbs free energy was determined for infinite dilution, with ΔG^0 = -22.8 kJ.mol^{-1} for MabSelect SuRe and ΔG^0= -24.9 kJ.mol^{-1} for TOYOPEARL AF-rProtein A HC. The two ΔG^0 values are highly similar because at infinite dilution ΔG^0 values translate only the specific interaction between the antibody and the Protein A, the primary event present in both resins.

It can be seen that both resins show a similar trend in the adsorption enthalpy, with greater enthalpy values at the very low linear range of the isotherm, with TOYOPEARL AF-rProtein A HC showing higher exothermic adsorption enthalpy values than MabSelect SuRe. If every binding site would be energetically equivalent, if the structure and the orientation of the adsorbed molecules would be independent of surface coverage, and if the adsorbed protein molecules would not interact laterally, the molar adsorption enthalpy would be invariant throughout the entire surface coverage (Norde, 1992). Given the fact that these concentrations are in the linear range of the isotherm, lateral interactions between adsorbed species are not likely to be prominent. Therefore, the heterogenous binding nature of the resins has to be a key element for the greater molar enthalpy values at low concentration. Conformational changes of the antibody upon adsorption are also probable at low surface coverage, as found by Beyer and Jungbauer, but they depend on the hydrophobicity of the ligands (Beyer & Jungbauer, 2018). TOYOPEARL AF-rProtein A HC has a greater enthalpy change possibly because of the greater number of binding possibilities when compared to MabSelect SuRe. After a certain surface concentration, but still in the linear range of the isotherm, the associated molar enthalpy tends to a stabilization. Therefore, the overall process enthalpy converges towards an energetic equilibrium.

2.4. Conclusions

The goal of this work was to understand antibody binding to Protein A resins in terms of its associated energy and kinetics. We showed the intrinsic link between surface concentration of biomolecules on chromatography resins and the necessary energy for adsorption. It seemed clear that the interaction between antibody and Protein A ligands upon loading is highly favorable at the studied low equilibrium concentrations. The antibody adsorption process can be subdivided into two sub-steps: a first moment of interaction and binding to a highly energetic Protein A binding site, and another moment of a rearrangement of the bound molecule in the ligand. These two sub-steps are energetically significant and evolve towards energy stabilization with surface concentration. At low equilibrium times, the antibody binding follows the shrinking core model, but when enough time is given to the adsorbed molecules to be in equilibrium with the unbound the model becomes less accurate because of the heterogeneity binding nature of MabSelect SuRe. Microcalorimetric data is a valuable addition for the uptake rate studies, suggesting also a heterogenous nature of the binding sites on the surface of this type of affinity resins.

2.5 References

Aguilar, P. A., Twarda, A., Sousa, F., & Dias-Cabral, A. C. (2014). Thermodynamic study of the interaction between linear plasmid deoxyribonucleic acid and an anion exchange support under linear and overloaded conditions. Journal of Chromatography A, 1372, 166–173. https://doi.org/10.1016/j.chroma.2014.11.002

Bellot, J. C., & Condoret, J. S. (1993). Review modelling of liquid chromatography equilibria. Process Biochemistry, 28, 365–376. https://doi.org/10.1016/0032-9592(93)80023-A

Beyer, B., & Jungbauer, A. (2018). Conformational changes of antibodies upon adsorption onto hydrophobic interaction chromatography surfaces. Journal of Chromatography A, 1552, 60–66. https://doi.org/10.1016/j.chroma.2018.04.009

Boyle, M. D. P. (1990). The type I bacterial immunoglobulin-binding protein: Staphylococcal protein A. In Bacterial Immunoglobulin-Binding Proteins (Vol. 1, pp. 17–28). Academic Press, Inc., San Diego. https://doi.org/10.1016/B978-0-12-123011-1.50006-X

Carta, G., & Jungbauer, A. (2010). Protein Chromatography: Process Development and Scale-Up. Weinheim: Wiley-VCH Verlag GmbH & Co. KGaA. https://doi.org/10.1002/9783527630158

DeLano, W. L., Ultsch, M. H., de Vos, A. M., & Wells, J. A. (2000). Convergent solutions to binding at a protein-protein interface. Science, 287, 1279–1283. https://doi.org/10.1126/science.287.5456.1279

Ecker, D. M., Jones, S. D., & Levine, H. L. (2015). The therapeutic monoclonal antibody market. MAbs, 7(1), 9–14. https://doi.org/10.4161/19420862.2015.989042

Gagnon, P., Nian, R., Leong, D., & Hoi, A. (2015). Transient conformational modification of immunoglobulin G during purification by protein A affinity chromatography. Journal of Chromatography A, 1395, 136–142. https://doi.org/10.1016/j.chroma.2015.03.080

Ghose, S., Allen, M., Hubbard, B., Brooks, C., & Cramer, S. M. (2005). Antibody variable region interactions with protein A: Implications for the development of generic purification processes. Biotechnology and Bioengineering, 92, 665–673. https://doi.org/10.1002/bit.20729

Ghose, S., Hubbard, B., & Cramer, S. M. (2007). Binding capacity differences for antibodies and Fc-fusion proteins on Protein A chromatographic materials. Biotechnology and Bioengineering, 96, 768–779. https://doi.org/10.1002/bit.21044

Hahn, R., Bauerhansl, P., Shimahara, K., Wizniewski, C., Tscheliessnig, A., & Jungbauer, A. (2005). Comparison of protein A affinity sorbents II. Mass transfer properties. Journal of Chromatography A, 1093, 98–110.

https://doi.org/10.1016/j.chroma.2005.07.050

Hahn, R., Schlegel, R., & Jungbauer, A. (2003). Comparison of protein A affinity sorbents. Journal of Chromatography B, 790, 35–51. https://doi.org/10.1016/S1570-0232(03)00092-8

Hober, S., Nord, K., & Linhult, M. (2007). Protein A chromatography for antibody purification. Journal of Chromatography B, 848, 40–47. https://doi.org/10.1016/j.jchromb.2006.09.030

Katiyar, A., Thiel, S. W., Guliants, V. V., & Pinto, N. G. (2010). Investigation of the mechanism of protein adsorption on ordered mesoporous silica using flow microcalorimetry. Journal of Chromatography A, 1217(10), 1583–1588. https://doi.org/10.1016/j.chroma.2009.12.058

Li, R., Dowd, V., Stewart, D. J., Burton, S. J., & Lowe, C. R. (1998). Design, synthesis, and application of a Protein A mimetic. Nature Biotechnology, 16(2), 190–195. https://doi.org/10.1038/nbt0298-190

Lin, F.-Y., Chen, W.-Y., & Hearn, M. T. W. (2002). Thermodynamic analysis of the interaction between proteins and solid surfaces: application to liquid chromatography. Journal of Molecular Recognition, 15(2), 55–93. https://doi.org/10.1002/jmr.564

Ljungquist, C., Jansson, B., Moks, T., & Uhlén, M. (1989). Thiol-directed immobilization of recombinant IgG-binding receptors. European Journal of Biochemistry, 186(3), 557–561. https://doi.org/10.1111/j.1432-1033.1989.tb15244.x

Mazzer, A. R., Perraud, X., Halley, J., O'Hara, J., & Bracewell, D. G. (2015). Protein A chromatography increases monoclonal antibody aggregation rate during subsequent low pH virus inactivation hold. Journal of Chromatography A, 1415, 83–90. https://doi.org/10.1016/j.chroma.2015.08.068

Morrison, C., & Lähteenmäki, R. (2017). Public biotech in 2016 - The numbers. Nature Biotechnology, 35, 623–629. https://doi.org/10.1038/nbt.3917

Müller, E., & Vajda, J. (2016). Routes to improve binding capacities of affinity resins demonstrated for Protein A chromatography. Journal of Chromatography B, 1021, 159–168. https://doi.org/10.1016/j.jchromb.2016.01.036

Norde, W. (1992). Energy and entropy of protein adsorption. Journal of Dispersion Science and Technology, 13(4), 363–377. https://doi.org/10.1080/01932699208943322

Pabst, T. M., Thai, J., & Hunter, A. K. (2018). Evaluation of recent Protein A stationary phase innovations for capture of biotherapeutics. Journal of Chromatography A, 1554, 45–60. https://doi.org/10.1016/j.chroma.2018.03.060

Perez-Almodovar, E. X., & Carta, G. (2009). IgG adsorption on a new protein A adsorbent based on macroporous hydrophilic polymers. I. Adsorption equilibrium and kinetics. Journal of Chromatography A, 1216, 8339–8347.

https://doi.org/10.1016/j.chroma.2009.09.017

Rosa, S. A. S. L., da Silva, C. L., Aires-Barros, M. R., Dias-Cabral, A. C., & Azevedo, A. M. (2018). Thermodynamics of the adsorption of monoclonal antibodies in phenylboronate chromatography: Affinity versus multimodal interactions. Journal of Chromatography A, 1569, 118–127.
https://doi.org/10.1016/j.chroma.2018.07.050

Salvalaglio, M., Zamolo, L., Busini, V., Moscatelli, D., & Cavallotti, C. (2009). Molecular modeling of Protein A affinity chromatography. Journal of Chromatography A, 1216, 8678–8686.
https://doi.org/10.1016/j.chroma.2009.04.035

Shukla, A. A., Hubbard, B., Tressel, T., Guhan, S., & Low, D. (2007). Downstream processing of monoclonal antibodies — Application of platform approaches. Journal of Chromatography B, 848, 28–39.
https://doi.org/10.1016/j.jchromb.2006.09.026

Silva, G. L., Marques, F. S., Thrash, M. E., & Dias-Cabral, A. C. (2014). Enthalpy contributions to adsorption of highly charged lysozyme onto a cation-exchanger under linear and overloaded conditions. Journal of Chromatography A, 1352, 46–54.
https://doi.org/10.1016/j.chroma.2014.05.049

Silva, G. L., Plewka, J., Lichtenegger, H., Dias-Cabral, A. C., Jungbauer, A., & Tscheließnig (2019). The pearl necklace model in protein A chromatography: Molecular mechanisms at the resin interface. Biotechnology and Bioengineering, 116, 76–86.
https://doi.org/10.1002/bit.26843

Suzuki, M. (1990). Adsorption engineering. Reactive Polymers (Vol. 14). Tokyo and Amsterdam: Kodansha Ltd. and Elsevier Science Publishers B.V.

Tao, Y., Perez-Almodovar, E. X., Carta, G., Ferreira, G., & Robbins, D. (2011). Adsorption kinetics of deamidated antibody variants on macroporous and dextran-grafted cation exchangers. III. Microscopic studies. Journal of Chromatography A, 1218(44), 8027–8035.
https://doi.org/10.1016/j.chroma.2011.09.010

Teo, W. K., & Ruthven, D. M. (1986). Adsorption of water from aqueous ethanol using 3-A molecular sieves. Industrial & Engineering Chemistry Process Design and Development, 25(1), 17–21.
https://doi.org/10.1021/i200032a003

Ueberbacher, R., Rodler, A., Hahn, R., & Jungbauer, A. (2010). Hydrophobic interaction chromatography of proteins: Thermodynamic analysis of conformational changes. Journal of Chromatography A, 1217(2), 184–190.
https://doi.org/10.1016/j.chroma.2009.05.033

Uhlén, M., Guss, B., Nilsson, B., Gatenbeck, S., Philipson, L., & Lindberg, M. (1984). Complete sequence of the Staphylococcal gene encoding Protein A. A gene evolved through multiple duplications. The Journal of Biological Chemistry, 259, 1695–1702.

Yu, D., Song, Y., Huang, R. Y.-C., Swanson, R. K., Tan, Z., Schutsky, E., … Li, Z. J. (2016). Molecular perspective of antibody aggregates and their adsorption on Protein A resin. Journal of Chromatography A, 1457, 66–75. https://doi.org/10.1016/j.chroma.2016.06.031

Zandian, M., & Jungbauer, A. (2009). Engineering properties of a camelid antibody affinity sorbent for Immunoglobulin G purification. Journal of Chromatography A, 1216(29), 5548–5556. https://doi.org/10.1016/j.chroma.2009.05.051

3. Publication III

The pearl necklace model in Protein A chromatography – molecular mechanisms at the resin interface

Goncalo L. Silva,[1,2,3] | Jacek Plewka,[3,4] | Helga Lichtenegger,[3,4] | Ana C. Dias-Cabral,[1,2] | Alois Jungbauer,[3,5] | Rupert Tscheließnig,[3,5]

[1]CICS-UBI – Health Sciences Research Centre, University of Beira Interior, Av. Infante D. Henrique, 6201-001 Covilhã, Portugal
[2]Department of Chemistry, University of Beira Interior, R. Marquês d'Ávila e Bolama, 6201-001 Covilhã, Portugal
[3]Austrian Centre of Industrial Biotechnology, Muthgasse 18, 1190 Vienna, Austria
[4]Department of Material Science and Process Engineering, University of Natural Resources and Life Sciences, Peter-Jordan Strasse 82, 1190 Vienna, Austria
[5]Department of Biotechnology, University of Natural Resources and Life Sciences, Muthgasse 18, 1190 Vienna, Austria

Corresponding author

Rupert Tscheließnig: Austrian Centre of Industrial Biotechnology, Muthgasse 18, 1190 Vienna, Austria
Email: rupert.tscheliessnig@boku.ac.at

Funding information

Austrian Research Promotion Agency FFG – grant number 824186
Fundação para a Ciência e Tecnologia in Portugal – grant number SFRH/BD/104498/2014

Goncalo L. Silva and Jacek Plewka contributed equally to this work.

Abstract

Staphylococcal Protein A chromatography is an established core technology for monoclonal antibody purification and capture in downstream processing. MabSelect SuRe involves a tetrameric chain of a recombinant form of the B domain of staphylococcal Protein A, called Z domain, however little is known about the stoichiometry, binding orientation, or preferred binding. We analyzed small-angle X-ray scattering data of the antibody–Protein A complex immobilized in an industrial highly relevant chromatographic resin at different antibody concentrations. From scattering data, we computed the normalized radial density distributions. We designed 3D models with protein data bank crystallographic structures of an IgG1 (the isoform of trastuzumab, used here) (Protein Data Bank: 1HZH) and the staphylococcal Protein A B-domain (the native form of the recombinant structure contained in MabSelect SuRe resin) (Protein Data Bank: 1BDD). We computed different binding conformations for different antibody to Protein A stoichiometries (1:1, 2:1, and 3:1) and compared the normalized radial density distributions computed from 3D models with those obtained from experimental data. In the linear range of the isotherm we favor a 1:1 ratio, with the antibody binding to the outer domains in the Protein A chain at very low and at high concentrations. In the saturation region, a 2:1 ratio is more likely to occur. A 3:1 stoichiometry is excluded because of steric effects.

Keywords

Monoclonal antibodies, staphylococcal Protein A, affinity chromatography, small-angle X-ray scattering, radial density distribution, pearl necklace model

Acknowledgments

This work has been supported by the Federal Ministry for Digital and Economic Affairs (bmwd), the Federal Ministry for Transport, Innovation and Technology (bmvit), the Styrian Business Promotion Agency SFG, the Standortagentur Tirol, Government of Lower Austria and ZIT - Technology Agency of the City of Vienna through the COMET-Funding Program managed by the Austrian Research Promotion Agency FFG. The funding agencies had no influence on the conduct of this research

This work was carried out in cooperation with Boehringer Ingelheim RCV, Process Science, and Novartis/Sandoz.

G.L.S. acknowledges his doctoral fellowship SFRH/BD/104498/2014 to Fundação para a Ciência e Tecnologia in Portugal.

Notes

The authors declare no competing financial interest.

3.1. Introduction

Staphylococcal Protein A chromatography is the capture step of choice in the manufacturing of monoclonal antibodies because of its high selectivity and robustness (Hahn et al. 2005, 2006; Shukla et al. 2007). Staphylococcus aureus Protein A is a cell wall 56-kDa protein with five homologous binding domains, designated as E, D, A, B, and C, in order from the N-terminal (Ghose et al. 2005; Graille et al. 2000; Hober, Nord, & Linhult 2007; Starovasnik et al. 1999; Uhlén et al. 1984). MabSelect SuRe (GE Healthcare) is one of the most widely used Protein A resins. It has a tetrameric chain of synthetically engineered Z-domains, which are derived from the B-domain with point mutations to improve alkaline stability (Ghose et al. 2005).

Protein A binding to immunoglobulins G (IgG) occurs through the hydrophobic region between the CH_2 and CH_3 domains of the Fc, known as consensus binding site (Deisenhofer 1981; DeLano et al. 2000; Gagnon et al. 2015; Salvalaglio et al. 2009; Shukla et al. 2007). Despite having physical-chemical properties that make it prone to establishing hydrogen bonds and electrostatic interactions, it is because of its exposed hydrophobic moiety that the consensus binding site shows preferential binding with Protein A ligands (Salvalaglio et al. 2009). Regardless of the abundant information regarding Fc recognition by Protein A, antibody structural rearrangement upon adsorption to Protein A ligands and the associated stoichiometry are not fully understood. However, some authors have reported the possibility of multiple binding to Protein A chains, but with Protein A in solution (Ghose, Hubbard, & Cramer 2007). Others have also addressed this issue, reporting the possible antibody binding orientations of an IgG4 to immobilized Protein A in silica (Mazzer et al. 2017).

Molecular models have been applied to study antibody form and flexibility in aqueous solutions (Brandt, Patapoff, & Aragon 2010; Sandin et al. 2004) for a better understanding of antibody aggregate adsorption to Protein A resins (Yu et al. 2016) and to characterize the nature of antibody binding to Protein A (Salvalaglio et al. 2009; Zamolo et al. 2008). Cavallotti and co-workers (Salvalaglio et al. 2009; Zamolo et al. 2008) have described which regions and amino acids play a major role in the interaction with chromatography matrices based on the crystal structure of CH_2 and CH_3 of an IgG1 coupled with fragment B of Protein A determined by Deisenhofer (Deisenhofer 1981) (PDB: 1FC2). However, despite this high economic value, a real 3D structure of the antibody-staphylococcal Protein A complex based on experimental data at different antibody loadings has not been elucidated. The current state-of-the art on antibody-Protein A conformations is solely attributed to computational simulations (Busini et al. 2006; Salvalaglio et al. 2009).

Here we present a methodology capable to experimentally assess normalized radial densities of antibody-Protein A conformations at a resin surface by small angle X-ray scattering (SAXS). SAXS provides information at the structural level of particle systems of the colloidal size (to thousands of angstroms, Å), such as antibodies (Boldon, Laliberte, & Liu 2015; Glatter and Kratky 1982) SAXS is based on the concept that a particle of relatively greater size than the X-ray wavelength will scatter the incident X-ray. Based on the scattering intensity, it is

possible to assess form, shape, and size of the scatterer. Therefore, it would be possible to establish an approximation of the "spatial extension of the particle" (Glatter and Kratky 1982). SAXS can provide information from a dynamic system and take into account molecular flexibility and different configurations (Boldon, Laliberte, & Liu 2015).

The aim of our work was to investigate the adsorption of a monoclonal antibody to MabSelect SuRe. More concisely, we sought to obtain an overview of the structural rearrangement of the antibodies in the tetrameric Protein A and to estimate the evolution of surface layer thickness with antibody concentration, as well as the antibody–ligand stoichiometry. We compared the antibody-Protein A complex radial densities provided by SAXS with theoretical configurations (Protein A B domain from the crystal structure 1BDD and the antibody from the crystal structure 1HZH from Protein Data Bank (PDB)) and spatial rearrangement of antibodies and staphylococcal Protein A ligands using a molecular model approach. We implemented this model to simulate different binding orientations of a crystallographic structure of an IgG1 to a tetrameric B-domain Protein A chain attached to an agarose structure to mimic the experimental system of a monoclonal antibody to MabSelect SuRe. In the present work, the methodology is explored on this very specific system of high industrial relevance, but it is also applicable to a broad range of protein-surface adsorption systems and can improve the understanding of protein binding in those systems.

3.2. Materials and Methods

3.2.1. Materials

Trastuzumab was purchased from Roche (Basel, Switzerland) (Lot. B1050B07). All the following reagents were purchased from MilliporeSigma (Burlington, MA, USA): sodium phosphate dibasic ($Na_2HPO.2H_2O$) (Lot. K450726804049), sodium dihydrogen phosphate ($NaH_2PO.2H_2O$) (Lot. K93717142706), glycine ($C_2H_5NO_2$) (Lot. VP614601407), and sodium chloride (NaCl) (Lot. K48705904713). MabSelect SuRe resin was purchased from GE Healthcare (Uppsala, Sweden) (Lot. 10247535).

3.2.2. Adsorption isotherms

The antibody solutions were prepared in 0.02 M phosphate buffer with 0.15 M sodium chloride at pH 7.4 in a range from 0.01 to 10 mg/mL. A volume of 0.025 mL of resin was added to the antibody solution with a total volume of 0.25 mL. The samples were incubated for 24 h in a thermomixer (ThermoScientific) at 20°C and 900 rpm. After incubation the bulk concentration was measured at Abs 280 nm using a UV plate reader (Tecan).

3.2.3. Scanning electron microscopy

The MabSelect SuRe beads were first submerged in a cryoprotectant 2.3M sucrose solution. The sample was then frozen with liquid nitrogen and the beads cut into slices 30 µm thick using a tungsten carbide knife in a MT-990 Motorized Precision Microtome (RMC Boeckeler). The bead slices were dehydrated with ethanol series and then dried with CO_2 in a Critical Point Dryer Leica EM CPD030. For the visualization, we used a Scanning Electron Microscope Quanta™ 250 FEG, and the dried slices were placed on an aluminum slab and coated with a gold layer.

3.2.4. SAXS

The SAXS measurements were performed in the beamlines BM26B (Portale et al. 2013) and BM29 (Pernot et al. 2013) at the European Synchrotron Radiation Facility, Grenoble, France. The antibody sample preparation followed the same procedure as for the adsorption isotherm measurements. After the incubation, the solution was resuspended, and 100 µL of incubated sample was loaded into a quartz capillary. The capillary was then placed aligned to the beam. The scattering images were collected in 10 frames at 1-s exposure each using Pilatus 1M detector at 12keV (λ=1.033Å).

3.3. Modeling

SAXS is a powerful and effective technique for determining molecule shapes and sizes at the nanoscale length. This approach measures the scattering intensity $I(Q)$ function of a scattering vector Q resulting from a scattering angle 2θ, at a given wavelength λ, where $Q = 4\pi \sin\theta\,/\lambda$. Q values are correlated to real-space distances d with $d = 2\pi/Q$ (Glatter and Kratky 1982; Hayter and Penfold 1983; Zhang et al. 2007).

3.3.1. A fractal pearl necklace model

The antibody binds to Protein A ligands and a complex is formed. This complex can be described by its characteristic pair density distribution. The Fourier transform of the pair density distribution gives the form factor, $P(Q)$, which is the scattering intensity of the complex according to its characteristics, such as shape, size, or concentration. Additionally, pair density distributions of complexes randomly arranged in the fractal network of the agarose resin contribute to the structure factor, $S(Q)$, and can be described by $p_S(r) \propto r^{D_f}\exp(-\kappa r)$. Under the assumptions of the scattering theory, the scattering intensity of the whole system is not more than the product of the form and structure factor: $I(Q) = P(Q)S(Q)$. The scattering intensity curve is obtained by:

$$I(Q) = \mathcal{F}(p(r))[Q] = \int_0^\infty dr\, p_P(\mathrm{r})\, J_{1/2}(Qr)/(Qr)^{1/2}\, Q^{-(D_f+1)} \quad (1)$$

where $J_{1/2}$ is a Bessel function of the first kind of order ½. The form factor is the Fourier transform of the radial density distribution: $P(Q) = \mathcal{F}\left(p_p(r)\right) = \int_0^\infty dr\, p_p(\mathrm{r})\, J_{1/2}(Q\mathrm{r})/(Qr)^{1/2}$. The structure factor is the Fourier transform of the pair density distribution of the fractal network: $S(Q) = \mathcal{F}\big(p_S(r)\big) \propto Q^{-(D_f+1)}$.

It is challenging to normalize any scattering intensity. The scattering intensity depends on the chemical contrast of each entity and may decrease despite the increasing number of scatterers. We shift the normalization issue to real space. We introduce the normalized pair density distribution of spherical hulls $p_p(r,R) \propto \mathrm{r}/R^2\ \mathrm{H}(2\,\mathrm{R} - \mathrm{r})$ and hereby enforce radial symmetry. It is an essential step that solves the normalization problem in a very elegant way. We define our working equation as:

$$I(Q)Q^{(D_f+1)} \propto \int_0^\infty dR\ 4\pi\ R^2\ p'(\mathrm{R})|J_{1/2}(Q\mathrm{R})/(QR)^{1/2}|^2 \tag{2}$$

The variable R is the measured distance from the scattering site relative to the backbone of the agarose. This mathematical model resembles a fractal folded pearl necklace, made from pearls with an average radial density distribution of matter, $p'(\mathrm{R})$.

3.3.2. The fractal network of the resin imposes a fractal structure factor

In the present case, we monitor antibody adsorption at high concentrations. Thus, the antibody concentration in the proximity of the surface is high. This is the reason why the infinite dilution argument no longer holds true. We have to take into account complex-complex pair density distributions. It seems appropriate to characterize their structure by the fractal pair density distribution: $p_S(r) \propto r^{D_f}\exp(-\kappa r)$, with κ as the screening length. Then, the structure factor of protein ligand complexes resembles:

$$S(Q) = \mathcal{F}(p_S(r))[Q] = \int_0^\infty p_S(r) J_{1/2}(Qr)/(Qr)^{1/2} \tag{3}$$

It is a *sin*-transform of the fractal pair density distribution:

$$\mathcal{F}_{D=3}(p(r))[Q] = C_{D_f}/(\kappa^2 + Q^2)^{(D_f+1)/2}\sin\left((D_f+1)\tan^{-1}\left(\frac{Q}{\kappa}\right)\right) \tag{4}$$

where C_{D_f} is a proportional constant of the gamma function Γ: $C_{D_f} = \sqrt{\frac{2}{\pi}}\frac{\Gamma(D_f+2)}{\kappa^{D_f+1}D_f+1}$. In the case of infinitely small κ, it simplifies to: $\mathcal{F}(p(r))[Q] \propto 1/Q^{D_f+1}$.

3.3.3. Bi-Langmuir adsorption

MabSelect SuRe is known for its tetrameric chain of B-domain–derived ligands. These four theoretical antibody binding domains may be a source of energetic heterogeneity.

Therefore, the Langmuir isotherm may incorrectly predict adsorption for this system. High energy adsorption sites become saturated (*i.e.*, are occupied first) at low concentrations, while at high concentrations, molecules adsorb to high and low energy sites (Gritti & Guiochon 2010). The system is better described by a bi-Langmuir model, which takes into account this possible heterogeneous adsorption as it is based on the coexistence of two (or more) independent non-cooperative sites (Bellot & Condoret 1993; Gritti & Guiochon 2005). The amount of adsorbed protein q in equilibrium with equilibrium solution concentration C is modeled by:

$$q = \sum_{i=1}^{2} q_{i,m} b_i C/(1 + b_i C) \tag{5}$$

where $q_{i,m}$ gives the maximum adsorbed capacity at any site, and b_i values are the sample equilibrium constants between the bulk solution and the multiple adsorption sites and $b_i > 0$.

3.4. Results and Discussion

The scope of this work is to understand the rearrangement and orientation of antibodies on MabSelect SuRe. SAXS is the fingerprint technique used here, and antibody–Protein A interaction data interpretation was done in terms of radial density distribution. We computed hypothetical 3D models and thereof radial density distributions. We compared the results to radial density distributions we computed from experimental scattering data. We found favored binding orientations and stoichiometry. Scanning electron microscopy (SEM) imaging was employed to validate the determination of the structure factor of a defined fractal network composed by the resin's cross-linked agarose.

3.4.1. Scattering profiles

The SAXS data were analyzed according to the theory drafted in the theory section and outlined in Figure II.3.1. In the present work, we assumed that the scattering intensities could be split into a product of form and structure factors. This simplification was made because of the different scales of the radial density distribution of both the antibody Protein A–ligand complex and the distribution of these particular complexes in the resin. The form factor, $P(Q)$, computed from the radial density distribution, mimics the statistics of the distances measured within the antibody–Protein A ligand complex, with a typical distribution as depicted in Figure II.3.1A. The red disk is a schematic representation of the Protein A ligand; the larger green disk mimics the immobilized antibody. The structure factor, $S(Q)$, takes into account the distribution of these complexes throughout the resin network, with a possible arrangement shown in red in Figure II.3.1B. We assume a random distribution of ligands, and it is the particular structure of the resin that imposes the characteristic shape of the pair density distribution from that the antibody–ligand complex structure factor is computed.

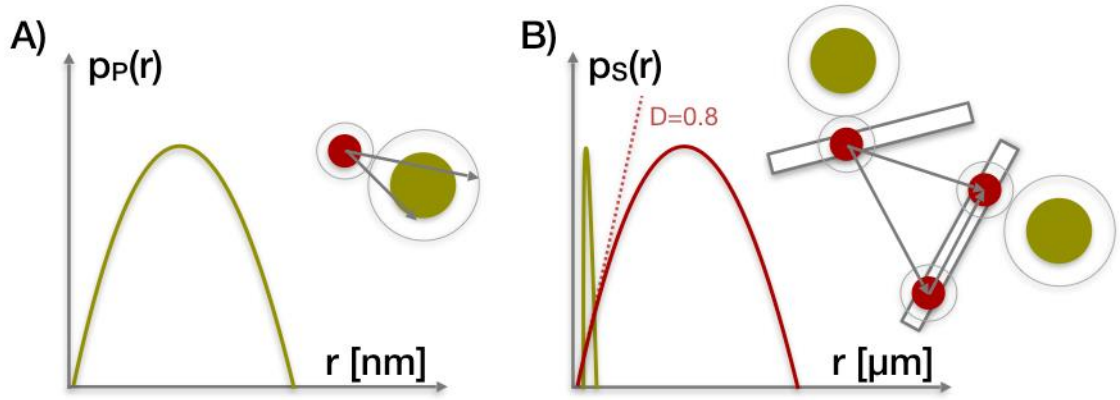

Figure II.3.1 - Schematic representation of the antibody (green disks) complexed with the Protein A ligand (red disks), their distribution across the resin network (grey rectangles), and the respective pair density distributions for *form* and *structure* factors. A) The green line is the hypothetical pair density distribution $p_p(\mathrm{r})$ of the antibody in reference to the ligand; B) the hypothetical pair density distribution, $p_s(\mathrm{r})$, of the agarose is presented by the red line. The hypothetical $p_p(\mathrm{r})$ is superimposed by a green line for scale. The slope of the tangent at small r to $p_s(\mathrm{r})$ is the fractal dimension D of the agarose network.

3.4.2. SEM

Parallel to SAXS data, we used SEM to visualize the agarose beads of MabSelect SuRe. From the SEM image, we could computationally generate the structure factor of the fractal network and compare it with the obtained value from SAXS.

Figure II.3.2A shows a SEM image of MabSelect SuRe resin's network. The magnification indicates a typical diameter of approx. 34 nm. The SEM image was binarized, resulting in Figure II.3.2B, where grey areas indicate the agarose network and white areas mark the pores. From the binarized image, we chose 10,000 sites randomly distributed in two zones. First, we constrained the site choices to the grey areas, *i.e.*, the agarose network, and displayed them with red dots in Figure II.3.2C. Then, we randomly chose pixels from both the grey and the white areas (random noise over the whole picture), marking them with blue dots in Figure II.3.2D; these are considered white noise. Figure II.3.2E is a magnified overlay of Figure II.3.2C and D. From Figure II.3.2E, we computed the normalized pair density distribution to the same amount of relative distances from the red and blue sites and plotted them in Figure II.3.2F. The pair density distribution can be estimated with $p_S(r) = r^{D_f}$. Therefore, from these pair density distributions, we computed the dimensionality D_f of the system. Whereas the white noise data gave a value $D_f = 1.0$, the fractal dimension of the agarose network returned a value $D_f = 0.74$, both represented as the slope of the fit curve to the data in Figure II.3.2G. The pair density fluctuations were determined with $\Delta p_S(r) = r^{0.74} - r^{1.0}$. It is an approach to estimate the average pore form and average pore sizes at small scale. Figure II.3.2H shows the pair density fluctuations of the MabSelect SuRe resin as assessed by the SEM image, with the typical small pores close to 80 nm in diameter (Pabst, Thai, & Hunter 2018).

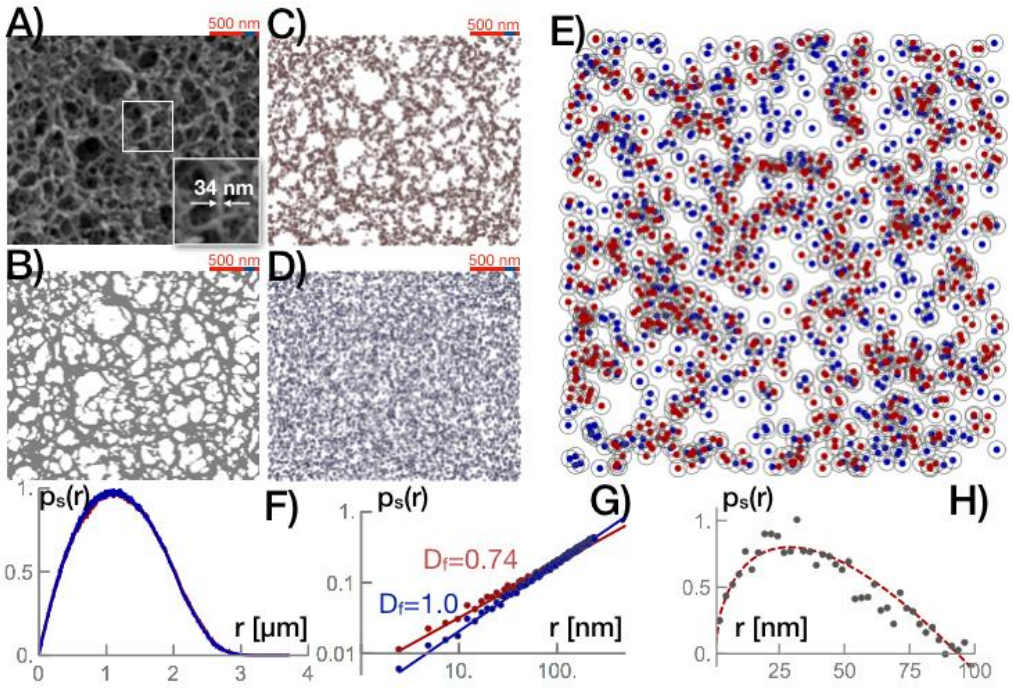

Figure II.3.2 - A) SEM image of MabSelect SuRe resin. The red scale bar indicates a 500 nm distance. The insert is a magnification of a typical agarose strand. Strands are up to 34 nm in diameter. B) Binarized SEM image. The pores are identified as white areas and the agarose as grey. C) Random choice of 10000 pixels distributed across the agarose fractal network (red); D) random choice of 10000 pixels of SEM image (agarose fractal network and the pores – white noise) (blue); E) Magnification of the overlay of C) and D), where the red dots represent the random distribution of the agarose, and the blue dots the random distribution of the agarose and the pores; F) pair density distribution of both the fractal network (red) and white noise (blue); G) determination of the dimension of the fractal network (D = 0.74) and white noise (D = 1.02); H) subtraction of the pair density distribution of the fractal network and white noise: pore size distribution, with the largest being 80 nm.

3.4.3. Antibody solution

To appropriately describe the adsorption mechanism, it is essential to evaluate the antibody state of aggregation at the used solution concentrations. The form factor of the antibody was computed from measurements of antibody in solutions at 8 mg/mL, 16 mg/mL, and 30 mg/mL. Figure II.3.3A shows in the insert the scattering intensity curves from the antibody in solution samples and the respective pair density distribution, as well as the pair density distribution of two antibody crystallographic structures (PDB: 1IGT – IgG2, and PDB: 1HZH – IgG1) to complement SAXS data evaluation.

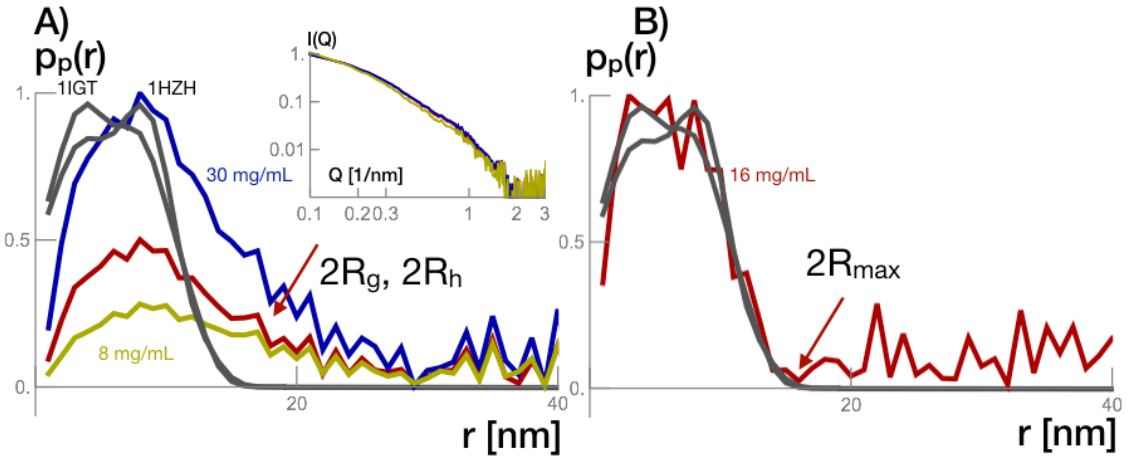

Figure II.3.3 - A) Normalized scattering intensity (insert) from antibody in solution at 8 mg/mL (green), 16 mg/mL (red), and 30 mg/mL (blue). The respective pair density distributions plotted with the pair density distribution from the crystallographic structures 1HZH and 1IGT; B) overlay of the pair density distribution from the crystallographic structures 1HZH and 1IGT with the pair density distribution of the subtracted scattering intensities from the antibody in solution at 16 mg/mL and 8 mg/mL. We corrected the scattering data of 36 mg/mL by a factor to $S(Q) = Q^{-0.3}$.

The pair density distributions from the crystallographic structures were computed from the centroids of the amino acids. They present maxima at 3 and 7 nm values that in literature are associated to the hydrodynamic radius of an IgG1 and would match well with the experimental data for the antibody in solution (Gagnon et al. 2015). Pair densities can be found up to relative distances of 12 nm. Indeed, this value is an estimation of the hydrodynamic diameter of the antibody in solution considering all the associated intrinsic flexibility (Gagnon et al. 2015; Gagnon & Nian 2016).

The relative pair density $p_P(r)$ from the experimental samples show, however, a tailing profile up to relative distances larger than the antibody size. This behavior may be characteristic of pair-wise interactions between molecules in solution that are near each other and consequently these additional relative distances contribute to the scattering signal. It would be as well valid to accuse a certain biologic flexibility of the antibody molecules in solution (Boldon, Laliberte, & Liu 2015), opposed to their rigid structures in crystals. Indeed, one of the advantages of SAXS over crystallographic data in terms of distance assessment measurements relies on the fact that the scattering intensity of a particle is measured in solution. Both interpretations, the pair wise interactions of antibody molecules and the flexibility of a monomer, are attributed similarly to the scattering intensity. Both contributions can be addressed by a factor $\propto Q^D$. The physical interpretation of the exponent D differs though. First, in the case of pair wise interactions, it would be the parameter of an interaction potential. Second, it would be interpreted as a measure of size distributions of the protein taking into account the intrinsic biological flexibility of the monomer. Both interpretations impacted the possible adsorption process.

We suggest a different evaluation. To assess the pair density distributions of the monomeric form, we subtracted the appropriately normalized pair densities from the sample

at solution concentration 8 mg/mL from that at solution concentration 16 mg/mL. The signal is plotted in Figure II.3.3B along with the pair density from the crystallographic structures. The results match the crystallographic data and we may argue that up to 16 mg/mL protein solutions are monomeric. Consequently, we anticipate, that antibody monomers adsorb and that the tailings in pair densities are due to parasitic background. For 30 mg/mL we indeed do monitor a factor of $Q^{-0.3}$. However, 16 mg/mL is well above the antibody starting concentration at which we perform our measurements.

3.4.4. The structure factor

The scattering intensity of the antibody adsorbed to the Protein A ligand at the resin surface was measured and plotted in Figure II.3.4A. The black curve corresponds to the MabSelect SuRe resin scattering intensity. Brighter red curves correspond to scattering intensity of MabSelect SuRe resins that have been incubated with a range of antibody concentrations.

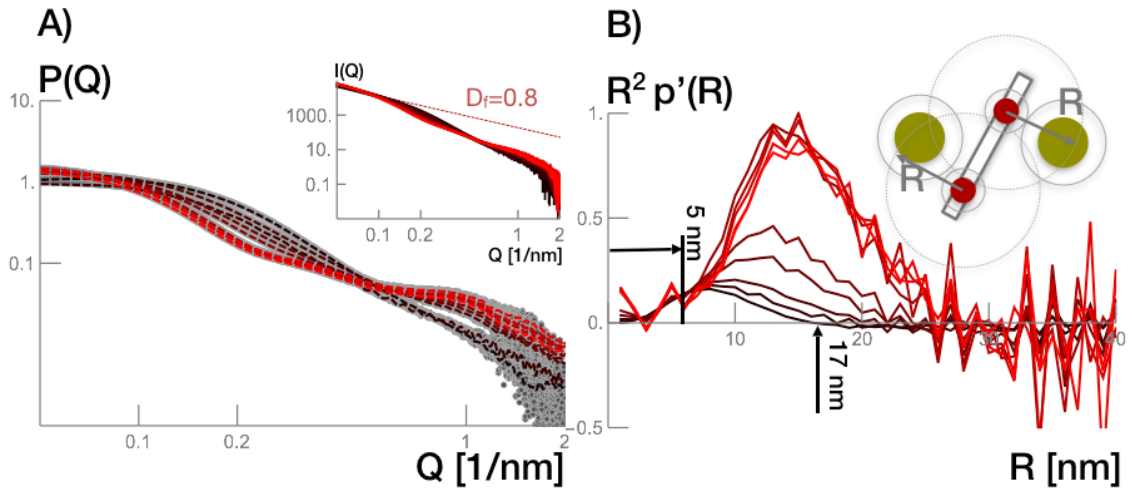

Figure II.3.4 - A) The scattering intensity, $\boldsymbol{P(Q)}$, given as a function of the scattering vector, $\boldsymbol{Q}$ [1/nm], from antibody bound to MabSelect SuRe 0-80 mg/mL resin by gray disks. Fits are represented in black and evolve towards red with increasing antibody concentration. Insert shows the raw experimental datasets. The fractal dimension (D = 0.8) is determined from the slope of scattering data from blank resin at low Q (red dashed line); B) Radial density distribution computed from the scattering intensity plots from blank resin and antibody bound to MabSelect SuRe 0-80 mg/mL resin. The resin signal is represented in black and evolves towards red with increasing surface concentration.

The structure factor dimension can be determined by calculating the absolute tangential slope to the low Q range of the scattering intensity of the resin. We found $D_f = 0.8$, which is in good agreement with the calculated value from the SEM image ($D_f = 0.74$). The computed fractal dimension from the fractal network of the SEM image matches the estimated fractal dimension we found from the low Q range of the experimental scattering intensities because both are 2D projections. One is an Abel transformation of the 3D pair density distribution and the other a binarized microscopy image of a 2D cut of the resin.

To assess the form factor contribution of the antibody–ligand complex distributed across the resin network at different equilibrium concentrations, we corrected the experimental scattering intensity $I(Q)$ by the fractal structure factor $S(Q) \propto 1/Q^{1.8}$. The resulting $P(Q)$ is seen in Figure II.3.4A, where the experimental data are represented with grey disks and the curve fits with dashed lines. The signal fluctuations are visible along the different Q ranges, a sign of different surface coverage by the antibody as a function of its bulk concentration.

3.4.5. The appropriate normalization of radial densities

A standard approach for background correction was to subtract the scattering intensity of the antibody-free resin sample from all of the complement data by $I_c(Q) = I(Q) - cI_b(Q)$ and then perform the inverse Fourier transform of the remaining scattering intensity: $p(r) = \mathcal{F}^{-1}(I_c(Q))$. However, this approach is biased because of the adjustment of factor c by matching both scattering curves at high Q range.

We propose a modified approach for a more realistic background correction. First, we corrected all scattering intensities by the structure factor, $S(Q)$, and then computed the radial density distributions: $p(r_c) = \mathcal{F}^{-1}(P(Q))$. Figure II.3.4B shows the radial density distributions, $p(r_c)$, from the scattering intensity profiles of antibody adsorption to MabSelect SuRe at the concentrations displayed in Figure II.3.4A. As in Figure II.3.4A, the curves go from black to red with increasing antibody concentration, with the black curve indicating the radial density distribution of the antibody-free resin sample. The resin signal (black line) has a maximum at 5-6 nm, which can be interpreted as the minimum radius of an agarose strand. We assume that the antibody molecules bind to the Protein A ligands and do not penetrate the cross-linked agarose strand. Therefore, the radial density distributions for every antibody concentration needs to match until 6 nm, resulting in the normalization of the radial density distributions.

3.4.6. Background corrected radial density distribution

To background-correct the normalized radial density distributions we subtracted the normalized radial density distribution of the resin from the normalized radial density distribution of the signals from samples with antibody bound to Protein A. The normalized and background corrected pair density distributions are shown in Figure II.3.5A. It shows the radial density distribution for different antibody concentrations. The most distinct feature is the increasing magnitudes with the increasing antibody concentration. The net area of the profiles resemble the surface excess, given by Γ.

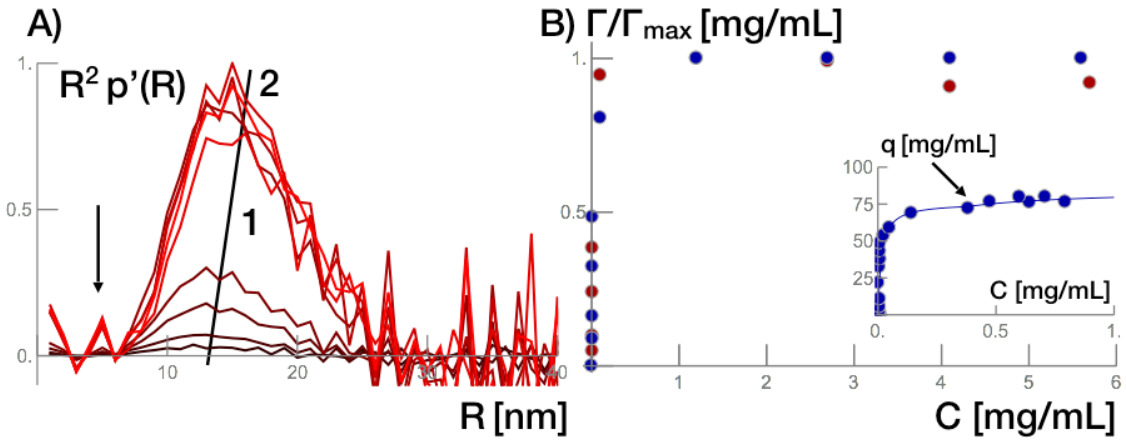

Figure II.3.5 - A) Background-corrected radial density distributions, $p'(\mathrm{R})$. B) Surface excess computed from the normalized areas from $R^2\,p'(\mathrm{R})$ as a function of antibody equilibrium concentration (red disks). Adsorbed amount derived from the equilibrium state of the samples before X-ray exposure (blue disks). The insert shows the experimental determined adsorption isotherm of antibody adsorption to MabSelect SuRe (blue disks).

3.4.7. Assessing the surface excess

If plotted with respect to the equilibrium bulk concentration of the antibody, the net area of the normalized radial density distribution profiles give a surface excess adsorption isotherm. The normalization of the isotherm was done in respect to the value at the highest concentration (Figure II.3.5B). The normalized surface excess values computed from the radial density distributions are shown in red, and the normalized isotherm derived from the equilibrium state of the samples before X-ray exposure is given in blue. This match supports the approach of how to assess radial density distributions from scattering intensity data.

Figure II.3.5B also shows an insert with the experimentally determined adsorption isotherm. It follows the favorable binding rectangular profile characteristic of Protein A resins in the antibody uptake. At equilibrium, the data show a second plateau to greater q_{max}. The data were fitted with a bi-Langmuir model, as described in the Theory section. Results favor a multi-point attachment due to heterogeneous binding sites with a weaker binding of a second antibody molecule to the Protein A ligand (Bellot & Condoret 1993). But how in particular does it bind and how is the form of the antibody-Protein A complex affected?

3.4.8. Form of antibody-Protein A 3D complex by molecular simulation

MabSelect SuRe is a tetrameric Protein A chain, thus multipoint attachment is theoretically possible (Gagnon & Nian 2016; Ghose, Hubbard, & Cramer 2007; Mazzer et al. 2017). Focused research is lacking. We have addressed it on basis of the normalized and background-corrected radial pair densities at different antibody bulk concentrations.

3.4.8.1. Antibody–Protein A–agarose complex

To visualize SAXS data, and to ease or support their interpretation, we perform model simulations. They are a powerful tool to help the interpretation of the nature of the present. In this work, we modeled the antibody–Protein A complex form by a rigid body approach.

As already mentioned, MabSelect SuRe Protein A chain is a recombinant polymer of four units of staphylococcal Protein A B-domain, called the Z-domain. This Z-domain is engineered through a point mutation of the B-domain to give the ligand improved alkaline stability (Ghose et al. 2005). To mimic as closely as possible the chromatographic system involved in this work, we used the crystallographic structure of Protein A B-domain (PDB: 1BDD) and built a four-fragment chain.

The model used to represent MabSelect SuRe agarose was kindly provided by Carlo Cavallotti from his group's publication (Salvalaglio et al. 2009), because they have recently employed such a model to predict which amino acid residues contribute the most to IgG binding to Protein A. The construct of this agarose model is described in detail in Ref. (Busini et al. 2006). The tetrameric Protein A chain was covalently linked to the agarose with an ester bond, and no spacer was introduced.

The final part of the model were the antibodies. We used the crystal structure of an IgG1 (PDB: 1HZH) and bound them through the consensus binding site located between the CH2 and CH3 Fc domains to the Fc binding site of one of Protein A B-domains. Deisenhofer has determined a complex of one half of the antibody Fc fragment and one Protein A B-domain (PDB: 1FC2) (Deisenhofer 1981). Our model matched Deisenhofer's proposed structure.

3.4.8.2. Random sampling

After designing the model complex, we ran simulations. We employed a rigid body random walk model in which we did not enable flexibility of any of the different species. All system components were considered rigid entities. Different orientations of the Protein A fragments and the antibodies were allowed. Each Protein A fragment is considered as a single-point attachment domain to the antibody. Therefore, in the whole chain there are four potential binding sites; one per fragment.

The first set of molecular simulations regarded the binding of one antibody molecule to the Protein A chain. We simulated a library of at least 10,000 potential forms of antibody in complex with the Protein A tetramer ligands. From the conformations, we assessed the respective radial density distributions. Figure II.3.6A shows the rigid body models of a selected conformation and Figure II.3.6B shows the radial density distributions of 1:1 antibody to Protein A chain stoichiometry.

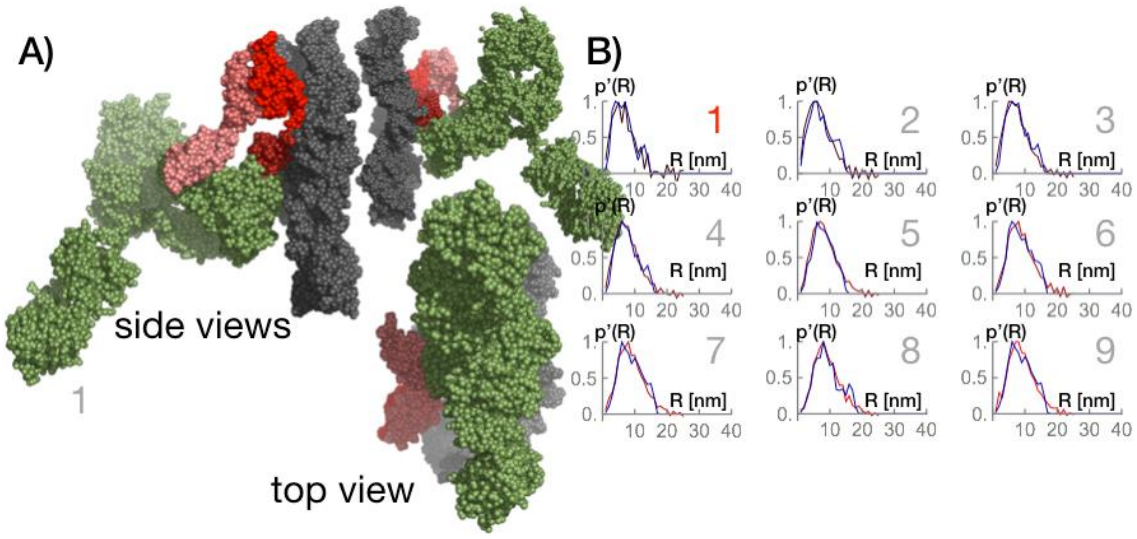

Figure II.3.6 - Rigid body models and radial density distributions of 1:1 antibody to Protein A stoichiometry. A) Selected configuration of the complex; the grey bead model indicates the resin; the red bead models mimic the MabSelect SuRe Protein A tetrameric chain; the green bead model marks the antibody. B) Radial density distributions computed from SAXS data (dark red to bright red lines) are compared to radial density distributions (blue line) computed from random walk models. The data enumerated 1-9 correspond to different antibody bulk concentrations, with the correspondence given in the text.

With increasing equilibrium concentration (we number them from 1 to 9 in Figure II.3.6B), the best results for 1:1 antibody–Protein A stoichiometry show a binding preference for the: 4th (solution 1: C = 0.01 mg/mL; q = 25.8 mg/mL resin), 3rd (solution 2: C = 0.01 mg/mL; q = 25.8 mg/mL resin), 1st (solution 3: C = 0.01 mg/mL; q = 25.8 mg/mL resin), 1st (solution 4: C = 0.01 mg/mL; q = 38.7 mg/mL resin), 3rd (solution 5: C = 0.1 mg/mL; q = 64.5 mg/mL resin), 3rd (solution 6: C = 1.2 mg/mL; q = 80.0 mg/mL resin), 3rd (solution 7: C = 2.7 mg/mL; q = 80.0 mg/mL resin), 4th (solution 8: C = 4.7 mg/mL; q = 80.0 mg/mL resin), and 3rd (solution 9: C = 5.6 mg/mL; q = 80.0 mg/mL resin) domain counting from the agarose surface. The obtained preferential binding is speculative as it does not take into account any energy minimization. Simulations indicate that at low bulk concentrations and very low surface concentrations (solutions 1 and 2) the antibody binds to the outermost ligands (4th and 3rd) but finds itself in the proximity of the first ligand. Engineered Protein A in commercial media has a tentacle form and the chain can be extended in the surface (Gagnon & Nian 2016). We have implemented the possibility for the Protein A chain for a loop-like conformation (see its form in Figures II.3.6, II.3.7, or II.3.8). Within our random walk model the Protein A chain is flexible and a transfer from the outermost to the innermost ligand seems feasible. Biologically, antibody dual-site binding to Protein A is possible (Gagnon & Nian 2016). With increasing surface concentration but still at low equilibrium concentration (solutions 3 and 4), the first ligand is the most favored. At elevated concentrations (solutions 5-9) the outermost become favored again. At these concentrations the radial densities of the simulated configurations lack the

tailing we find in the experimental data, as seen in Figure II.3.6B. Therefore, a second antibody molecule to recover this particular tailing is needed.

Following a 1:1 stoichiometry, we attached two antibody molecules to every possible combination of B fragments and allowed every possible orientation. Figure II.3.7A shows possible orientations of two antibody molecules bound to the inner and outermost fragments in the Protein A. Again, the radial density distributions of these models were determined and scanned for similarity to radial densities computed from the experimental SAXS data. Figure II.3.7B shows the radial density distributions of this 2:1 stoichiometry.

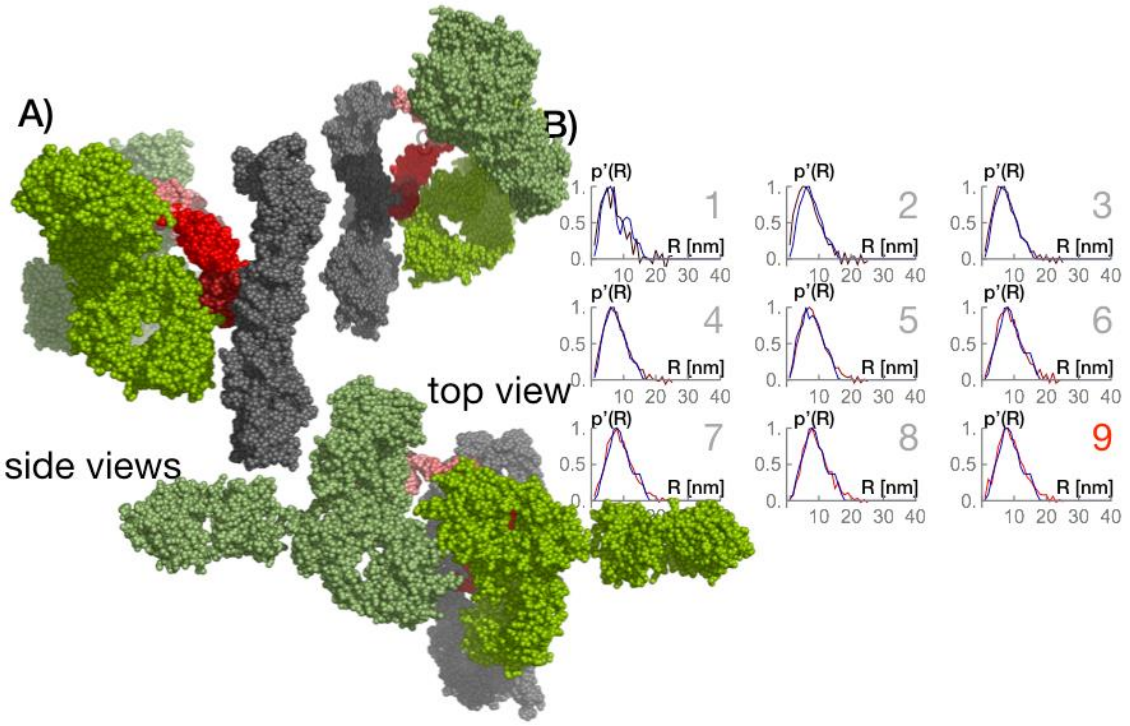

Figure II.3.7 - Rigid body models and radial density distributions of 2:1 antibody Protein A stoichiometry. A) Selected configuration of the complex; the grey bead model indicates the resin; the red bead models mimic the MabSelect SuRe Protein A tetrameric chain; the green bead model marks the antibody. B) Radial density distributions computed from SAXS data (dark red to bright red lines) are compared to radial density distributions (blue line) computed from random walk models. The data enumerated 1-9 correspond to different antibody bulk concentrations, with the correspondence given in the text.

Antibody molecules bound to the two outermost fragments returned the best radial density distributions, matching the distribution at high antibody concentration provided by SAXS. It can be assumed that the steric hindrance from the agarose would be greater in comparison to the resulting hindrance of the close proximity of another antibody molecule. The radial density distributions at this moment showed a maximum detected relative distance at around 21 nm. This value could correspond to the largest possible scattering distance between the two antibody molecules (approximately the sum of two hydrodynamic radius) or the distance from the most external antibody to the agarose.

These modeled data support the isotherm prediction. At saturation more than one antibody molecule can bind to the Protein A ligands with the support of binding heterogeneity proposed by bi-Langmuir isotherm model. Data based on equilibrium binding capacities definitely support the idea that two antibody molecules can be bound to the MabSelect SuRe ligand. This was already suggested by other authors with Protein A in solution studies (Ghose, Hubbard, & Cramer 2007) and with neutron reflectivity studies with Protein A attached to silica (Mazzer et al. 2017).

Finally, we ran models with three antibody molecules bound to different Protein A fragments within the same chain. The configurations computed are densely packed. Figure II.3.8A shows a selected configuration of these models. Figure II.3.8B shows the radial density distributions of this stoichiometry overlapped with experimental data.

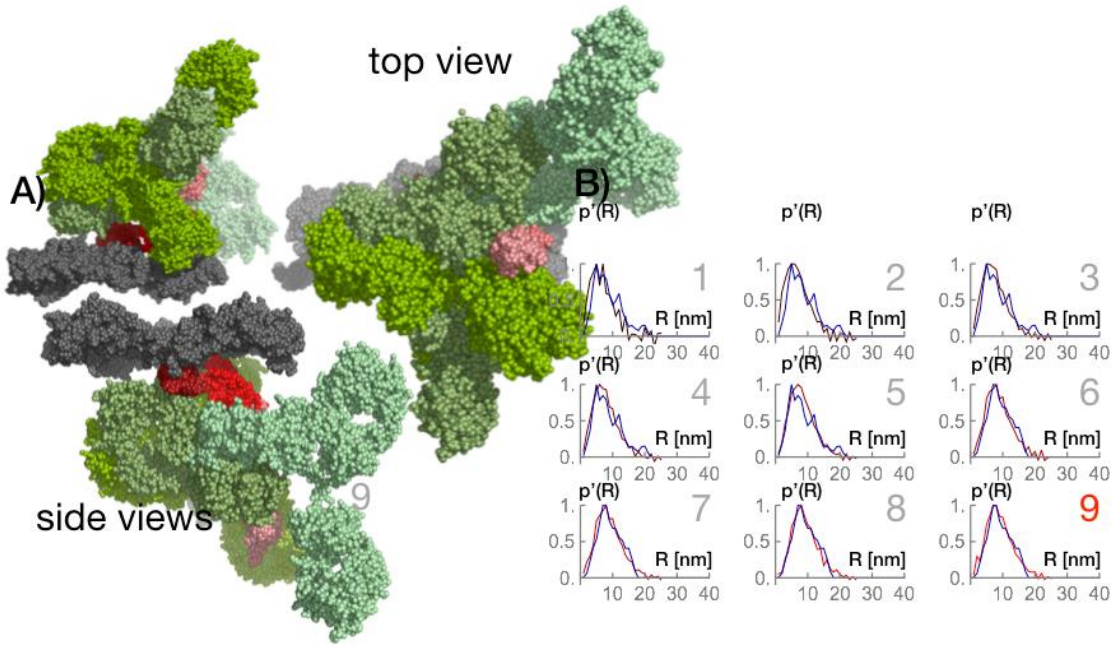

Figure II.3.8 - Rigid body models and radial density distributions of 3:1 antibody Protein A stoichiometry. A) Selected configuration of the complex; the grey bead model indicates the resin; the red bead models mimic the MabSelect SuRe Protein A tetrameric chain; the green bead model marks the antibody. B) Radial density distributions computed from SAXS data (dark red to bright red lines) are compared to radial density distributions (blue line) computed from random walk models. The data enumerated 1-9 correspond to different antibody bulk concentrations, with the correspondence given in the text.

We are convinced that a 3:1 stoichiometry possibility can be excluded because of steric effects. We would need to consider all atomistic pair wise interactions to argue their feasibility. In the present work, we limited ourselves to geometrical considerations.

3.5. Conclusions

In this work we experimentally assessed radial density distributions and, on basis of this experimental value, hypothesized possible antibody-Protein A forms and configurations in a chromatographic resin.

We used small angle X-ray scattering as experimental method to model and speculate on the 3D form of antibody in solution and after binding to tetrameric staphylococcal Protein A in MabSelect SuRe. We compared the experimentally assessed radial density distribution with ones computed from molecular simulations. Computational models were restricted to crystallographic data and to data derived from molecular dynamic simulations.

We reason that the antibodies bind to the Protein A ligand at different stoichiometries because of the existence of heterogeneous binding sites. At low antibody concentrations (< 40 mg/mL resin) we argue that the probable binding stoichiometry is 1:1, whereas at higher concentrations (> 40 mg/mL resin) a 2:1 stoichiometry is favored. At low concentrations, and assuming a 1:1 stoichiometry, the random walk models point towards configurations where the antibody binds at the outermost ligands at very low and at high concentrations and in perpendicular form in respect to the surface. At 2:1 stoichiometry, we favor propeller-like configurations of the immobilized antibodies, which are more preferentially bound to the 1st and 4th ligand. From our data, a 3:1 stoichiometry, albeit theoretically possible, is excluded here because of the steric effects. We are convinced that our paper, in which we outlined how to rationally assess 3D forms of the antibody-Protein A complexes at different antibody concentrations next to a resin surface, will trigger the rational design of this technology of high industrial relevance. Our experimental design can be potentially used to investigate molecule binding on other chromatographic systems in terms of stoichiometry, binding configurations, and distal spacing. Therefore, it can be implemented as a monitoring tool in industrial applications where it is necessary to purify large amounts of product while obeying to certain Quality by Design parameters.

3.6 References

Bellot, J. C., & Condoret, J. S. (1993). Review modelling of liquid chromatography equilibria. Process Biochemistry, 28, 365–376. https://doi.org/10.1016/0032-9592(93)80023-A

Boldon, L., Laliberte, F., & Liu, L. (2015). Relevant Integrated Application. Nano Reviews, 6, 1–22. https://doi.org/10.3402/nano.v6.25661

Brandt, J. P., Patapoff, T. W., & Aragon, S. R. (2010). Construction, MD simulation, and hydrodynamic validation of an all-atom model of a monoclonal IgG antibody. Biophysical Journal, 99, 905–913. https://doi.org/10.1016/j.bpj.2010.05.003

Busini, V., Moiani, D., Moscatelli, D., Zamolo, L., & Cavallotti, C. (2006). Investigation of the influence of spacer arm on the structural evolution of affinity ligands supported on agarose. Journal of Physical Chemistry B, 110, 23564–23577. https://doi.org/10.1021/jp0622278

Deisenhofer, J. (1981). Crystallographic refinement and atomic models of a human Fc fragment and its complex with fragment B of Protein A from Staphylococcus aureus at 2.9-and 2.8-A resolution. Biochemistry, 20, 2361–2370. https://doi.org/10.1021/bi00512a001

DeLano, W. L., Ultsch, M. H., de Vos, A. M., & Wells, J. A. (2000). Convergent solutions to binding at a protein-protein interface. Science, 287, 1279–1283. https://doi.org/10.1126/science.287.5456.1279

Gagnon, P., & Nian, R. (2016). Conformational plasticity of IgG during protein A affinity chromatography. Journal of Chromatography A, 1433, 98–105. https://doi.org/10.1016/j.chroma.2016.01.022

Gagnon, P., Nian, R., Leong, D., & Hoi, A. (2015). Transient conformational modification of immunoglobulin G during purification by protein A affinity chromatography. Journal of Chromatography A, 1395, 136–142. https://doi.org/10.1016/j.chroma.2015.03.080

Ghose, S., Allen, M., Hubbard, B., Brooks, C., & Cramer, S. M. (2005). Antibody variable region interactions with protein A: Implications for the development of generic purification processes. Biotechnology and Bioengineering, 92, 665–673. https://doi.org/10.1002/bit.20729

Ghose, S., Hubbard, B., & Cramer, S. M. (2007). Binding capacity differences for antibodies and Fc-fusion proteins on Protein A chromatographic materials. Biotechnology and Bioengineering, 96, 768–779. https://doi.org/10.1002/bit.21044

Glatter, O., & Kratky, O. (1982). Small Angle X-ray Scattering. Academic Press Inc., London.

Graille, M., Stura, E. A., Corper, A. L., Sutton, B. J., Taussig, M. J., Charbonnier, J. B., & Silverman, G. J. (2000). Crystal structure of a Staphylococcus aureus protein A domain complexed with the Fab fragment of a human IgM antibody: structural basis for recognition of B-cell receptors and superantigen activity. Proceedings of the National Academy of Sciences of the United States of America, 97, 5399–5404. https://doi.org/10.1073/pnas.97.10.5399

Gritti, F., & Guiochon, G. (2005). Critical contribution of nonlinear chromatography to the understanding of retention mechanism in reversed-phase liquid chromatography. Journal of Chromatography A, 1099, 1–42. https://doi.org/10.1016/j.chroma.2005.09.082

Gritti, F., & Guiochon, G. (2010). Comparison between heterogeneous multi-Langmuir and homogeneous electrostatically modified Langmuir models in accounting for the adsorption of small organic ions in reversed-phase liquid chromatography. Journal of Chromatography A, 1217, 5584–5594. https://doi.org/10.1016/j.chroma.2010.06.046

Hahn, R., Bauerhansl, P., Shimahara, K., Wizniewski, C., Tscheliessnig, A., & Jungbauer, A. (2005). Comparison of protein A affinity sorbents: II. Mass transfer properties. Journal of Chromatography A, 1093, 98–110. https://doi.org/10.1016/j.chroma.2005.07.050

Hahn, R., Shimahara, K., Steindl, F., & Jungbauer, A. (2006). Comparison of protein A affinity sorbents III. Life time study. Journal of Chromatography A, 1102, 224–231. https://doi.org/10.1016/j.chroma.2005.10.083

Hayter, J. B., & Penfold, J. (1983). Determination of micelle structure and charge by neutron small-angle scattering. Colloid & Polymer Science, 261, 1022–1030. https://doi.org/10.1007/BF01421709

Hober, S., Nord, K., & Linhult, M. (2007). Protein A chromatography for antibody purification. Journal of Chromatography B, 848, 40–47. https://doi.org/10.1016/j.jchromb.2006.09.030

Mazzer, A. A. R., Clifton, L. A., Butler, P. D., Roberts, C. J., & Bracewell, D. G. (2017). Neutron reflectivity measurement of protein A - antibody complex at the solid-liquid interface. Journal of Chromatography A, 1499, 118–131. https://doi.org/10.1016/j.chroma.2017.03.084

Pabst, T. M., Thai, J., & Hunter, A. K. (2018). Evaluation of recent Protein A stationary phase innovations for capture of biotherapeutics. Journal of Chromatography A, 1554, 45–60. https://doi.org/10.1016/j.chroma.2018.03.060

Pernot, P., Round, A., Barrett, R., De Maria Antolinos, A., Gobbo, A., Gordon, E., … McSweeney, S. (2013). Upgraded ESRF BM29 beamline for SAXS on macromolecules in solution. Journal of Synchrotron Radiation, 20, 660–664. https://doi.org/10.1107/S0909049513010431

Portale, G., Cavallo, D., Alfonso, G. C., Hermida-Merino, D., Van Drongelen, M., Balzano, L., … Bras, W. (2013). Polymer crystallization studies under processing-relevant conditions at the SAXS/WAXS DUBBLE beamline at the ESRF. Journal of Applied Crystallography, 46, 1681–1689. https://doi.org/10.1107/S0021889813027076

Salvalaglio, M., Zamolo, L., Busini, V., Moscatelli, D., & Cavallotti, C. (2009). Molecular modeling of Protein A affinity chromatography. Journal of Chromatography A, 1216, 8678–8686. https://doi.org/10.1016/j.chroma.2009.04.035

Sandin, S., Öfverstedt, L.-G., Wikström, A.-C., Wrange, Ö., & Skoglund, U. (2004). Structure and Flexibility of Individual Immunoglobulin G Molecules in Solution. Structure, 12, 409–415. https://doi.org/10.1016/j.str.2004.02.011

Shukla, A. A., Hubbard, B., Tressel, T., Guhan, S., & Low, D. (2007). Downstream processing of monoclonal antibodies — Application of platform approaches. Journal of Chromatography B, 848, 28–39. https://doi.org/10.1016/j.jchromb.2006.09.026

Starovasnik, M. A., O'Connell, M. P., Fairbrother, W. J., & Kelley, R. F. (1999). Antibody variable region binding by Staphylococcal protein A: Thermodynamic analysis and location of the Fv binding site on E-domain. Protein Science, 8, 1423–1431. https://doi.org/10.1110/ps.8.7.1423

Uhlén, M., Guss, B., Nilsson, B., Gatenbeck, S., Philipson, L., & Lindberg, M. (1984). Complete sequence of the Staphylococcal gene encoding Protein A. A gene evolved through multiple duplications. The Journal of Biological Chemistry, 259, 1695–1702.

Yu, D., Song, Y., Huang, R. Y.-C., Swanson, R. K., Tan, Z., Schutsky, E., … Li, Z. J. (2016). Molecular perspective of antibody aggregates and their adsorption on Protein A resin. Journal of Chromatography A, 1457, 66–75. https://doi.org/10.1016/j.chroma.2016.06.031

Zamolo, L., Busini, V., Moiani, D., Moscatelli, D., & Cavallotti, C. (2008). Molecular dynamic investigation of the interaction of supported affinity ligands with monoclonal antibodies. Biotechnology Progress, 24, 527–539. https://doi.org/10.1021/bp070469z

Zhang, F., Skoda, M. W. A., Jacobs, R. M. J., Martin, R. A., Martin, C. M., & Schreiber, F. (2007). Protein interactions studied by SAXS: effect of ionic strength and protein concentration for BSA in aqueous solutions. The Journal of Physical Chemistry B, 111, 251–259. https://doi.org/10.1021/jp0649955

CHAPTER III - Conclusions

Conclusions

The monoclonal antibody is an increasing market, contributing significantly to the global sales revenue of biopharmaceuticals. Therefore, and also given the wide range of the potential therapeutic applications of mAbs, pharmaceutical industry is becoming constantly subjected to regulatory constrains to ensure product quality and safety criteria are met.

One of the most important unit operations in the downstream processing of mAbs is their direct capture from cell supernatant, with Protein A chromatography being unarguably the most employed and robust method for antibody capture. However, antibody adsorption to Protein A resins is a complex process that requires full understanding.

This doctoral thesis had the main goal to understand from a biophysical standpoint the adsorption process of a commercially available therapeutic antibody to Protein A resins during the capture step of its purification. This work intended to highlight the importance of monitoring a chromatographic step *in situ* and provide valuable information regarding the binding process for a better understanding and optimization.

From the publications listed above, it was possible to have a thermodynamic, kinetic, and structural fingerprint of the antibody binding process to Protein A resins with different ligand structure and backbone nature.

The calorimetric studies showed that adsorption can be discriminated in two sub-processes of exothermic nature; binding and reorganization are the two proposed sources for the changes in enthalpy in this process. Also, the binding kinetics showed different effective diffusivities associated with equilibrium time; faster kinetics following the shrinking core model at early equilibrium times, and slower kinetics as the ultimate capacity is attained, consistent with the binding heterogeneity of the two resins studied. This conclusion was reinforced by the flow microcalorimetry studies.

SAXS was a valuable tool to assess the adsorption layer thickness, which was established as a 5.5 nm increase (the antibody hydrodynamic radius) with antibody loading and it was seen that it regenerates after elution. That led to the interpretation that the Protein A ligand in MabSelect SuRe has a preferred hook-like conformation as opposed to be fully stretched upon antibody binding.

SAXS also confirmed the possibility of antibody binding to MabSelect SuRe in multiple stoichiometry in batch operations depending on the isotherm region associated to the heterogeneous binding nature. A key fact is that regardless of the concentration, there would always be a mixture of different stoichiometry, depending on the ligand accessibility. However, it was found that at lower concentrations a 1:1 antibody to Protein A chain stoichiometry is favoured, and at higher concentrations 2:1 becomes more probable. 3:1 conformations, despite being possible at high binding capacity, were shown to be unlikely because of associated steric effects. Nevertheless, the proposed model still lacks the flexibility given by true molecular dynamic simulations.

The main conclusion of this thesis derived from the results of the experimental methodology is the heterogeneous biding nature of multimeric Protein A resins. It is suggested that the antibody adsorption is a stochastic phenomenon where the distribution of binding of the first molecules determines the binding probability of the subsequent. The small but valuable contribution from this thesis could potentially lead to a better understanding of Protein A chromatography and could help to predict any parameter associated to the capture step of mAbs at any point of the process.

Future perspectives

This work consisted in a deep calorimetric and structural investigation regarding antibody adsorption to Protein A in commercial synthetically engineered resins, in which it was proved the heterogeneous binding nature of such resins. With the antibodies having the possibility to bind to more than one domain in a single Protein A chain, it would be of utmost importance to link the thermodynamic data obtained to every possible conformation and stoichiometry. By doing this, it would be possible to discriminate at any surface concentration how favorable would be for the antibody to bind to any given Protein A domain.

The structural analysis by SAXS of antibody binding to TOYOPEARL AF-rProtein A is already under evaluation. The experiments were performed but the scattering intensity signal is smeared by the noise contribution of the less porous methacrylate-based backbone of this resin. So, a different model than the one used for MabSelect SuRe results interpretation has to be used. In addition, it would be of interest to perform a true molecular dynamics simulation with applied coarse grain force fields. In this way, the models representing the antibody and the resin would be approximate to the real conditions in chromatography.

Another valuable input to understand and optimize resin utilization by the antibody is the ligand density and ligand distribution in the backbone of the resin. It is important to understand its contribution to the steric hindrance associated to antibody molecules binding in the neighboring ligands. In ongoing studies, the resin backbone was modelled subdivided into clusters of spherical dimensions of the polymer (agarose or poly-methacrylate) thickness along the cross-linked network. The number of ligands per one of these spheres was already extrapolated in order to build a model that can mimic the entire bead piece by piece with the appropriate ligand distribution and binding capacity and see how the antibody molecules respond to their vicinity. By knowing this, resin manufacturers can exploit ligand accessibility and improve binding capacity and the costumers could potentiate the extent of the resin and optimize its limitations.